Computational models of motor adaptation under multiple classes of sensorimotor disturbance

Adrian Haith

Doctor of Philosophy

Institute of Perception, Action and Behaviour

School of Informatics

University of Edinburgh

2009

Abstract

The human motor system exhibits remarkable adaptability, enabling us to maintain high levels of performance despite ever-changing requirements. There are many potential sources of error during movement to which the motor system may need to adapt: the properties of our bodies or tools may vary over time, either at a dynamic or a kinematic level; our senses may become miscalibrated over time and mislead us as to the state of our bodies or the true location of an intended goal; the relationship between sensory stimuli and movement goals may change. Despite these many varied ways in which our movements may be disturbed, existing models of human motor adaptation have tended to assume just a single adaptive component.

In this thesis, I argue that the motor system maintains multiple components of adaptation, corresponding to the multiple potential sources of error to which we are exposed. I outline some of the shortcomings of existing adaptation models in scenarious where multiple kinds of disturbances may be present - in particular examining how different distal learning problems associated with different classes of disturbance can affect adaptation within alternative cerebellar-based learning architectures - and outline the computational challenges associated with extending these existing models.

Focusing on the specific problem in which the potential disturbances are miscalibrations of vision and proprioception and changes in arm dynamics during reaching, a unified model of sensory and motor adaptation is derived based on the principle of Bayesian estimation of the disturbances given noisy observations. This model is able to account parsimoniously for previously reported patterns of sensory and motor adaptation during exposure to shifted visual feedback. However the model additionally makes the novel and surprising prediction that adaptation to a force field will also result in sensory adaptation. These predictions are confirmed experimentally. The success of the model strongly supports the idea that the motor system maintains multiple components of adaptation, which it updates according to the principles of Bayesian estimation.

Acknowledgements

I would like to thank my supervisor, Sethu Vijayakumar, along with all the other members of the SLMC group for providing a hugely stimulating research environment and many fruitful and interesting discussions throughout my years at Edinburgh. I thank Carl Jackson and Chris Miall for hosting me in Birmingham while we performed the experiments described in Chapter 5 and introducing me to the world of experimental motor control research - in particular, thanks to Carl for running subjects while I wasn't able to be in Birmingham. Thanks to John Porrill and Paul Dean for their guidance in the early stages of my PhD. Thank you to Melissa for her inexhaustible patience, encouragement and enthusiasm. And, lastly, huge thanks to my parents for everything they've done for me along the way.

Declaration

I declare that this thesis was composed by myself, that the work contained herein is my own except where explicitly stated otherwise in the text, and that this work has not been submitted for any other degree or professional qualification except as specified.

(*Adrian Haith*)

Table of Contents

Chapter 1

Introduction

Both our bodies and our environment are constantly changing. In order to continue to execute accurate, efficient movements, it is imperative that we are able to recognize any such change and adapt future movements accordingly.

A popular theory of how our brains achieve accurate control over our bodies is that the brain explicitly represents the characteristics of our body and environment through *internal models* - networks in the brain whose input/output characteristics capture the functional relationship between our motor commands and their consequences.As we will describe in the next chapter, these internal models can be used directly for control, planning and for estimating the state of our bodies (Wolpert et al., 1998; Kawato, 1999). As the relationship between motor commands and outcomes changes, the internal model can be adapted, enabling accurate control over our bodies to be maintained.

There are, however, a wide variety of ways in which our movements may be disrupted. In this thesis, I will examine the implications of these different kinds of disturbances for models of human motor adaptation and consider how to extend existing models to account for patterns of human adaptation in scenarios where multiple different kinds of disturbance may be present.

1.1 Visual vs dynamic disturbances

Through fatigue, atrophy, growth, ageing, exercise, disease, etc., the properties of our musculo-skeletal system may change. The objects and tools we manipulate may also change their properties over time, becoming heavier, lighter, stiffer etc. In a laboratory setting, robotic devices are routinely employed to apply arbitrary forces to the hand or arm. In all of these cases, the effect of a given motor command on the state of our arm

will change, leading to errors in our movements. These kinds of disturbances will be referred to as *dynamics disturbances*.

Besides changes in the dynamics of our body and environment, our motor performance may also be disrupted if our visual feedback is distorted. Most movements we make are guided by visual cues, such as the target of a reach, or throw. If the relationship between the true state of the world and our visual observation of it is disrupted, there will be errors in our movement. For instance, wearing glasses with strong lenses can distort our visual field, causing us to misjudge the location of a target or our hand and therefore make inappropriate movements. Prism lenses, which shift or invert the visual field, are a more extreme example of this effect. In the laboratory, computer displays and virtual reality devices allow precise control over the visual feedback a subject receives and are widely used to induce adaptation. A more natural example of this kind of disturbance is the effect of refraction shifting the visually-perceived location of an underwater target, while spear-fishing, for instance. In all cases, the visual feedback of both the target and our end-effector is systematically altered. These kinds of disturbances will be referred to as *visual disturbances*.

Although these are very different kinds of disturbances, the movement error arising from them may well end up being very similar. In both cases, a similar adjustment to our motor commands must be made if the movement is repeated. So, in a way, it may not really matter what the real cause of the error was. Indeed, as we discuss in Chapter 2, most computational models of motor adaptation draw no distinction between the different possible causes of an error. They simply attempt to characterize motor adaptation in terms of the effect that a movement error experienced during one trial will generalize to performance in subsequent trials. If possible, however, the nervous system should adapt differently according to the underlying cause of the error, since different kinds of disturbances will affect future movements in different ways.

Consider, for instance, that we make an error while reaching to a visual target with our right hand and then attempt a subsequent reach with the left hand. If our initial miss had been due to a change in the dynamics of the right arm, then there would be no need to make any adjustment to the subsequent movement with the left hand. However, if the error really arose from a visual disturbance, then we clearly *should* also adjust our subsequent left-hand movement. On the other hand, if we reach with the right hand, but to an auditory or proprioceptively defined target rather than a visual target, we should ignore any visual disturbance, but still compensate for any disturbance to the dynamics.

Besides interlimb generalization, there can also be differences in how we should generalize adaptation to different movements with the same limb. Two movements with similar hand displacements might require very different joint-angle displacements if they have different initial arm postures. For a visual disturbance, such as a shift or rotation of visual feedback, any two hand movements with the same hand displacement should be compensated for during planning in a similar way, regardless of the initial posture of the arm. This is indeed how people generalize learning of rotated visual feedback (Krakauer et al., 2000). By contrast, subjects generalize learning of dynamics disturbances according to similarities in joint-angle displacements (Shadmehr and Mussa-Ivaldi, 1994). This clear difference in how visual and dynamics disturbances are generalized establishes clearly that, rather than simply compensating for all movement errors in a similar fashion, the motor system is able to recognize whether it is experiencing a visual or a dynamic disturbance and adapt appropriately.

1.2 Task vs plant disturbances

Both the motor and visual disturbances described above affect motor performance in a similar way - they modify the relationship between the motor commands sent to the muscles, and the eventual outcome of the movement. The goal of the movement remains the same, however the motor commands required to achieve it are altered. However, this is not the only way in which motor performance may be disturbed. Another possibility is that the requirements for successful completion of the task may change, i.e. the desired outcome associated with a given stimulus might be liable to change.

In many circumstances, the stimulus and the desired outcome of a movement are essentially equivalent. For example, in the case of reaching, the stimulus corresponds to the location of an object in the visual field and the task is to move the hand to that same location. This remains true even when visual feedback is tampered with or when the dynamics of the arm change. However, there are numerous examples where this is not the case. The most common examples are target-shifting paradigms, in which the goal endpoint of a hand or eye movement is shifted mid-movement (McLaughlin, 1967; Magescas and Prablanc, 2006). In order to compensate for such perturbations with relying solely on visual feedback, subjects must adjust the motor commands that they execute in response to a given stimulus. However, the actual dynamics of the arm remain the same.

Another example where this kind of disturbance can arise is in the vestibulo-ocular reflex (VOR). In the VOR, vestibular signals containing information about the angular velocity of the head trigger a movement of the eyes to stabilize gaze. If the visual field is enlarged with lenses, the eyes must move faster for the same head angular velocity in order to stabilize gaze. However. the dynamics of the eye remain the same as before.

We will refer to this kind of disturbance as a *task disturbance*, since it amounts to a change in the relationship between the stimulus and the conditions for successful completion of the task. We will refer to the more conventional dynamic and visual disturbances as *plant disturbances* since they both affect the relationship between the motor commands and the resulting movement.

Though these examples are from laboratory situations, there are more natural circumstances in which task disturbances can occur. A sportsman preparing to catch or strike a moving ball must initiate his movement based on the state of the ball mid-flight, before it arrives in the position at which he will actually make contact. Should the dynamics of the ball (i.e. flight or bounce characteristics) change, future movements should be adjusted. This is another example of a *task disturbance* - i.e. a change in the relationship between the stimulus (the mid-flight state of the ball) and the desired outcome (the catching/striking location).

Again, it is important to be able to distinguish this kind of disturbance from plant disturbance. A task disturbance should be compensated for regardless of the effector being used. The learned compensation, however, should ideally not be generalized to other behaviours. For instance, changes in VOR behaviour caused by wearing magnifying lenses should not be generalized to other oculomotor behaviours such as smooth pursuit, whereas a similar compensation for changes in eye dynamics *should* be generalized.

1.3 Distinguishing between different kinds of disturbance

The previous sections introduced three important categories of sensorimotor disturbances. It is important to adapt in a manner appropriate to each particular disturbance. But if a given error could be the result of many potential disturbances, how is it possible to determine which was the true cause? One potential aid in solving this credit assignment problem is that although the visual consequences of different disturbances may be very similar in each case, the motor system receives additional cues about the state of its body from proprioceptive feedback - afferents from muscle stretch recep-

tors which provide information about the kinematic state of the arm. Under changes in dynamics, proprioception will be affected similarly to visual feedback - both will deviate from what was expected. However under visual disturbances, visual feedback will again be disturbed, but proprioceptive feedback will match expectations. This critical difference should enable the motor system to distinguish between visual and dynamic disturbances by comparing visual and proprioceptive feedback with predictions. In principle, errors due to task disturbances can similarly be distinguished since both visual and proprioceptive feedback will match expectations.

The models of motor adaptation we will discuss in Chapter 2 all rely on a single estimate of hand position. It is not clear exactly how these models should be extended to incorporate multiple modalities. The relative contributions of visual and proprioceptive feedback to motor adaptation are still not entirely understood. It is easy to isolate the contribution of proprioceptive information to adaptation by simply not giving visual feedback. Visual feedback is not necessary for adapting to dynamics disturbances (Franklin et al., 2007), although learning is slightly faster when visual feedback is additionally available, (Tong et al., 2002).

Isolating the contribution of vision by eliminating proprioceptive feedback is technically more difficult to achieve. Proprioceptive feedback can be partially masked by vibrating the tendons of agonist/antagonist muscle pairs (Bock et al., 2007). Pipereit et al. (2006) showed that learning of a 60°rotation of visual feedback was not affected by muscle vibration, but learning of a velocity-dependent force field was substantially slowed. An alternative means to determine the contribution of proprioception in motor adaptation is offered through 'deafferented' patients who have suffered loss of proprioceptive sensation. Ingram et al. (2000) demonstrated that one such patient was able to adapt to an increase in visual feedback gains, (i.e. a cursor which moved slightly further than the hand). Another deafferented patient was reported by (Bernier et al., 2006) to be able to show comparable performance to healthy control in a 30°visuo-rotation learning task. However, evidence from deafferented patients is difficult to interpret since these patients have typically developed highly specialized compensatory strategies to cope with their impairment, and thus may not tell us very much about adaptation in healthy subjects.

Collectively, however, the results from tendon vibration experiments and studies of deafferented patients appear to suggest that proprioception is only relevant during learning of dynamic perturbations, and that visual perturbations are learnt using visual feedback alone. Indeed, Krakauer et al. (1999) suggested that kinematics and dynamics

are learnt independently using visual and proprioceptive feedback, respectively. Their argument was supported by an experiment assessing the extent to which learnt visual and dynamic disturbances interfere with one another. They found that subjects who learnt a 30°clockwise visual rotation showed strong retention of learning the next day despite having performed a secondary dynamics adaptation task which required an opposing compensation. This secondary learning session, in which an inertial load was attached to the arm, occured immediately after exposure to the visual rotation, but was learned without visual feedback. The results imply that the representation of the kinematic and dynamic components of the compensation were entirely independent.

Though this result supports the idea that visual and dynamic disturbances are represented independently, and potentially trained by different modalities, subsequent studies have failed to corroborate this finding in more general settings. Tong et al. (2002) found that learning to compensate for a position-dependent force, instead of an inertial load, *did* interfere with recall of a previously learnt visual rotation. Adaptation to changes in dynamics is also accelerated when visual feedback is available, suggesting that it cannot be purely driven by proprioceptive feedback.

Adaptation to visual disturbances is known to be multifaceted, comprising both sensory and motor components - some of which may be liable to interference by subsequent adaptation even in the absence of visual feedback. Proprioception is also notoriously liable to drift when visual feedback is not available. Indeed visual feedback is largely believed to maintain proprioceptive calibration.

It is well known that humans integrate visual and proprioceptive information during state estimation in order to decrease the negative effects of sensory noise. Similar advantages might also be obtained if vision and proprioception were integrated during adaptation. In Chapter 4, we propose an alternative model of how vision and proprioception can be combined to optimally guide adaptation among multiple components. We apply the principles of Bayesian estimation to derive a learning rule which characterizes the optimal way to integrate visual and proprioceptive feedback to guide adaptation. Within this framework, we can also easily incorporate prior knowledge about the statistical properties of different kinds of disturbance, to reflect the fact that, e.g. proprioception drifts out of calibration much more often than vision. Our model gives rise to novel and surprising predictions which we tested experimentally. Details of the experimental methods and results are given in Chapter 5.

1.4 Overview of thesis

In Chapter 2 we review existing approaches to modelling human motor adaptation. In Chapter 3 we examine the implications of adapting to task vs plant disturbances. We show that these two kinds of disturbances give rise to different distal learning problems which have contrasting effects on learning within different adaptive control architectures (Haith and Vijayakumar, 2009, 2007).

In Chapter 4 we focus attention on the question of how information from multiple sensory modalities should be used to guide adaptation among multiple components. We begin by reviewing existing computational models of sensory integration and adaptation which we then extend to derive a Bayesian model of concurrent sensory and motor adaptation (Haith et al., 2008b,a). This model makes strong and novel predictions. Experiment which we carried out to test these predictions are described in Chapter 5.

Chapter 6 concludes the thesis, discussing the implications of our experimental results, the limitations of the models we have presented and the scope for extending the Bayesian framework in the future to account for other experimental phenomena.

Chapter 2

Modelling human motor adaptation

In this chapter, we review existing approaches to modelling human motor adaptation. We begin with the concept of internal models, reviewing the evidence for internal-model based control, and providing a sketch of how such internal models may be represented and learnt in the cerebellum. We then introduce the idea of state-space models as a way of linking the internal model framework to behavioural data. These adaptation rules have an appealing Bayesian interpretation in which subjects are assumed to adapt by *inferring* the properties of their bodies and the environment from noisy observations of the outcome of their movements. We review existing Bayesian models of motor adaptation, arguing that that it provides a powerful framework for modelling motor adaptation, particularly where there may be multiple different kinds of disturbance which may have caused the error.

2.1 Internal models

The dynamics of any moving system to be controlled, e.g. the arm, can be characterized by a differential equation linking the current state, θ_t (e.g. joint angles and velocities), and control signals, $\mathbf{u}_t$ (joint torques or muscle activations), to changes in the state:

$$\dot{\theta}_t = f(\theta_t, \mathbf{u}_t). \tag{2.1}$$

The system under control is often referred to as the *plant*. One way of controlling the arm is to plan some desired sequence of state changes $\dot{\theta}_t^*$, and select appropriate motor commands at each instant in order to execute this plan. In order to do this, it is necessary to invert Equation 2.1, representing the required motor command at each

instant as a function of the current state and the desired change in state:

$$\mathbf{u}_t = f^{-1}(\theta_t, \dot{\theta}_t^*). \tag{2.2}$$

It has been widely hypothesized that the brain explicitly represents these mappings through *internal models* - networks in the brain whose input/output functionality mirror the relationship between current states, desired states and control described by Equations 2.1 and 2.2 (Wolpert et al., 1998; Kawato, 1999). Forward models, representing Equation 2.1, can be used to obtain a rapid estimate of the state of the body following an issued motor command, without needing to rely on large delays in sensory feedback. Inverse models, representing Equation 2.2, can be used directly for control, offering a means to compute the necessary motor command to achieve a particular desired change in state $\dot{\theta}^*$. As the dynamics of our bodies change, these internal models adapt accordingly so that accurate motor commands can continue to be executed and accurate predictions about changes in limb state can continue to be made.

What is the evidence in favour of the internal model hypothesis? If a perturbing force field is applied to the hand, subjects initially exhibit large movement errors, but these errors gradually diminish with practice. If the force field is suddenly removed after the subject has adapted to it, movement errors are observed in the opposite direction to the initial ones in the force field (Shadmehr and Mussa-Ivaldi, 1994). These *aftereffects* imply that accurate movements in the force field are achieved by feedforward control, rather than simply increasing feedback gains, an effect which is certainly consistent with the idea that inverse models are used for control.

However, this effect could also occur due to memorization of the required motor commands to achieve the task. A prediction which is more specific to internal models concerns their flexibility. The same inverse dynamics model can be used for a variety of different tasks simply by changing the desired change in state, θ_t^*. Thus, if people do use such an inverse dynamics model for control, changes in dynamics learnt while performing one task should generalize to other tasks. Conditt et al. (1997) demonstrated that this is indeed the case. Subjects who adapted to a velocity-dependent force field while making a series of straight reaching movements were subsequently able to successfully execute a circular movement in the same force field. This generalization implies that a single dynamics model is shared across different tasks - strong evidence in favour of inverse models.

As well as forming inverse models of objects being controlled, it may be advantageous to learn a model of the forward dynamics of the arm (i.e. Equation 2.1). Pre-

dictions of a forward model can help to augment noisy sensory feedback to improve estimation of the current state, θ_t. Wolpert et al. (1995) demonstrated that subjects' estimates of hand position under the influence of perturbing forces are indeed biased by predictions of a forward model which has no knowledge of the perturbing forces. During saccades, where no sensory feedback is available at all, such a forward model may provide the only estimate of the current state (Chen-Harris et al., 2008) to an internal feedback controller or inverse model.

It should be noted that, more recently, the mathematical framework of *optimal feedback control* has been proposed as a theory of human motor coordination (Todorov and Jordan, 2002; Scott, 2004). Optimal feedback control models essentially propose that, rather than computing a planned sequence of state changes θ_t^* and selecting actions according to an inverse model as in Equation 2.2, actions are selected according to a more general movement policy which depends only on the current state, elapsed time t and the goal of the movement,

$$\mathbf{u}_t = \pi(\theta_t, t), \tag{2.3}$$

eliminating the need to separately represent a desired trajectory θ_t^*. Algorithms for computing such optimal policies typically rely on a known forward dynamics model (Todorov and Li, 2005). Trajectories of human subjects following adaptation reflect accurate knowledge of the new dynamics (Izawa et al., 2008). Exactly how optimal control policies may be represented and adapted in the brain, and indeed whether they are at all, is at present poorly understood.

In addition to forward and inverse dynamics models, internal models might represent any kind of functional relationship between variables such as a forward kinematics mapping between arm state in joint angle coordinates and hand state in an extrinsic coordinate frame. In fact, in this thesis, we argue that the brain represents multiple different kinds of internal models.

2.2 Computational models of motor adaptation

In general, we assume that an internal model attempts to approximate some function with input $\mathbf{x}$ and output y, with

$$y = f(\mathbf{x}). \tag{2.4}$$

Note that, for the time being, we suppress the temporal dependence on the inputs and outputs and assume that y is scalar. The case that y is multidimensional can be treated

as simply learning a different internal model for each dimension.

From a purely theoretical perspective, an effective way to represent such a function is via a linear combination of basis functions:

$$\begin{aligned} \hat{f}(\mathbf{x}) &= \Sigma_i w_i \psi_i(\mathbf{x}) \\ &= \mathbf{w}^T \psi(\mathbf{x}). \end{aligned} \tag{2.5}$$

This linear representation is flexible enough to represent a broad class of functions, provided a suitable set of basis functions ψ is chosen. A typical set of basis functions is a set Gaussian radial basis functions:

$$\psi_i(\mathbf{x}) = \exp\left\{ \frac{(\mathbf{x}-\mathbf{c}_i)^2}{2l^2} \right\} \tag{2.6}$$

having different centres $\mathbf{c}_i$. The linearity of Equation 2.5 in the parameters $\mathbf{w}$ ensures that, regardless of the nature of the basis functions ψ, learning the optimal parameters is always straightforward. Suppose we wish to minimize the mean squared estimation error

$$E = \frac{1}{2} \int \left(y - \hat{f}(\mathbf{x}) \right)^2 d\mathbf{x}. \tag{2.7}$$

As each new pair of input/output observations $(y, \mathbf{x})$ becomes available, we can improve our estimate by adjusting the parameters $\mathbf{w}$ by gradient descent,

$$\begin{aligned} \Delta w_i &= -\eta \, \tfrac{\partial}{\partial w_i} \, \tfrac{1}{2} \left(y - \hat{f}(\mathbf{x}) \right)^2 \\ &= -\eta \, \left(y - \hat{f}(\mathbf{x}) \right) \psi_i(\mathbf{x}) \\ &= -\eta \, \tilde{y} \, \psi_i(\mathbf{x}), \end{aligned} \tag{2.8}$$

where η is some arbitrary learning rate and $\tilde{y} \equiv y - \hat{f}(\mathbf{x})$ is the error in the internal model output. Thus, the appropriate adjustment to the combination weights is proportional to both the approximation error $\tilde{y}$ and the output of each basis function $\psi(\mathbf{x})$.

While the more simplistic generalized linear model approach to learning internal models described in the section is largely motivated by theoretical considerations, this kind of model also has an appealing neural interpretation, with y representing the firing rate of a particular neuron, $\mathbf{x}$ representing the firing rates of presynaptic neurons, and the parameters $\mathbf{w}$ representing the corresponding synaptic weights. In principle, more sophisticated nonlinear regression algorithms such as locally weighted learning methods (e.g. Vijayakumar et al. (2005)) can also be employed as more abstract models of internal model learning (Shibata and Schaal, 2001; Mitrovic et al., 2008).

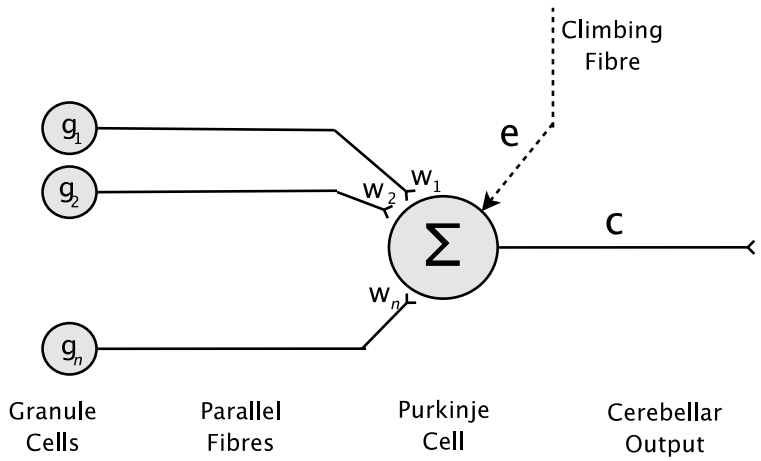

Figure 2.1: Schematic illustration of the Marr/Albus cerebellum model. Granule cell firing rates $g_{1:n}$ are combined linearly according the weights $w_{1:n}$ at the parallel fibre-Purkinje cell synapse, yielding cerebellar output c. Climbing fibre firing rate e signals error in c, which modulates synaptic plasticity.

2.2.1 Internal models in the cerebellum

Where exactly in the brain internal models are represented is not precisely known. Many brain regions contribute to the control of movement, however the cerebellum appears to be of particular importance for predictive control (Bastian, 2006). Damage to the cerebellum results in impairments in compensating for interaction torques between limb segments (Bastian et al., 1996), adapting to altered dynamics (Smith and Shadmehr, 2005; Rabe et al., 2009) and adapting to altered visual feedback (Rabe et al., 2009; Baizer et al., 1999). Iimaging studies of healthy subjects during have also revelaed heightened activity of the cerebellum during adaptation (Imamizu et al., 2000).

While the equations given above for representing and adapting internal models (Equations 2.5 and 2.8) were motivated by theoretical considerations, they correspond closely to models of cerebellar learning. A simplified schematic of the structure of the cerebellum is shown in Figure 2.1. The sole output pathway of the cerebellum comes via the axons of the Purkinje cells. The major input pathway arrives via granule cells, whose long axons travel in parallel lines along the surface of the cerebellar cortex, and are thus known as *parallel fibres*. These parallel fibres pass through the dendritic tree of the *Purkinje cells*, with which they form synapses. There are also numerous interneurons such as basket cells and stellate cells which we neglect for the sake of simplicity.

Mathematically, let us denote the parallel fibre input by $\mathbf{z}(t)$ and its output by $\mathbf{c}(t)$. In this model, the cerebellar output $\mathbf{c}(t) = C(\mathbf{z}(t))$ is given by a weighted sum of parallel fibre activities:

$$c_j(t) = \sum_i w_{ij} p_i(t), \tag{2.9}$$

where, $p_i(t)$ is the activity (i.e. firing rate) of the ith parallel fibre and w_{ij} is the strength of the synapse between the ith parallel fibre and the jth Purkinje cell. This can be written more compactly in vector notation as

$$\mathbf{c}(t) = \mathbf{W}^T \mathbf{p}(t). \tag{2.10}$$

Learning occurs through adaptation of the synaptic weights $\mathbf{W}$ over time.

The other major input to the cerebellar cortex arrives via the climbing fibres. These synapse directly onto the Purkinje cell. The sparse coverage of the climbing fibres (each Purkinje cell forms synapses with only one climbing fibre) and their relatively low firing rates ($\sim$ 1Hz) suggest that this input does not directly influence Purkinje cell activity in any significant way. Rather, the climbing fibres exert their influence by modulating synaptic plasticity between the parallel fibres and Purkinje cells.

A classical theory of cerebellar learning is the Marr-Albus-Ito theory (Marr, 1969; Ito, 2000). In this framework, climbing fibre activity is assumed to directly convey the error in the cerebellum's output. Despite having been around for some 40 years now, there is still considerable controversy surrounding this idea Simpson et al. (1996). In the VOR, the climbing fiber signal does indeed seem to relate to retinal slip (which constitutes an error signal in this case), though it is unclear exactly whether this error signal directly represents retinal slip or the error in outgoing motor commands (Wolpert et al., 1998; Yutaka Hirata and Highstein, 2004). In other behaviours, it is not so clear. During reaching, for instance, the climbing fibre signal does contain some error information, but also information about destinations of movements Kitazawa et al. (1998). It is still not clear exactly what information in general is represented in climbing fibres, however it appears that performance or prediction errors are strongly reflected in the pattern of climbing fibre activity. For the purposes of this thesis, we assume that the firing rate of climbing fibres encodes some transformed version of the error in task performance (e.g. in sensory or motor coordinates).

If the climbing fibre signal is taken to be equal to the error in the cerebellar output, then the learning rule of Equation 2.12 is, in fact, a reasonable approximation to the true plasticity laws at the Purkinje cell-parallel fibre synapses (Fujita, 1982). We

therefore assume that the error in the cerebellar output is equal to

$$\mathbf{e}_t = \mathbf{c}_t^* - \mathbf{c}_t. \tag{2.11}$$

The synaptic plasticity rule becomes

$$\Delta \mathbf{W} = \mathbf{p}(t)^T \mathbf{e}(t). \tag{2.12}$$

In reality, negative errors are not possible, however the 'firing rates' in this rule can be interpreted as deviations from some baseline firing rate. An alternative possibility is that different cells code for positive and negative errors.

In summary, there is strong evidence that internal models are represented at least partially in the cerebellum, and that these internal models are learnt and adapted in an error-driven fashion. We adopt the learning rule given by Equation 2.8 as a model of error-driven learning in the cerebellum due to its biological plausibility, mathematical simplicity and flexibility.

Equation 2.11 states that the climbing fibre signal should be equal to the error in the cerebellar output. The nature of this error depends on the particular role of the cerebellum in control. Furthermore, this error may not be precisely known, since all that can be measured by the subject is the sensory consequence of this error. This leads to a so-called *distal learning problem*. In Chapter 3 we describe two alternative models of how internal models learnt in the cerebellum can be used for control. In one model, the cerebellum learns a forward model, while in the other, the cerebellum learns an inverse model. We will examine the impact of the distal learning problem in these two models under different types of sensorimotor disturbance.

2.3 From continuous to discrete descriptions of internal models

The previous section offers one sketch of how internal models might be represented and adapted in the brain. In practice, however, it has proved very difficult to test such models based on neurophysiological data. However, changes in an internal model may be difficult to isolate at the neurophysiological level, they do lead directly to readily measurable behavioural consequences. Thoroughman and Shadmehr (2000) and later Donchin et al. (2003) proposed that subjects adapt to an external perturbing force field by building an internal model of the external force as a function of hand velocity.

Behaviouarally, subjects' feedforward control patterns are most easily quantified by measuring the directional error in the initial part of their hand trajectories (before the influence of feedback control kicks in). As shown by Donchin et al. (2003), this scalar measure of performance error can be related to the subject's internal model by averaging actual and predicted forces over the duration of a movement, yielding scalar estimates f and $\hat{f}$ of the force field and the subject's estimate of it respectively. The hand position error is then given by

$$\tilde{y}_n = D(f_n - \hat{f}_n) + \varepsilon_n, \tag{2.13}$$

where D is a stiffness coefficient transforming forces into hand positions and ε is motor execution noise. Representing the force field and internal model as functions of a whole movement rather than functions of state enables a compact representation of the state of learning, while retaining the most behaviourally-relevant aspects of the internal model, and greatly simplifies the analysis of behavioural data.

Crucially, if the internal model is represented and adapted as a generalized linear model with a gradient descent learning rule as in Equation 2.8, then this scalar representation of the internal model will also be linear in the error. Consequently, the *change* in the subject's reaching performance from trial to trial will also depend linearly on the error in the previous trial, but *not* on the underlying parameters $\mathbf{w}$. The update to the internal model is given by

$$\hat{f}_{n+1} = A\hat{f}_n + B\tilde{y}_n, \tag{2.14}$$

where, B is the rate of learning and A is a forgetting factor describing how quickly the prediction of the internal model decays back to zero over trials. This model predicts a series of hand position errors y_n, which are generated according to, and in turn modify, the state of the internal model $\hat{f}_n$. These state-space models yield very close agreement with subject data even in random force fields (Donchin et al., 2003).

As presented here, this system describes adaptation of reaches to a single target. Extensions to multiple targets are also possible, in which case f and $\hat{f}$ become vectors describing the true dynamics and the internal model of the dynamics along the different target directions. B becomes a vector describing how learning in the current direction is generalized to other directions. The pattern of this generalization can also be learnt from data.

In theory, the nature of generalization depends strongly on the shape of the basis functions in the representation of the underlying internal model. Ideally, we would

like to find out about the underlying basis functions from the parameters of the state-space model. However, while it is relatively straightforward to go from continuous to discrete descriptions of internal models, attempting to reverse engineer a neural representation of an internal model from a state-space model is much more difficult. Though attempts have been made (Donchin et al., 2003), in general it is not possible without making very strong prior assumptions about the form of the basis functions, since many different kinds of representations can give rise to identical behaviour.

State space models have emerged as a valuable tool for characterizing and quantifying motor adaptation (Cheng and Sabes, 2006, 2007). However, while the behaviour predicted by a state-space model may be consistent with an underlying internal model-based representation, a good state space model fit does not necessarily imply the existence of such an underlying representation. In this sense, the state-space model approach may be considered more phenomenological in spirit than the more connectionist approach described in the previous section.

There may be other very good reasons why human adaptive behaviour is well-described by the state-space approach. As we describe in the next Section, the kind of error-driven adaptation rules emerging from these models may in fact be the *optimal* way to adapt based on behavioural-level considerations rather than low-level neurological detail.

2.4 Bayesian models of motor adaptation

One difficulty with the models of adaptation presented above is that the learning rate η in Equation 2.8 appears to be entirely arbitrary. We can easily estimate this parameter by fitting the model to data, but it is not clear from the models why adaptation occurs at the rate it does. Even the choice of gradient descent updates in the first place was entirely arbitrary. In principle, one-shot learning might even be possible, i.e. subjects should be able to adapt to a step change in the environment given a single observation of their errors. The fact that learning does seem to be well-described by a more incremental gradient-descent rule could perhaps be due to biological constraints at the synaptic level. A more plausible explanation, however, is that the error signal used for adaptation is unreliable, and therefore a more cautious approach is adopted when updating the parameters. A one-shot learning strategy or large learning rate would be liable to suffer from severe fluctuations in performance due to adaptation to the noise rather than any true change in the dynamics. On the other hand, too slow a learn-

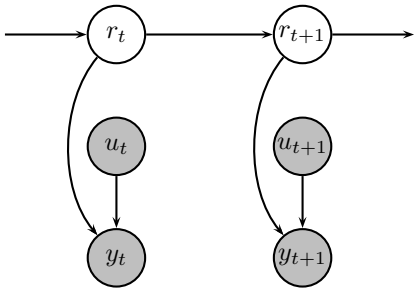

Figure 2.2: Basic 1-dimensional Kalman filter model. On trial t, hand position y_t depends noisily on motor command u_t and an unknown disturbance r_t. In addition, the disturbance r is assumed to vary smoothly, but randomly between trials.

ing rate would lead to more stable adaptation but might be unnecessarily slow if the environment is changing relatively rapidly. A balance must be achieved.

This intuition about appropriate learning rates can be formalized through a Bayesian approach to modelling motor adaptation, an idea first proposed by Korenberg and Ghahramani (2002). The key idea behind the Bayesian approach is that, rather than following a gradient descent learing rule with an arbitrarily chosen learning rate, we view the subjects as attempting to *infer* the disturbances based on his observations. We consider a probabilistic *generative model* of the outcome of a series of reaching movements, i.e. a model which gives us the full probability distribution of both disturbances and resulting hand positions. We assume that the relationship between final hand position y_t and motor command u_t is given by

$$y_t = u_t + r_t + \varepsilon_t, \tag{2.15}$$

where $\varepsilon_t \sim N(0, \sigma^2)$ represents the combined effects of motor execution noise and observation noise, and r_t is the average effect of an external force over the duration of the movement, analogous to f_n in the state space model in Equation 2.13. We also assume that the disturbance r_t is itself liable to fluctuate randomly from trial to trial according to

$$r_{t+1} = r_t + \xi_t, \tag{2.16}$$

where $\xi_t \sim N(0, Q)$. This generative model is illustrated in Figure 2.2.

The subject maintains an estimate of the disturbance on each trial as a probability distribution over possible disturbances. We assume that, after trial $t-1$, the subject's belief is described by a Gaussian with mean $\hat{r}_{t-1|t-1}$ and variance (i.e. uncertainty)

$P_{t-1|t-1}$, i.e.

$$p(r_{t-1}|u_{t-1},y_{t-1}) \sim N(\hat{r}_{t-1|t-1}, P_{t-1|t-1}). \tag{2.17}$$

The subscripted $t-1|t-1$ indicates that this is the estimate of r_{t-1} given observations from trials up to *and including* trial $t-1$.

Before the start of the next trail, the subject must predict what the disturbance will be. He should do so according to his statistical model of how the disturbances vary over time, i.e. Equation 2.16. The appropriate updates to the subject's estimates are found by considering the joint probability of r_{t-1} and r_t and marginalizing over possible values of r_{t-1}:

$$p(r_t|u_{t-1},y_{t-1}) = \int p(r_t|r_{t-1},u_{t-1},y_{t-1})p(r_{t-1}|u_{t-1},y_{t-1})dr_{t-1}. \tag{2.18}$$

This leads to a Gaussian prior over the disturbance on trial t,

$$p(r_t) \sim N(A\hat{r}_{t-1|t-1}, P_{t-1|t-1}+Q), \tag{2.19}$$

where we have suppressed the conditioning on observations in previous trials. We write the prior mean as

$$\hat{r}_{t|t-1} = A\hat{r}_{t-1|t-1} \tag{2.20}$$

and the prior variance

$$P_{t|t-1} = P_{t-1|t-1} + Q. \tag{2.21}$$

The subscripted $t|t-1$ indicates that this is the estimate of r_t given observations from trials up to $t-1$, but *not* trial t.

The subject selects his movement on each trial according to the desired hand position y^* and the predicted disturbance so that

$$\mathbb{E}[y_t] = y_t^*, \tag{2.22}$$

which is achieved by selecting

$$u_t = y_t^* - \hat{r}_{t|t-1}. \tag{2.23}$$

As new observations become available, the subject updates his estimates according to Bayes' rule:

$$p(r_t|y_t,u_t) = \frac{p(y_t|r_t,u_t)p(r_t)}{p(y_t|u_t)}. \tag{2.24}$$

The prior $p(r_t)$ is as described above [1]. The *likelihood* $p(y_t|r_t,u_t)$ is given directly by Equation 2.15. $p(y_t|u_t)$ is just a normalizing constant which doesn't depend on r_t

[1] Note that in the general statement of Bayes rule this should be $p(r_t|u_t)$, however we assume that the disturbance r_t does not depend on the motor command u_t and so is equal to $p(r_t)$

and can be ignored, since we are dealing with Gaussians which are easy to normalize anyway. We can then calculate the posterior: The *posterior*, $p(r_t|y_t,u_t)$ is therefore given by

$$\begin{aligned} p(r_t|y_t,u_t) &\propto p(y_t|r_t,u_t)p(r_t) \\ &\propto \exp\left\{-\frac{1}{2}\left[\frac{(r_t-(y_t-u_t))^2}{\sigma^2}+\frac{(r_t-\hat{r}_{t|t-1})^2}{P_{t|t-1}}\right]\right\} \\ &\propto \exp\left\{-\frac{1}{2}\frac{\left[r_t-w_y(y_t-u_t)-(1-w_y)\hat{r}_{t|t-1}\right]^2}{w_y(1-w_y)}\right\}, \end{aligned} \tag{2.25}$$

where $w_y = \frac{P_{t|t-1}}{\sigma^2+P_{t|t-1}}$.

Equation 2.25 describes a Gaussian probability distribution over r_t with mean [2]

$$\hat{r}_{t|t} = w_y(y_t-u_t)+(1-w_y)\hat{r}_{t|t-1} \tag{2.26}$$

$$= \hat{r}_{t|t-1}+w_y(r_t+\varepsilon_t-\hat{r}_{t|t-1}) \tag{2.27}$$

and variance $P_{t|t} = w_y(1-w_y) = \frac{\sigma^2 P_{t|t-1}}{\sigma^2+P_{t|t-1}}$. The subscript $t|t$ indicates that these parameters relate to the estimate of r_t given observations up to *and including* time t. Throughout this thesis, wherever we write just $\hat{r}_t$ in the context of a Bayesian adaptation model - typically for clearer comparison with other, non-Bayesian models - we refer to the prior estimate $\hat{r}_{t|t-1}$ since this is the estimate which is used for selecting the motor command u_t.

This Bayesian adaptation model we have derived here is essentially a 1-dimensional Kalman filter. Note that the update to the mean of the disturbance estimate is linear in the observed error, much like the state-space models described earlier. Indeed, as long as the variance of the execution noise σ^2 remains constant, the Kalman gain will converge to a constant given enough trials, making it even more similar to a state-space model.

Note the resemblance of the update between the prior and the posterior given in Equation 2.27 and the gradient descent learning rule given in Equation 2.8. Neglecting the noise term ε_t (i.e. concentrating on the *expected* update), both updates are linear in the error in estimating the disturbance r_t. One key difference between the Bayesian model and a state-space model is that, in the Bayesian model, the adaptation rate is determined by the noise structure of the underlying model, rather than being an open parameter. Specifically, the adaptation rate depends on the observation noise σ^2 and the variability of the disturbance, Q. The Bayesian model predicts that if either of these

[2] Note the similarity between Equation 2.27 and the cue combination procedure described later in Section 4.1. One way of interpreting the inference is as a cue combination procedure, with the prior acting as one 'cue' and the observation another.

change, the rate of adaptation will change in a predictable way. Burge et al. (2008) tested this idea in a visuomotor adaptation paradigm in which a cursor representing hand position was artificially shifted. The observation uncertainty σ^2 was manipulated by blurring a cursor representing hand position. The disturbance variability was manipulating by randomly changing the disturbance from trial to trial with different levels of variability Q for different subject groups. In both cases, subjects' adaptation rates changed in accordance with the predictions of the Bayesian model, with learning slower for more blurry targets and faster for more variable disturbances. [3]

2.4.1 More general Bayesian models

The model presented in the previous section is highly simplified. However it represents the key aspects of the Bayesian approach to modelling motor adaptation. It would not be exaggerating to say that all Bayesian models in some sense amount to variations on the generative model illustrated in Figure 2.2. Where individual models differ is in the specific details of their generative models: the number of unknown disturbances, the number and nature of the observations, the structure of the conditional dependencies between disturbances and observations and between disturbances on different trials. Regardless of the nature of this generative model, taken together with an appropriate criterion for selecting the motor command u_t on each trial, the properties of the generative model specify a model of human motor adaptation through the normative principle that subjects adapt by optimally inferring the disturbances, given their observations.

Whenever the generative model is linear, with Gaussian noise, the inference of the disturbances corresponds to a Kalman filter. In general, there will be a vector of disturbances $\mathbf{r}_t$, which vary from trial to trial according to

$$\mathbf{r}_{t+1} = A_t \mathbf{r}_t + \xi_t, \tag{2.28}$$

with $\xi_t \sim N(0, Q_t)$. There will also be a vector of observations $\mathbf{z}_t$, which depend linearly on the disturbances via

$$\mathbf{z}_t = H_t \mathbf{r}_t + \varepsilon_t, \tag{2.29}$$

with $\varepsilon_t \sim N(0, R_t)$. H is called the *observation matrix*. The motor command $\mathbf{u}_t$ will affect either in the observation $\mathbf{z}_t$ or in the observation matrix H_t, or both.

[3] It is worth noting that the fact that subjects were able to actually *learn* the change in disturbance variability is not predicted by the model, which proposes that subjects assume that this variability is constant.

As before, the subject maintains an estimate of the disturbance after each trial

$$p(\mathbf{r}_{t-1}|\mathbf{z}_{t-1}) \sim N(\hat{\mathbf{r}}_{t-1|t-1}, P_{t-1|t-1}). \tag{2.30}$$

In the prediciton step of the Kalman filter, the subject forms a prediction about trial t based on the posterior from trial $t-1$:

$$\hat{\mathbf{r}}_{t|t-1} = A_t \hat{\mathbf{r}}_{t-1|t-1} \tag{2.31}$$

$$P_{t|t-1} = A_t^T P_{t-1|t-1} A_t + Q_t. \tag{2.32}$$

After trial t, the subject updates his prior estimate to a posterior:

$$K_t = P_{t|t-1} H_t^T \left(H_t P_{t|t-1} H_t^T + R_t\right)^{-1} \tag{2.33}$$

$$\hat{\mathbf{r}}_{t|t} = \hat{\mathbf{r}}_{t|t-1} + K_t \left(\mathbf{z}_t - H_t \hat{\mathbf{r}}_{t|t-1}\right) \tag{2.34}$$

$$P_{t|t} = (I - K_t H_t) P_{t|t-1}. \tag{2.35}$$

There are two key things worth noting about these update equations: i) The update to the mean is always linear in the prediction error, i.e.

$$\hat{\mathbf{r}}_{t|t} = \hat{\mathbf{r}}_{t|t-1} + K_t(H\mathbf{r}_t + \boldsymbol{\varepsilon} - \hat{\mathbf{r}}_{t|t-1}). \tag{2.36}$$

ii) If the matrices A_t, H_t, Q_t and R_t remain constant, then the update matrix K_t (often referred to as the Kalman gain) converges to a constant over time, as does the uncertainty $P_{t|t}$. Simulations of human motor adaptation according to this model also typically include an initialization phase to allow the Kalman gain and uncertainty to converge to appropriate values, to eliminate any dependence on the arbitrarily-chosen prior uncertainty $P_{1|0}$.

All of the models we consider in this thesis are linear and Gaussian and the inference can therefore be solved by these equations. In cases where there are nonlinear relationships between variables or non-Gaussian random variables involved, there is a wealth of literature on appropriate methods for calculating the posterior disturbance estimates. The general problem of inferring a dynamic latent variable online given a sequence of previous observations is referred to in the statistics and machine learning literature as *filtering*. Nonlinear dynamics can be handled by extensions to the Kalman filter - the extended Kalman filter or unscented Kalman filter. In general, sampling-based methods such as the particle filter can provide an arbitrarily good approximation to the exact posterior, though the computational complexity may be high.

2.4.2 Previous Bayesian models of motor adaptation

As we noted in the previous section, the Bayesian framework can lead to equivalent predictions to those given by state-space models when the generative model is *stationary*, i.e. when the parameters A, Q, H and R are fixed. For non-stationary models, however, the Bayesian modelling framework makes very strong predictions about how adaptation will proceed.

Returning to a simple example with a one-dimensional disturbance r_t and a one-dimensional observation z_t, suppose the observation z_t is unavailable for a few trials, for instance while performing saccades in the dark, how will this affect the estimate of the disturbance r_t and subsequent learning? Formally, this can be modelled by setting the observation uncertainty R to infinity. Note that this is different from setting the observation mapping H to 0. The consequence of this in terms of the updates is that the Kalman gain K_t becomes zero (from Equation 2.33), therefore the posterior mean and uncertainty remain the same as the prior (Equations 2.34 and 2.35).

The only changes to the disturbance estimate over time come from the prediction updates in (Equations 2.31 and 2.32). The disturbance mean $\hat{r}_t$ is multiplied by A. Since A is typically a number just less than 1, this corresponds to a gradual 'forgetting' of the disturbance over time. The disturbance uncertainty P_t increases on each trial by Q, though the multiplication by A means that the variance is bounded as the number of blind trials tends to infinity. The consequence of this increase in uncertainty is that the rate of learning will be much faster once the observation is restored. Effectively, the weight on the prior in Equation 2.26 is reduced. So the Bayesian framework makes two specific predictions about what will happen if a subject is deprived of sensory feedback - firstly, that there will be some forgetting of the disturbance and secondly, that the rate of adaptation when feedback is restored will be faster.

Körding et al. (2007b) proposed a Bayesian model of saccade adaptation supported by the fact that both of these phenomena are exhibited in saccade adaptation in monkeys (based on data from (Kojima et al., 2004)). Their model is illustrated in Figure 2.3. The model of Körding et al. also contained multiple disturbance components with different timescales and variabilites, i.e. A and Q were diagonal 30×30 matrices.The intuition behind these multiple components is that different sources of error have different characteristic timescales, e.g. illness and fatigue. In terms of the data, these multiple components with different timescales can account for changes in adaptation rate during repeated gain-up/gain-down training, also know as *savings*, even when vi-

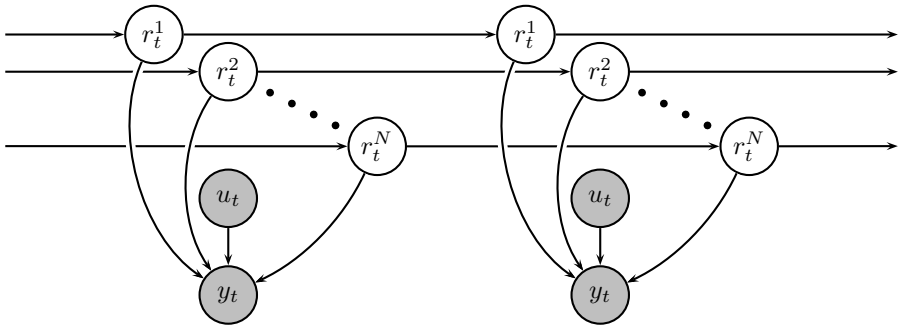

Figure 2.3: Bayesian saccade adaptation model with multiple timescales proposed in (Körding et al., 2007b). Eye position y_t depends on motor command u_t and multiple unknown disturbances $r_{1:n}$. Each disturbance is assumed to have different timescale of decay and random variability between trials.

sual feedback is not removed. Note, however, that the ability of the model to account for savings, and the ability to predict forgetting when sensory feedback is deprived, do not depend on any Bayesian assumptions. A similar state-space model makes identical predictions (Smith et al., 2006). The key insight from the Bayesian model is that prolonged sensory deprivation will lead to an increase in uncertainty, which will then lead to more rapid adaptation.

The experiments on saccade adaptation were limited to extended blocks of either full sensory feedback of performance or blocks of total darkness. The study by Burge et al. (2008) also held visual feedback quality fixed for extended blocks at a time. It is possible that these changes in adaptation rate occurred gradually over the course of the block. The Bayesian model, however, predicts that the rate of adaptation will be continually adjusted from one trial to the next, rather than just across blocks. Wei and Körding (2008) investigated the potential of the Kalman filter model to account for human behaviour under these conditions by presenting subjects with a cluster of cursors which were either very close (high feedback certainty), or spread out (low feedback certainty). They found that, although the predictions of the Kalman filter model did not match human behaviour exactly, the rate of learning on individual trials did depend strongly on the quality of feedback on each individual trial.

Besides changes in the quality of observations, there may also be changes in the form of the observations, i.e. in the observation matrix H. Krakauer et al. (2006) proposed a model of motor adaptation under switching contexts in which two different contexts c_1 and c_2 were modelled by different observation matrices H_1 and H_2.

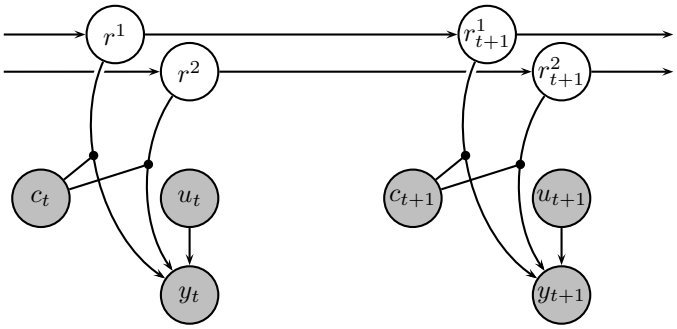

Figure 2.4: Bayesian model of adaptation under switching contexts proposed in (Krakauer et al., 2006). Hand position y_t depends on motor command u_t and two unknown disturbances r^1 and r^2. However, the context c determines exactly how the disturbances influence the hand position.

The strength of the model in explaining the data depends crucially on the way uncertainty is handled in the Kalman filter model. The specific setting for their model was adaptation of reaching movements to a rotation of visual feedback. The two contexts corresponded to movement of the hand using either only the wrist or only the shoulder. Again, the performance on each trial is modelled as a single observation y_t, corresponding to the initial directional error of the cursor. According to the model, the subject assumes that the disturbance may be related to either hand movement, or arm movement or possibly both. Thus there are two latent disturbance components to be estimated: $\mathbf{r} = \left(r^{\text{hand}}, r^{\text{arm}}\right)$. The subject believes that these vary over time according to the usual state dynamics given in Equation 2.16.

If only the wrist is being moved, then the cursor position is given by $y_t = u_t + r^{\text{hand}}$. If the arm is also moving, then the cursor position is given by $y_t = u_t + r^{\text{hand}} + r^{\text{arm}}$. More succinctly, this can be written in terms of two different observation matrices, $H_1 = (1,\ 1)$ and $H_2 = (1,\ 0)$. The model is illustrated in Figure 2.4 This model is able to account qualitatively for a wide variety of phenomena observed experimentally - particularly the fact that learning was transferred from the arm to the wrist but not from the wrist to the arm. After optimizing the open parameters in the model, the model was able to provide a good quantitative fit to the average subject performance.

Finally, Berniker and Körding (2008) considered the problem of credit assignment between intrinsic and extrinsic sources of error. Intrinsic sources of error correspond to changes in arm dynamics due to e.g. fatigue, injury etc. Extrinsic sources of error correspond to external perturbations from the environment or a tool being used. They

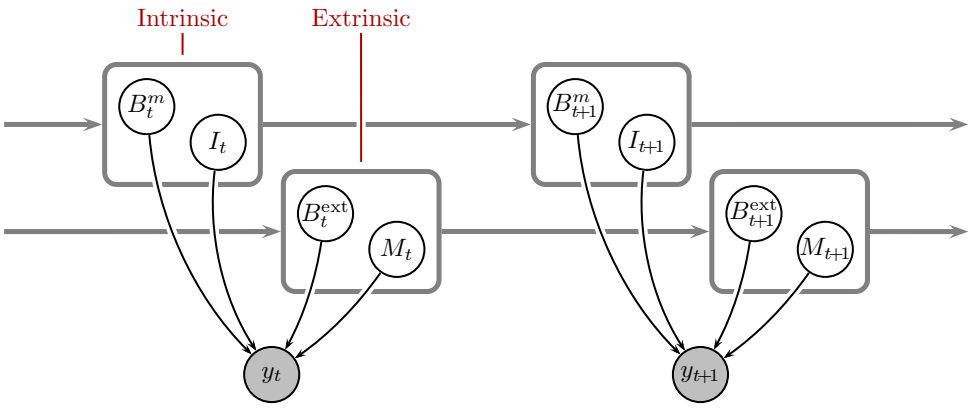

Figure 2.5: Graphical model illustration of model from (Berniker and Körding, 2008). A variety of parameters influence the hand position. Some parameters relate to the body (intrinsic), e.g. arm inertia I, joint viscosity B^m, while others relate to the world (extrinsic), e.g. object inertia M, object viscosity B^{ext}.

hypothesized that the intrinsic components of adaptation would generalize to the other arm, while the intrinsic components would not.

Unlike in the previous models, adaptation took place *within* trials, with variables updated six times during each movement. The model is illustrated in Figure 2.5. The dynamics of the arm are modelled as

$$I(\mathbf{q})\ddot{\mathbf{q}} + C(\mathbf{q},\dot{\mathbf{q}})\dot{\mathbf{q}} + B_m\dot{\mathbf{q}} + K_m\mathbf{q} = \tau_{\text{motor}} + \tau_{\text{world}} + \tau_{\text{noise}}. \tag{2.37}$$

The authors assume that the subject approximates the inertia matrix $I(\mathbf{q})$, a matrix-valued function of limb posture $\mathbf{q}$, with a single matrix $\hat{I}$ which does not depend on $\mathbf{q}$. Similarly the Coriolis matrix-valued function $C(\mathbf{q},\dot{\mathbf{q}})$ is approximated by a single matrix $\hat{C}$. They give little justification for this approximation. During the course of a reaching movement, the inertia of the arm is likely to vary substantially, although across many trials, the inferred value would likely fluctuate around the mean value over the six time-steps sampled per trial.

2.5 Summary

In summary, the notion of internal models has proven to be a very succesful framework for accounting for patterns of human motor adaptation - formulated either in terms of a continuous function describing the dynamics of the body in detail, or as a finite-dimensional state-space representation which is more convenient for comparison with experimental data.

Human motor adaptation appears to be well-described by a gradient-descent learning rule on the parameters of the internal model. An alternative interpretation of this adaptation is that subjects attempt to *infer* the properties of their bodies and environments given noisy observations of their performance. This Bayesian view of motor adaptation gives rise to a richer model in which uncertainty about properties of the world also plays a prominent role in adaptive behaviour. Several experiments have now demonstrated that human behaviour at least partially reflects uncertainty in internal model learning as predicted by the Bayesian model.

The Bayesian framework provides a principled means to determine the rate of adaptation, and also a principled means to determine the assignment of credit among multiple potential sources of error. All of the generative models presented in the previous section contained multiple disturbances which are assumed to represented as distinct components of adaptation. In all of these cases, the credit assignment problem is solved by applying prior knowledge about the statistics of the disturbances and the way in which they affect performance, which are captured in the generative model.

All of these models contain only a single observation of performance. As we argued in Section 1.3, exploiting information from multiple different modalities - in particular vision and proprioception - is likely to be of critical importance in determining the true cause of an error among multiple potential sources. In Chapter 4 we propose a Bayesian model of motor adaptation in which both visual and proprioceptive observations of performance are available, and in which multiple different kinds of disturbance affect these observations in different ways. This model makes strong predictions about how humans will adapt, which we test experimentally in Chapter 5.

Chapter 3

Distal learning in cerebellar-based motor adaptation models

In this chapter, we examine the computational challenges associated with adaptation to both task and plant disturbances. We examine two alternative models of cerebellar-based motor adaptation - one based on a feedforward architecture and one based on a recurrent architecture. We show how both models face a *distal learning problem* in which the relationship between observed performance errors and errors in internal model output is not known precisely. The nature of the two different distal learning problems is related to the distinction between task and plant disturbances. We examine the implications for behaviour both theoretically and through simulations of the vestibulo-ocular reflex, saccades and reaching, and consider possible solutions to overcome the distal error problem.

3.1 Task vs plant disturbances

In general, a motor control task involves generating appropriate motor commands in response to some stimulus to bring about a desired outcome. There are two fundamental types of change which can alter what the appropriate motor commands are in response to a given stimulus (see Figure 3.1). Firstly, the relationship between the motor commands and the resulting outcome can be altered. This typically involves changes in the motor plant dynamics (e.g. through injury, disease, growth or ageing); however some changes which are more kinematic in nature, such as distortions of visual feedback, can also be grouped into this category. We will refer to disturbances of this kind as *motor disturbances*.

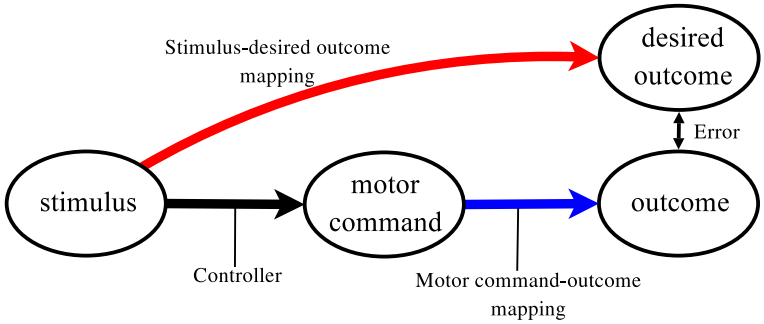

Figure 3.1: Illustration of task vs motor adaptation. Task adaptation is compensation for changes in the mapping between stimulus and desired outcome. Motor adaptation is compensation for changes in the mapping between motor command and actual outcome.

A second kind of change is in the relationship between the initial stimulus and the desired outcome following that stimulus. This kind of change is more subtle than the previous one but examples do occur in the context of most motor behaviours - either naturally or under experimental conditions. After such a change, the original response to the stimulus will no longer be appropriate and a new pattern of responses must be learnt. We refer to these kinds of disturbance as *task disturbances*.

In many circumstances, the stimulus and the desired outcome can be considered to be equivalent. For example, in the case of reaching, the stimulus is the location of an object in the visual field and the task is to move the hand to that same location (note that this is true even when visual feedback is tampered with). Nevertheless, there are numerous examples where the stimulus-desired outcome relationship is not so trivial and subject to change. As we will describe in later sections, many common experimental paradigms in oculomotor adaptation actually fall into the latter category rather than the former. Adaptation to these kinds of changes can also be induced in reaching tasks (Lurito et al., 1991; Magescas and Prablanc, 2006) where they are sometimes referred to as ‘non-standard mappings’ or ‘transformational mappings’ (Shadmehr and Wise, 2005).

We examine the problem of adapting to both kinds of disturbance within two alternative cerebellar-based adaptive control architectures based on the kinds of error-driven learning models introduced in the previous chapter. Before going into the details of the different architectures, we will first illustrate the discussion with a concrete example in which both kinds of sensorimotor change occur naturally - the vestibulo-ocular reflex (VOR).

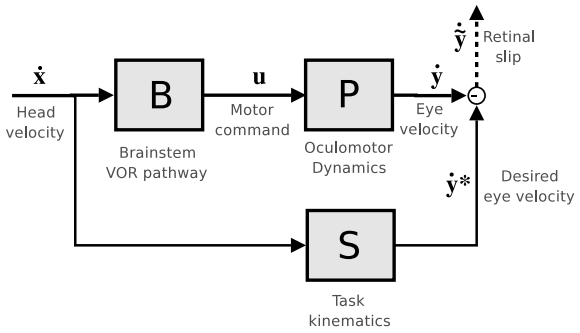

Figure 3.2: Schematic of the VOR.

3.1.1 Kinematics and Dynamics of the VOR

The vestibulo-ocular reflex in mammals acts to stabilize gaze during head rotations by counter-rotating the eyes. The characteristics of this reflex are not fixed, but can be modified through experience in response to changes in conditions which lead to a reduction in performance. After a suitable amount of training under these new conditions, the VOR becomes recalibrated so that even in the dark, the response of the VOR is altered (Boyden et al., 2004).

For illustrative purposes, and since the oculomotor plant is known to have negligible inertia (Robinson, 1964), we consider a first-order dynamics model of the oculomotor plant. We denote the current eye position by $\mathbf{y}$. The relationship between the motor command $\mathbf{u}$ and the resulting eye velocity $\dot{\mathbf{y}}$ (see Figure 3.2) is determined by the forward dynamics of the oculomotor plant,

$$\dot{\mathbf{y}} = P(\mathbf{y}, \mathbf{u}). \tag{3.1}$$

The inverse dynamics model is correspondingly defined as

$$\mathbf{u} = P^{-1}(\mathbf{y}, \dot{\mathbf{y}}^*). \tag{3.2}$$

The inverse dynamics P^{-1} map the current eye position $\mathbf{y}$ and desired eye velocity $\dot{\mathbf{y}}$ to a motor command $\mathbf{u}$ which would achieve that eye velocity when acting through the plant.

The desired outcome in this case is that the gaze be stabilized, i.e. that the eye velocity $\dot{\mathbf{y}}$ be equal to some gaze-stabilizing eye velocity $\dot{\mathbf{y}}^*$. Any deviations of eye velocity from this desired value will be perceived as retinal slip - movement of the visual image across the retina. We denote this retinal slip by $\dot{\tilde{\mathbf{y}}}$ and it is given by

$$\dot{\tilde{\mathbf{y}}} = \dot{\mathbf{y}}^* - \dot{\mathbf{y}}. \tag{3.3}$$

In most VOR models, desired eye velocity is taken as equal and opposite to head velocity, i.e. $\dot{\mathbf{y}}^* = -\dot{\mathbf{x}}$. However, in general this is not the case. Most VOR gain adaptation experiments work by directly manipulating the relationship between head velocity and desired eye velocity, not by changing the properties of the oculomotor plant. This includes any experiment using prisms or lenses and vestibular mismatch experiments in which an external visual stimulus is moved concurrently with head movements to alter the gaze-stabilizing eye velocity required for a given head velocity. If the stimulus is moved in phase with head movements, this achieves a change in the gain of the required response.

VOR adaptation therefore cannot be regarded as simply a process of learning the relationship between motor commands and resulting movement of the oculomotor plant. Fundamental to VOR adaptation is that the kinematic relationship between the stimulus (vestibular signal, indicating head velocity) and the desired outcome (gaze-stabilizing eye velocity) is also subject to change and must be compensated for, as illustrated in Figure 3.2. As well as the experimental manipulations described above, this kinematic component also encompasses more natural disturbances such as off-axis effects (Coenen and Sejnowski, 1996) and inaccuracies or nonlinearities in the relationship between the vestibular signal and the true head velocity $\dot{\mathbf{x}}$. VOR adaptation must, either explicitly or implicitly, reflect learning of this relationship as well as of the plant dynamics.

Mathematically, we can describe this relationship as a function mapping head velocity $\dot{\mathbf{x}}$ and current eye position $\mathbf{y}$ to a desired eye velocity $\dot{\mathbf{y}}^*$,

$$\dot{\mathbf{y}}^* = S(\mathbf{y}, \dot{\mathbf{x}}) \tag{3.4}$$

and a corresponding inverse mapping

$$\dot{\mathbf{x}}' = S^{-1}(\mathbf{y}, \dot{\mathbf{y}}). \tag{3.5}$$

This *task* mapping S relates the current head velocity $\dot{\mathbf{x}}$ to an appropriate gaze-stabilizing eye velocity $\dot{\mathbf{y}}$, while S^{-1} gives the head rotation $\dot{\mathbf{x}}'$ that would have required an eye movement $\dot{\mathbf{y}}$ to stabilize gaze.

Hence, from Equations 3.2 and 3.4, the overall mapping which must be learnt is a composite function

$$\mathbf{u}^* = P^{-1}(\mathbf{y}, S(\mathbf{y}, \dot{\mathbf{x}})). \tag{3.6}$$

This equation states exactly how each kind of mapping describing either the plant (P) or the task (S), influences the required motor command $\mathbf{u}$.

In general, we can describe any task disturbance in terms of a function mapping the stimulus $\mathbf{x}$ (e.g. observed target location) to desired outcome $\mathbf{y}^*$ (e.g. desired hand location). We refer to S as the *task*.

3.2 Alternative architectures for cerebellar-based adaptive control

It is well known that the cerebellum plays a critical role in VOR adaptation. Although a variety of brainstem circuitry contributes to the VOR, the basic reflex is largely mediated by a fast three-synapse pathway in the brainstem (Boyden et al., 2004). This brainstem pathway is augmented by an adaptive pathway through the cerebellum. It is known that among its many inputs, the region of the cerebellum involved in the VOR receives a variety of parallel-fibre inputs including vestibular-related signals and efferent copies of outgoing oculomotor commands (Hirata and Highstein, 2001).

Two distinct kinds of control architectures have previously been proposed as models of this circuitry. Most commonly, the brainstem and cerebellar pathways are modelled as having a purely feedforward organization (Gomi and Kawato, 1990; Kawato and Gomi, 1992; Shibata and Schaal, 2001), disregarding the motor command efferent copies. This model, with a *feedforward architecture* is illustrated in Figure 3.3(a). More recently, Porrill et al. (2004) have argued that the efferent copy inputs may in fact be of critical importance and should not be ignored. They propose a model of VOR adaptation in which efferent copy information *alone* is sufficient for successful adaptive control. This model, in which the cerebellum is connected with the brainstem via a recurrent architecture, is illustrated in Figure 3.3(b).

These two alternative models of VOR adaptation each effectively assume that either the feedforward or the recurrent (efferent copy) inputs to the cerebellum dominate, with the other inputs playing a more minor role in generating the cerebellar output. The true contributions from each of these pathways to the cerebellar output is unknown. Although both architectures are capable of generating appropriate motor commands, the nature of the internal model learnt and the respective learning capabilities and dynamics turn out to be quite different, particularly in how they perform under task vs plant disturbances.

We use the model of cerebellar learning presented in Section 2.2.1. Recall that this model proposes that the cerebellar output is constructed from a weighted combination

of the inputs to the cerebellum,

$$\mathbf{c}_t = \mathbf{W}^T \mathbf{p}_t, \tag{3.7}$$

and that these weights are adapted according to an error-driven gradient descent learning rule,

$$\Delta \mathbf{W} = -\beta \, \widetilde{\mathbf{c}}_t \mathbf{p}_t^T. \tag{3.8}$$

Here, $\widetilde{\mathbf{c}}_t$ is the error in the cerebellar output at time t. We do not, however, have direct knowledge of this error. The error in performance can only be measured in terms of retinal slip. This poses a distal learning problem which can be solved by transforming the observed outcome error (retinal slip $\dot{\widetilde{\mathbf{y}}}$ in the case of the VOR) into an error in the cerebellar output $\widetilde{\mathbf{c}}$.

In order to do this, we need to know exactly what the desired output of the cerebellum is. As we shall see, this depends critically on whether the cerebellum is being used in a feedforward or a recurrent architecture. Previous analyses of cerebellar VOR adaptation have tended to consider only plant disturbances, neglecting the fact that experiments typically employ task disturbances.

If we assume that head velocity and desired eye velocity are always equal and opposite, the error in the cerebellar output $\widetilde{\mathbf{c}}$ under the feedforward architecture is equal to the error in the motor command,

$$\widetilde{\mathbf{c}} = \mathbf{u}^* - \mathbf{u}. \tag{3.9}$$

As we shall see below, this motor error can be estimated from the retinal slip by transforming it through an inverse model of the plant dynamics. Under the recurrent architecture, on the other hand, Porrill et al. (2004) have shown that the error in the cerebellar output is equal to the raw retinal slip signal $\dot{\widetilde{\mathbf{y}}}$ and thus the distal learning problem is circumvented. However, their analysis was restricted to adaptation to changes in the oculomotor plant dynamics.

We will now examine learning within each of these architectures in the case that the task S, i.e. the relationship between head velocity and the gaze-stabilizing eye velocity, is also subject to change. In both cases, we require an expression for the error in the cerebellar output, $\widetilde{\mathbf{c}}$, in terms of the observed output error (retinal slip, $\dot{\widetilde{\mathbf{y}}}$, in the case of the VOR).

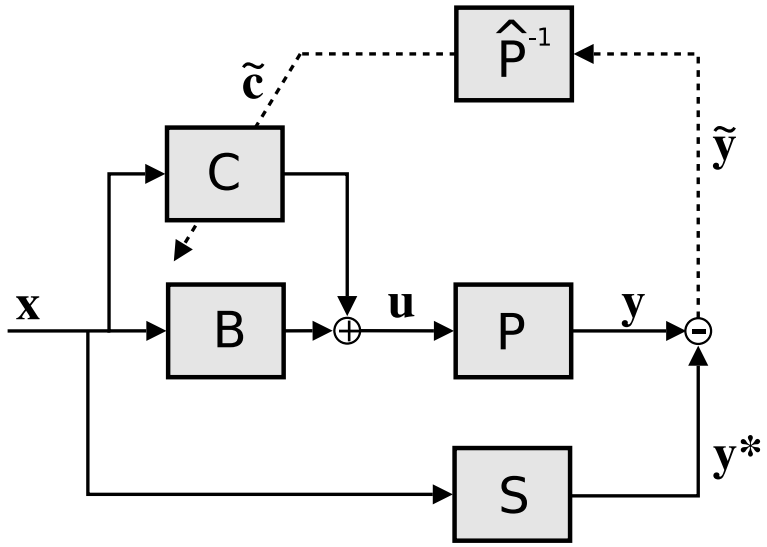

(a) Feedforward Architecture

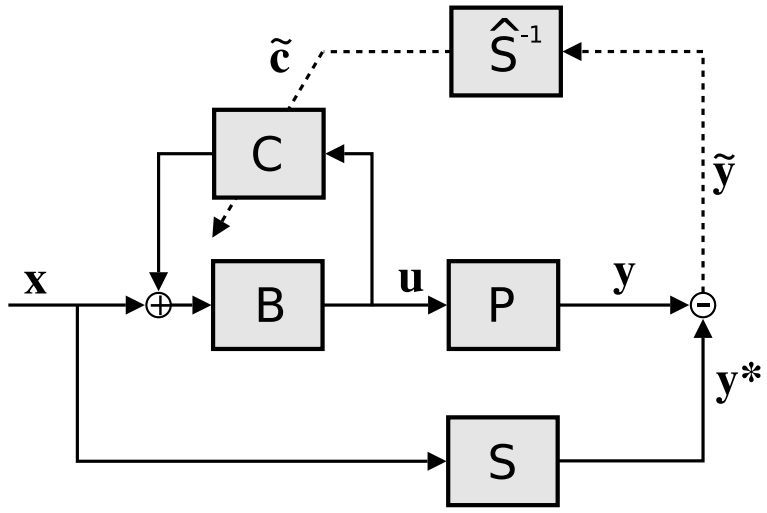

(b) Recurrent Architecture

Figure 3.3: Schematic of feedforward and recurrent architectures. In the feedforward architecture, output from cerebellum C is combined with output from brainstem B to form the motor command u which is sent to the plant P. The task S specifies desired output given stimulus x. Sensory error $\tilde{y}$ must be transformed through an inverse model of the plant to reflect error in the cerebellar output. In the recurrent architecture, cerebellum C receives output of the brainstem as input and sends its ouput as input to the brainstem. Sensory error must be transformed through inverse model of the task S.

3.2.1 Learning in the Feedforward Architecture

Referring to the feedforward architecture shown in Figure 3.3(a), the inputs to the cerebellum in this model are head velocity $\dot{\mathbf{x}}$ and head position $\mathbf{x}$ ($\dot{\mathbf{x}}$ is omitted from the figure for clarity). We assume that an optimal cerebellar model C^* exists. This corresponds to a set of optimal weights $\mathbf{W}^*$ for the cerebellum model outlined in the previous section. The error in the cerebellar output is then given by

$$\widetilde{\mathbf{c}}(\mathbf{x},\dot{\mathbf{x}}) = C^*(\mathbf{x},\dot{\mathbf{x}}) - C(\mathbf{x},\dot{\mathbf{x}}), \tag{3.10}$$

and we wish to express this in terms of the retinal slip $\dot{\tilde{\mathbf{y}}}$.

The motor command is generated by combining the output from the brainstem and cerebellum

$$\mathbf{u} = C(\mathbf{x},\dot{\mathbf{x}}) + B(\mathbf{x},\dot{\mathbf{x}}), \tag{3.11}$$

where $B(\mathbf{x},\dot{\mathbf{x}})$ describes the brainstem dynamics. Similarly for the optimal cerebellum model

$$\mathbf{u}^* = C^*(\mathbf{x},\dot{\mathbf{x}}) + B(\mathbf{x},\dot{\mathbf{x}}). \tag{3.12}$$

Noting that the optimal motor command $\mathbf{u}^*$ is given by $P^{-1}(\mathbf{y},S(\mathbf{y},\dot{\mathbf{x}}))$, we can see that the optimal cerebellum model C^* satisfies

$$C^*(\mathbf{x},\dot{\mathbf{x}}) = P^{-1}(\mathbf{y},S(\mathbf{y},\dot{\mathbf{x}})) - B(\mathbf{x},\dot{\mathbf{x}}). \tag{3.13}$$

The cerebellum must therefore learn a composite of a forward task model and an inverse dynamics model, while also compensating for the contribution from the brainstem B.

Now, taking the difference between Equations 3.11 and 3.12 and comparing it to Equation 3.10 illustrates that we can express the error in the cerebellar output as:

$$\widetilde{\mathbf{c}} = \mathbf{u}^* - \mathbf{u}, \tag{3.14}$$

that is, $\widetilde{\mathbf{c}}$ is equal to the *motor error*. Rewriting the right hand side of Equation 3.14 in terms of the inverse plant model (Equation 3.2), we have

$$\widetilde{\mathbf{c}} = P^{-1}(\mathbf{y},\dot{\mathbf{y}}^*) - P^{-1}(\mathbf{y},\dot{\mathbf{y}}). \tag{3.15}$$

For linear plant dynamics, we can directly simplify and rewrite the expression in terms of the retinal slip $\dot{\tilde{\mathbf{y}}}$,

$$\widetilde{\mathbf{c}} = P^{-1}(\mathbf{y},\dot{\tilde{\mathbf{y}}}). \tag{3.16}$$

For nonlinear plant dynamics, Equation 3.15 can be approximated by the first term of the Taylor expansion of P^{-1} about $(\mathbf{y},\dot{\mathbf{y}})$:

$$\widetilde{\mathbf{c}} \approx J_{P^{-1}}(\mathbf{y},\dot{\mathbf{y}})\widetilde{\mathbf{y}}, \tag{3.17}$$

where $J_{P^{-1}}(\mathbf{y},\dot{\mathbf{y}})$ is the Jacobian of P^{-1} at the point $(\mathbf{y},\dot{\mathbf{y}})$.

Equations 3.16 and 3.17 show that the error in the cerebellar output can be calculated from the retinal slip via the inverse dynamics of the plant, i.e. the inverse of the mapping from motor commands to observed outcome. We assume that some internal model is available to compute this, which may reside elsewhere in the cerebellum (Wolpert et al., 1998). Alternatively, the error signal might be the direct output of a feedback controller, (Gomi and Kawato, 1990; Shibata and Schaal, 2001). In any case, if the plant dynamics change, the transformation of the sensory error into motor error will still reflect the old dynamics and we can no longer be confident that our estimate of the cerebellar output error is accurate. The required training signal is, however, independent of the task *S*.This is an important but usually overlooked advantage of employing this kind of feedforward learning architecture.

In general, then, we expect learning under the feedforward architecture to be impaired (i.e. converge more slowly) or even made entirely unstable (not converge at all) following a change in the motor command-outcome (dynamics) mapping. However, we expect learning to be unaffected by a change in the kinematics.

3.2.2 Learning in the Recurrent architecture

Next, we derive an expression for the error in the cerebellar output in terms of the measured retinal slip for the recurrent architecture (Figure 3.3(b)), following a similar argument to Porrill et al. (2004). We assume that the inputs to the cerebellum are the head position $\mathbf{x}$ and the afferent motor command $\mathbf{u}$ (the head-position input is omitted in Figure 3.3(b) for clarity).

We begin by noting that the input to the brainstem model is given by $C(\mathbf{x},\mathbf{u})+\dot{\mathbf{x}}$, which is equal to the motor command transformed under the brainstem inverse model, i.e.,

$$\mathbf{u} = B(\mathbf{x}, C(\mathbf{x},\mathbf{u})+\dot{\mathbf{x}}) \tag{3.18}$$

$$\Longrightarrow \quad C(\mathbf{x},\mathbf{u})+\dot{\mathbf{x}} = B^{-1}(\mathbf{x},\mathbf{u}). \tag{3.19}$$

Again, as in the feedforward case, we assume there exists an optimal cerebellar model

C^* which yields exactly the desired motor command (this corresponds to optimal weights $\mathbf{W}^*$ in the cerebellum model outlined previously).

Note that the motor command $\mathbf{u}$ would be optimal for some alternate head velocity $\dot{\mathbf{x}}'$, i.e.

$$C^*(\mathbf{x},\mathbf{u}) + \dot{\mathbf{x}}' = B^{-1}(\mathbf{x},\mathbf{u}), \tag{3.20}$$

with $\dot{\mathbf{x}}' = S^{-1}(\mathbf{y}, P(\mathbf{y},\mathbf{u}))$, by definition of S^{-1} from Equations 3.1 and 3.5. Rearranging this, we have

$$C^*(\mathbf{x},\mathbf{u}) = B^{-1}(\mathbf{x},\mathbf{u}) - S^{-1}(\mathbf{y}, P(\mathbf{y},\dot{\mathbf{u}})). \tag{3.21}$$

Under the recurrent architecture then, the cerebellum must learn a composite of a forward dynamics model and an inverse task model. This is in direct contrast to the feedforward case in Equation 3.13.

Taking the difference between Equations 3.19 and 3.20, we can express the cerebellar output error as:

$$\begin{aligned} C^*(\mathbf{x},\mathbf{u}) - C(\mathbf{x},\mathbf{u}) &= \dot{\mathbf{x}}' - \dot{\mathbf{x}} \\ &= S^{-1}(\mathbf{y},\dot{\mathbf{y}}) - S^{-1}(\mathbf{y},\dot{\mathbf{y}}^*). \end{aligned} \tag{3.22}$$

If we assume that S is linear then we can express this directly in terms of the retinal slip,

$$\widetilde{\mathbf{c}}(\mathbf{x},\mathbf{u}) = S^{-1}(\mathbf{y},\dot{\widetilde{\mathbf{y}}}). \tag{3.23}$$

If S is nonlinear, we can use a first order Taylor approximation as before,

$$\widetilde{\mathbf{c}} \approx J_{S^{-1}}(\mathbf{y},\dot{\mathbf{y}})\dot{\widetilde{\mathbf{y}}}, \tag{3.24}$$

where $J_{S^{-1}}(\mathbf{y},\dot{\mathbf{y}})$ is the Jacobian of S^{-1} at the point $(\mathbf{y},\dot{\mathbf{y}})$.

Equations 3.23 and 3.24 show that the error in the cerebellar output is given by the retinal slip transformed via the inverse of the task S, i.e. the inverse of the mapping from the stimulus to the desired outcome. This can be thought of as an error in the original vestibular signal $\dot{\mathbf{x}}$.

So in general, we expect learning under the recurrent architecture to be impaired under task disturbances but not plant disturbances. This reveals a duality between the feedforward and recurrent architecture models. The properties of learning in the feedforward architecture are mirrored by those of learning in the recurrent architecture with the roles of the two kinds of transformation reversed.

Although we have illustrated the argument with the specific example of the VOR, the arguments presented here are entirely general and can be applied to any other motor

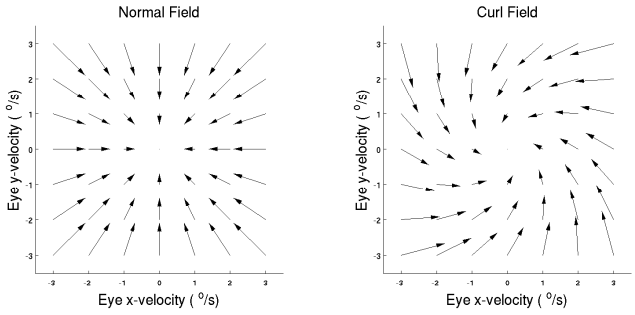

(a) Plant disturbance

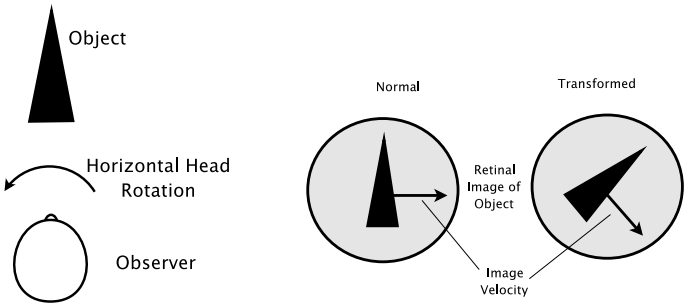

(b) Task disturbance

Figure 3.4: Example of dynamic and kinematic transformations. a) A change in the viscosity field of the oculomotor plant. b) Effect of rotation of visual feedback on image velocity during head rotations.

behaviour. Furthermore, the only point at which linearity was assumed was in the final step in each derivation combining the terms in Equations 3.15 and 3.22. For nonlinear P and S, a Taylor expansion gives a simple approximation to the cerebellar output error in terms of the observed output error, provided the error is not too large.

3.2.3 VOR simulations

In order to test the performance of each of the two alternative VOR models in adapting to a range of task and plant disturbances, we simulated adaptation of a 2 degree-of-freedom oculomotor plant under a range of transformations of the kinematics and the plant dynamics. The simulated oculomotor plant had simplified dynamics initially given by

$$\dot{\mathbf{y}} = \mathbf{u}, \tag{3.25}$$

and an initial relationship between head velocity and gaze-stabilizing eye velocity given by

$$\dot{\mathbf{y}}^* = -\dot{\mathbf{x}}. \tag{3.26}$$

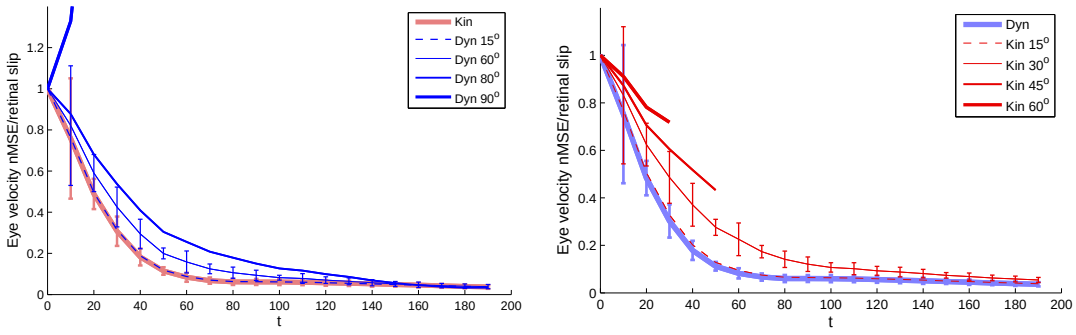

(a) Feedforward Architecture (b) Recurrent Architecture

Figure 3.5: Timecourse of adaptation for VOR model using 3.5(a) feedforward architecture and 3.5(b) recurrent architecture. Both figures display average normalized mean squared eye velocity error (retinal slip), averaged over 10 trials. Different traces show response to different conditions - either a change in dynamics (viscous curl field) or a change in kinematics (visual field rotation) of differing magnitudes.

To simulate a change in the relationship between motor command and observed outcome, we changed the dynamics from the ordinary resistive viscosity field described by Equation 3.25 to a viscous curl field (Figure 3.4(a)) in which there is an angle ϕ between the eye velocity and the force, i.e.

$$\mathbf{u} = P_1 \dot{\mathbf{y}}, \tag{3.27}$$

where

$$P_1 = \begin{pmatrix} \cos\phi & \sin\phi \\ -\sin\phi & \cos\phi \end{pmatrix}. \tag{3.28}$$

Due to the first-order dynamics assumed here, this had the effect of rotating the angle of actuation for a given motor command.

To change the relationship between head velocity and gaze-stabilizing eye velocity, we employed a rotation of the visual field (Figure 3.4(b)) by angle ψ. Following this transformation, the desired eye velocity is rotated by angle ψ relative to the head velocity, i.e.

$$\dot{\mathbf{y}}^* = S_1 \dot{\mathbf{x}}^*, \tag{3.29}$$

where

$$S_1 = \begin{pmatrix} \cos\psi & \sin\psi \\ -\sin\psi & \cos\psi \end{pmatrix}. \tag{3.30}$$

In all experiments, the head position repeatedly traced out a figure-of-eight:

$$\mathbf{x}(t) = \begin{bmatrix} \sin(0.1t) \\ \sin(0.2t) \end{bmatrix}^T. \tag{3.31}$$

All experiments were run 10 times, with different initial positions around the figure-of-eight on each trial. Full implementation details are given in Appendix B.

First, we tested the performance of the feedforward architecture in adapting to the visuomotor rotation. Analyzing the normalized mean-squared (nMSE) velocity error (i.e., retinal slip), we found no significant difference in the learning rate when adaptation to different magnitudes of rotation ($\psi = [15, 135]$) were compared. Figure 3.5(a) plots the average nMSE over time for $\psi = 45^\circ$ which is representative of all values of ψ. The error bars represent one standard deviation above and below the mean.

We then tested the performance of the feedforward architecture in adapting to novel dynamics. Figure 3.5(a) plots the evolution of the nMSE over time for different values of ϕ. For $\phi = 15^\circ$, performance is the same as under the visuomotor rotation. As ϕ increases, however, the rate of learning is reduced. Error bars representing standard deviation across runs with differing initial conditions are plotted for the $\phi = 60^\circ$ case to show that the difference from the 15° case is significant (error bars on other plots are omitted for clarity). At $\phi = 90^\circ$, the VOR no longer converges and updates of the cerebellar weights no longer improve performance. This is equivalent to always moving perpendicularly to the direction of steepest slope. For $\phi > 90^\circ$, changes in the cerebellar weights led to deteriorating performance and unstable adaptation.

For the recurrent architecture, we first tested the performance under the change in dynamics. For $\phi < 60^\circ$, we found no significant difference in performance between different values of ϕ. For larger values of ϕ, however, the recurrent loop tended to become unstable after a period of initial improvement. Figure 3.5(b) shows the nMSE over time for $\phi = 45^\circ$ which was representative of all trials for $\phi < 60^\circ$.

Finally, we tested the performance of the recurrent architecture in adapting to the visuomotor rotation. Results from these trials are also plotted in Figure 3.5(b). Again, for clarity, error bars are only plotted for representative transformations. For $\psi = 15^\circ$, performance is similar to that under the change in the dynamics. For $\psi = 45^\circ$, however, the adaptation is significantly slower. For $\psi = 50^\circ$ and greater, the recurrent loop tended to become unstable resulting in an exponential increase of the error over a very short timescale. The plots have therefore been curtailed at this point. The initial rate

of improvement in performance is nevertheless reflective of the quality of the estimate of the cerebellar output error.

For the linear models considered in this section, the problem of instability in the brainstem-cerebellum loop under the recurrent architecture can be attributed to the eigenvalues λ of the matrix BC (refer Figure 3.3(b)) having magnitude $|\lambda| > 1$. The output at time t is given by

$$\begin{aligned} u_T &= \sum_{t=1}^{T} B(\dot{\mathbf{x}}_t + C\mathbf{u}_t) \\ &= \sum_{t=1}^{T} B\dot{\mathbf{x}}_t + BC\mathbf{u}_t. \end{aligned} \tag{3.32}$$

Thus, if the matrix BC has any eigenvalue with magnitude greater than 1, the motor command will grow exponentially over time. A given desired motor output can still be computed with the recurrent architecture (i.e. Equation 3.21 can still be satisfied along with stability requirements) if a different value of B is used. It may be possible to avoid entering into unstable regions of the parameter (cerebellar weight) space by also adapting B, using the output of C as a training signal. This 'learning transfer' from C to B would steer the loop away from regions of instability by ensuring that C^* (which would now depend on B) would tend asymptotically to 0. Learning transfer of this kind is supported by physiological evidence (Boyden et al., 2004) and Porrill and Dean (2007a) have suggested it may be used as a mechanism to enhance VOR response at high frequencies. So, although, problematic, the instability issues with the recurrent architecture do not preclude it as a biologically plausible model of cerebellar learning.

In summary, as predicted by the theory, performance of the feedforward architecture was impaired following changes in the oculomotor plant dynamics, but was not affected by changes in the kinematics. Performance of the recurrent architecture, on the other hand, was affected by changes in the kinematics but not by changes in the dynamics.

3.3 Saccades

So far we have described adaptation of the VOR in response to two distinct kinds of disturbances and described how two existing cerebellar-based learning frameworks are each well-suited to learning one of these kinds of transformation but not so well-suited to the other. In this section we show how these same arguments carry over to the saccadic system and in particular, we use this example to examine the effect on the timecourse of adaptation more closely.

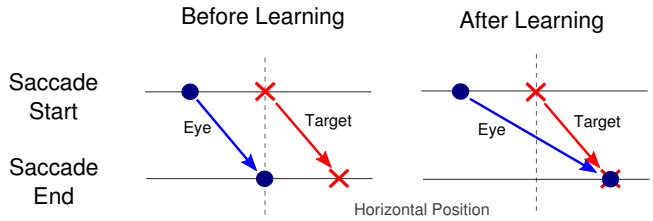

Figure 3.6: Illustration of target shifting paradigm.

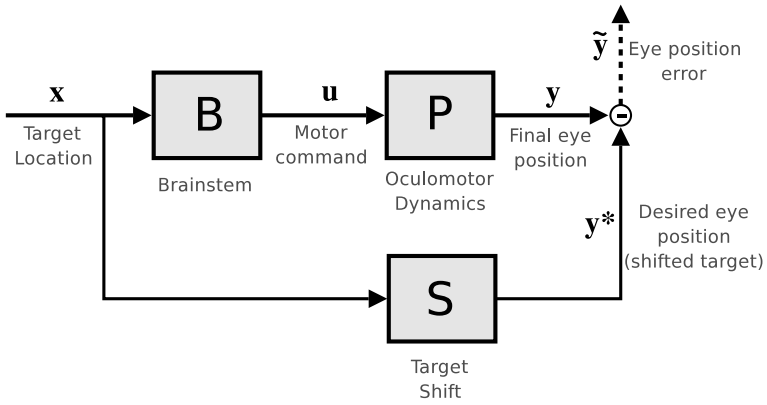

Figure 3.7: Simplified saccadic adaptation framework

Saccades are rapid eye movements used to change gaze fixation from one point to another. It is known that saccades are planned as a difference vector in retinotopic coordinates between the current fixation point and the desired fixation point (Hopp and Fuchs, 2004). An open-loop sequence of motor commands based on this difference vector is then issued to guide the eye to the planned new position, with the eye typically following a minimum-jerk-like trajectory (Harris and Wolpert, 1998).

The *gain* of a saccade is the ratio between the distance of the planned saccade and the distance the eye ultimately moves. Under ordinary circumstances the gain of the saccadic system should be equal to 1, but through physical changes to the eye or experimental intervention, the gain of saccades can change leading to systematic errors in the saccadic endpoint. Whenever such errors are experienced, the gain of the saccadic controller is adapted so as to reduce future errors. As in the VOR, this adaptation is known to be cerebellar-dependent (Optican and Robinson, 1980).

3.3.1 Experimental saccade adaptation paradigms

Two different experimental paradigms have primarily been used to elicit adaptation of saccadic gain. One method is to surgically weaken one or more of the extra-ocular

muscles. This procedure directly alters the plant dynamics so that the same motor command (stimulation of the extraocular muscles by motor neurons) will result in a different (smaller) eye movement. Initially, the impaired eye will fall short of its target but, after practice, will adapt and eventually exhibit more accurate saccades.

The saccadic gains for each eye are coupled - if one eye is patched while the other undergoes gain adaptation, the gain of saccades in the patched eye will also change. Therefore, by operating only on one eye and by alternately patching either the normal eye or the weakened eye, adaptation can be repeatedly induced either from low gain to normal gain (moving the patch from the weakened eye to the normal eye) or from high gain to normal gain (moving the patch from the normal eye to the weakened eye) (Scudder et al., 1998).

An alternative, non-surgical method to elicit adaptation of saccadic gain is to shift the position of the target during the saccade. Subjects are unable to see this movement since vision is suppressed during saccades. If the target is shifted further away from its original position, this has a similar effect to having weakened muscles in that there is still some distance to go to the target at the end of the saccade. After many trials (typically hundreds), the saccadic system adapts and the size of saccades changes to reduce the endpoint error.

Although it is tempting to view the latter experimental paradigm as a way of simulating a change in the plant dynamics, it should, in fact, be viewed as a change in the relationship between the stimulus the desired outcome, i.e. as a task disturbace, rather than a plant disturbance. The plant dynamics, that is the relationship between motor commands and resulting eye movements, remain constant throughout. The shifted target location depends only on the original position of the target and not on the intermediate motor commands or the final eye position.

3.3.2 Implications for learning

Following the discussion of VOR adaptation in the previous section, we should likewise expect these different training paradigms to elicit different patterns of adaptation. In the case of the VOR, adaptation to a rotation of the visual field under the recurrent architecture was hampered by the fact that the estimate of the cerebellar output error was rotated relative to the true error. In the case of saccadic gain adaptation under the target shift paradigm, there is no rotation and, for the recurrent architecture, the estimate of the cerebellar output error will remain parallel to the true error. This is analogous to a

magnification or shrinking of the visual field for the VOR. Non-parallel, or 'cross-axis' shifting of saccade targets has been elicited in some studies but this is less commonly done. Under the normal gain-up (gain-down) adaptation paradigm, however, errors in movement will be exacerbated (diminished) and the estimated error in the cerebellar output will therefore be inflated (or reduced). This will affect the rate of adaptation. A similar argument applied to adaptation in the feedforward model under changes in the dynamics. For a weakened plant, the additional motor command required to successfully reach the target will actually be greater than the estimate, which is based on dynamics of a normal eye.

So while in the case of the VOR we showed how learning can fail completely under drastic enough transformations, we will use the example of saccades to illustrate how different architectures lead to different predictions for the time-course of learning.

3.3.3 Saccade adaptation model

In order to make concrete arguments about the role of the cerebellum and the impact of different training paradigms on the timecourse of learning, we introduce a simplified model of the saccadic system, illustrated in Figure 3.7. In this section, for mathematical simplicity, we represent all variables as scalars and assume all mappings are linear. The stimulus, x, in this case is the initial target location relative to the current eye position. The brainstem B issues a sequence of motor commands based on this target location which we represent by a single scalar u characterizing its magnitude.

We model the plant dynamics as a simple linear relationship between motor command u and final eye position y, i.e.

$$y = P_0 u, \tag{3.33}$$

where P_0 denotes the normal plant dynamics. We model the surgical weakening of the eye by replacing P_0 with P_1 in (3.33) with $P_1 < P_0$. To model the target shift paradigm, we assume that the mapping S is linear, corresponding to a change in the required gain, i.e.

$$y^* = S_1 x \tag{3.34}$$

so that S_1 is the new gain to be learnt. The baseline (i.e. before adaptation is elicited) saccadic gain is assumed to be equal to 1. The distance remaining to the target $\widetilde{y} = y^* - y$ is the raw performance measure used to drive adaptation - analogous to the retinal slip in VOR adaptation. We consider a simplified experiment in which saccades are only made in one direction and the distance x to the initial target is constant.

By analogy with the VOR, we assume the adaptive capabilities of saccades arise from a cerebellar pathway working in tandem with the brainstem B and that the cerebellar weights are updated on a trial-to-trial basis based on an estimate of the cerebellar output error.

We now seek to describe the time-course of learning mathematically under both the feedforward and recurrent architectures, and examine how the various parameters P_1, S_1 and x affect this time-course. Since saccade adaptation typically takes place over timescales of thousands of saccades, it seems reasonable to adopt a continuous-time approximation to simplify the derivations, rather than describing the trial-to-trial learning dynamics as a discrete-time dynamical system.

3.3.3.1 Feedforward Architecture

First, we note that the motor command u is generated as the sum of brainstem and cerebellar outputs,

$$u = Bx + Cx. \tag{3.35}$$

The observed error in the eye position is given by $\tilde{y} = y^* - y$. Substituting the expressions for y and y^* into this we obtain

$$\tilde{y} = S_1 x - P_1(Bx + Cx) \tag{3.36}$$

and taking the time derivative we have

$$\dot{\tilde{y}} = -P_1 x\dot{C}, \tag{3.37}$$

where $\dot{C}$ corresponds to the rate of cerebellar weight adaptation as given by the cerebellar learning rule. We will assume the same gradient descent cerebellar learning rule as we employed for VOR adaptation (Equation 3.8), i.e.

$$\dot{C} = \beta x P_0^{-1} \tilde{y}. \tag{3.38}$$

Note that we use the old dynamics P_0 and the not the new dynamics P_1 to approximate the motor error, since the new dynamics are unknown. Substituting this into Equation 3.37 we obtain

$$\dot{\tilde{y}} = -\beta x^2 \frac{P_1}{P_0} \tilde{y}. \tag{3.39}$$

This can easily be solved to reveal exponential decrease in performance error over time. Crucially this performance error is independent of S_1, i.e. the relationship between the initial target location (the stimulus) and the shifted target location (desired outcome).

Table 3.1: Dynamics of learning for different adaptation strategies

Model	Error Dynamics
Feedforward	$\dot{\tilde{y}} = -\beta x^2 \frac{P_1}{P_0}\tilde{y}$
Recurrent	$\dot{\tilde{y}} = -\beta P_1 x \left(\frac{S_1 x - \tilde{y}}{P_1 x}\right)^3 \tilde{y}$

3.3.3.2 Recurrent Architecture

For the recurrent architecture, as in the case of the VOR, the motor command u satisfies

$$u = B(x + Cu). \tag{3.40}$$

Rearranging and substituting this into the definition of $\tilde{y}$ we have

$$\tilde{y} = S_1 x - \frac{P_1 B x}{1 - BC}. \tag{3.41}$$

Taking the derivative with respect to time, we obtain

$$\dot{\tilde{y}} = \frac{-P_1 B^2 x}{(1 - BC)^2}\dot{C}. \tag{3.42}$$

Again, $\dot{C}$ is given by the cerebellar learning rule (Equation 3.8). According to the theory presented in Section 3.2, the error in the cerebellar output is obtained by transforming the observed eye position error $\tilde{y}$ via the inverse of the task mapping S. In this case this yields $e_C = \tilde{y}$ (since we assume initially $S = 1$, i.e. the target does not move) and the full cerebellar learning rule is then given by

$$\dot{C} = -\beta u \tilde{y}. \tag{3.43}$$

Substituting this into the equation above we have

$$\dot{\tilde{y}} = -\beta P_1 x \left(\frac{B}{1 - BC}\right)^3 \tilde{y}. \tag{3.44}$$

Finally, by rearranging Equation 3.41 we can obtain an expression for $B/(1 - BC)$ which we can substitute in here to obtain

$$\dot{\tilde{y}} = -\beta P_1 x \left(\frac{S_1 x - \tilde{y}}{P_1 x}\right)^3 \tilde{y}. \tag{3.45}$$

Table 3.1 summarizes the difference in learning dynamics between the two architectures. Note that these equations describe both the sensitivity to changes in the dynamics ($P_0 \rightarrow P_1$) and to shifting of the target ($S_1 \neq 1$).

The most significant different between the two architectures is in what parameters affect the timescale of learning. The rate of learning in the feedforward architecture depends only on the initial plant dynamics P_0 (i.e. the dynamics model assumed to estimate the motor error), the novel plant dynamics P_1 and the initial distance to the target, x (regardless of whether or not it is subsequently shifted). It is independent of any change in gain (i.e. target-shifting) so that no difference in learning rate should be observed between large gain changes and small gain changes. In the recurrent architecture, on the other hand, the adaptation rate depends on the novel plant dynamics P_1 and the target shift size S_1, as well as the initial distance to the target x.

Another notable difference is that the feedforward architecture predicts an exponential decay of the learning rate over trials. The equation governing learning under the recurrent architecture, on the other hand, is non-linear and does not predict purely exponential decay. This is ultimately due to the fact the learning rule in Equation 3.8 was devised to minimize the error in the cerebellar output and this has a nonlinear relationship with the performance error $\widetilde{y}$.

3.3.4 Simulation of saccade adaptation

We simulated trial-to-trial adaptation and subsequent recovery of saccades under both the target shift and surgical weakening paradigms. In addition to the elements of the model described above, we introduced signal-dependent noise in the motor command so that the actual output of the plant on trial n was given by

$$y_n = P_1 u_n (1 + \varepsilon_n), \tag{3.46}$$

with the ε_n's independent and drawn from a normal distribution, $\varepsilon_n \sim N(0, .05^2)$. The value of .05 for the standard deviation of the distribution was chosen to give a spread of saccades and timecourse of learning which visually resembled the data presented in (Straube et al., 1997). Similarly, a value of 2×10^{-5} was chosen for the learning rate β. The same value was used for both the forward and recurrent architectures. Further implementation details can be found in Appendix B.

Figure 3.8 shows the simulated data for adaptation and subsequent recovery to a gain decrease of 30% induced by target-shifting. The top pair of figures shows the data for adaptation under the feedforward architecture while the middle pair of figures shows the data for adaptation under the recurrent architecture. Experimental data from Straube et al. (1997) is shown below for comparison. Each dot represents the magni-

tude of an individual saccade while the solid line displays the results of adaptation in the noiseless case to more easily see the trend.

During the initial gain-down adaptation phase, the time-course of adaptation is more or less indistinguishable between the feedforward and recurrent architectures. In the recovery phase, however, adaptation under the recurrent architecture exhibits an initially linear decrease in the error over the first 500-1000 saccades, before becoming more exponential-like as the gain approaches 1. Under the feedforward architecture, on the other hand, a much sharper increase in performance is visible over the first 500-1000 saccades, with a clearly exponential shape to the adaptation curve. It is plausible, therefore, based on this analysis, that differences between architectures might have observable consequences at a behavioural level. However, comparison with the data from Straube et al. (1997) is inconclusive.

3.3.5 Comparison with experiments

Experimentally, the rate of saccade adaptation is typically estimated as the rate-constant (measured in number of saccades) of an exponential curve fitted to the data. In the context of our model, the trend of adaptation under the feedforward architecture truly is exponential, while for the recurrent architecture, an exponential function still offers a reasonably good fit, despite the nonlinearities in the adaptation dynamics.

An experiment by Scudder et al. (1998) directly compared the timecourse of learning between the two paradigms. The learning rates were estimated by fitting exponentials as described above. The authors found that, during gain-down adaptation, learning under the target-shift paradigm was markedly faster than under the surgical weakening paradigm, which is predicted by the feedforward architecture model, but not the recurrent architecture model. During gain-up adaptation, no such difference in learning rates was observed. In this case, however, for the dynamics disturbance, adaptation was being performed in the healthy eye, with the weakened eye patched. Under the feeforward model, the motor error in this case would be accurate if it were calculated according a model of the normal dynamics of the eye. The patterns of adaptation found in this study therefore tend to favour a feedforward model over a recurrent model.

Straube et al. (1997) examined how various properties of the timecourse of saccadic gain adaptation varied with the change in gain and with the change in the initial distance to the target under the target shifting paradigm. They found that changing the size of the planned saccade had little effect on the rate constant of the fitted exponen-

tial. Decreasing the gain, however did affect the rate of adaptation with more substantial gain decreases having a larger rate constant and therefore slower adaptation. This observation is certainly compatible with a recurrent architecture model. Under the feedforward architecture, our simplified model predicts that a change in gain should have no impact on the learning rate.

Not all saccade adaptation experiments follow the target-shifting paradigm we described here. Robinson et al. (2003) performed an experiment in which the position of the shifted target depended on the final eye position in such a way that the perceived error ($\widetilde{y}$) remained constant, irrespective of the actual final eye position. A study by Albano (1996) also varied the target location in response to the eye position. Unfortunately, neither of these studies present any data on the timescales of adaptation, which would potentially enlighten the present discussion. Precise control over the errors experienced by subjects may enable a more detailed identification of the learning algorithms at the cerebellar level. Methods like this also offer the possibility of directly simulating a change in the plant dynamics by shifting the target in a way which is consistent with a weakened muscle.

Complicating the interpretation of these results within the context of our simplified models is the fact that our model of cerebellar learning (Equation 2.12) can only be taken seriously up to a point. In reality it is not clear exactly how real-valued (positive or negative) variables such as this are really represented in terms of neural firing. At a behavioural level though, the effect of errors on learning (i.e. the cerebellar learning rule in our model) is only appears to depend strongly on the size of the error itself (Straube et al., 1997) and even the sign of the error - overshoots are adapted to more strongly than undershoots (Robinson et al., 2003). In other words, the actual learning rule employed by the nervous system is certainly not linear in $\widetilde{y}$. Deviations from the linear learning rule we have assumed could potentially have a far greater impact on the time-course of learning than the difference between architectures. It is difficult, therefore to draw any firm conclusions about the underlying cerebellar architecture for saccade adaptation from behavioural data. Furthermore, it is impossible to discount the fact that the behavioural trends we observe are governed primarily by normative principles (Körding et al., 2007b; Chen-Harris et al., 2008; Ethier et al., 2008), rather than by low-level implementational details.

In conclusion, we have shown how the two primary experimental paradigms for inducing saccadic gain adaptation are fundamentally different in nature - surgical weakening of the extraocular muscles falls into the category of a plant disturbance, while the

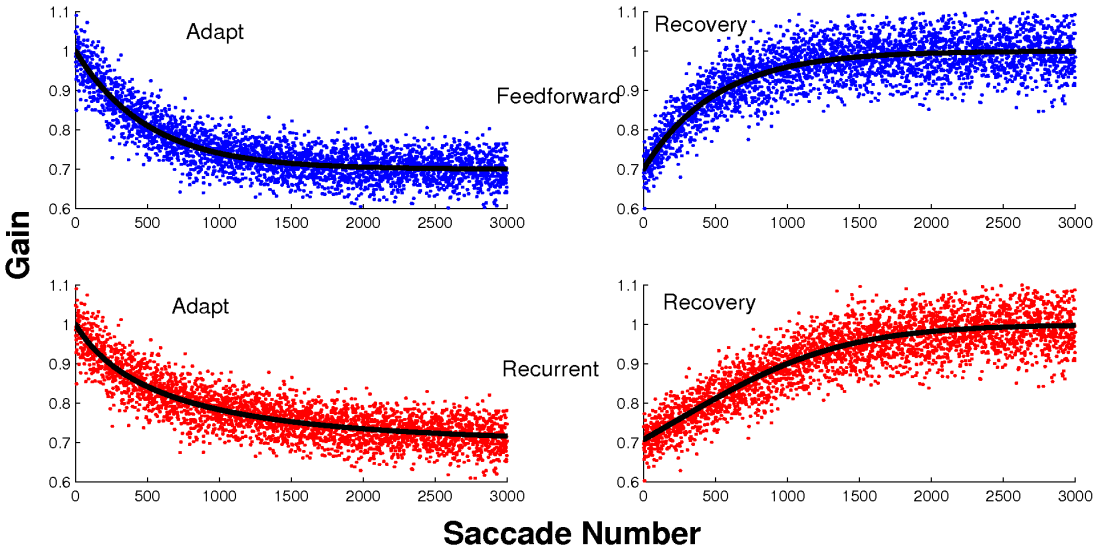

(a) Simulated Data

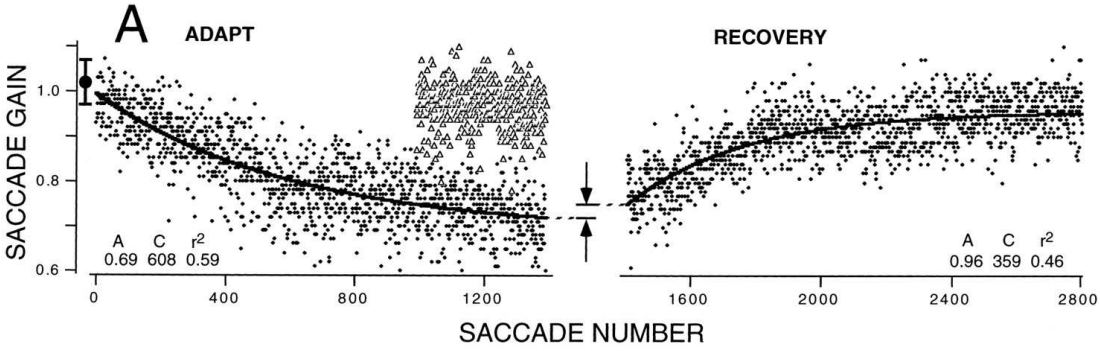

(b) Experimental Data

Figure 3.8: Comparison of simulated saccadic gain adaptation and experimental data under the target-shift paradigm. Simulated saccade adaptation trials under the feedforward architecture (top) and recurrent architecture (middle). Each scatter dot indicates gain of saccade for an individual trial. Solid black line indicates timecourse of learning in the noiseless condition. Experimental data are shown at the bottom, reproduced from (Straube et al., 1997) with permission.

intra-saccadic shift paradigm is a task disturbance. Currently available data, however, does not seem to be sufficient to infer both the learning rules and the underlying cerebellar architecture. Nevertheless, we have highlighted how the timecourse of learning can differ between the different learning architectures. Although we have illustrated these aspects of the alternative cerebellar-based learning models in the context of a relatively simple model, the basic insights in this section apply quite generally.

3.4 Reaching and catching

Arm movements are considerably more complex than eye movements, having more degrees of freedom and nonlinear dynamics. Nevertheless, many of the control principles observed in oculomotor control can be easily generalized to this setting, as we shall describe in this section.

While the exact role of the cerebellum in reaching movements is not entirely understood, cerebellar involvement has been demonstrated in compensating for interaction torques between limb segments (Bastian et al., 1996), adapting to altered dynamics (Smith and Shadmehr, 2005), adapting to altered visual feedback (Baizer et al., 1999) and in learning to manipulate an on-screen cursor (Imamizu et al., 2000). The role of motor command generation in reaching is largely attributable to the primary motor cortex (Todorov, 2000; Shadmehr and Wise, 2005). It therefore seems reasonable to extend the cerebellar-based adaptation frameworks for the VOR from Section 3.2 to model the cerebellum's role in reaching adaptation.

Indeed, Schweighofer et al. (1998) have suggested that the cerebellum generates feedforward motor commands which refine those generated by the cortex, effectively assuming a feedforward cerebellar architecture. By contrast, Porrill and Dean (2007b) have proposed a model of arm control which employs a recurrent cerebellar architecture to learn an inverse kinematics model of the arm. Each of the architectures considered in the previous sections might therefore be considered plausible abstract models of the cerebellum's role in the adaptive control of reaching.

As discussed in Chapter 1, the most common experimental paradigms for eliciting adaptation of reaching movements include application of an external force field to the hand via a robotic manipulandum (e.g., Shadmehr and Mussa-Ivaldi (1994)), or tampering with visual feedback - usually in the form of a rotation of the visual field about the initial position of the hand (Krakauer et al., 2000). Both of these manipulations amount to changing the relationship between the motor command and the eventual

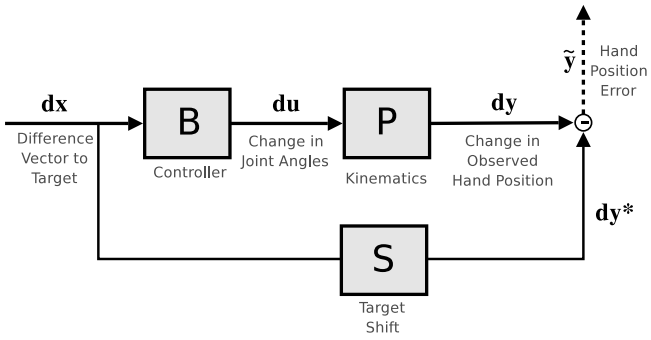

Figure 3.9: Schematic of human reaching model.

observed outcome, and are therefore categorized as plant disturbances.

A few studies have, however, explored adaptation to changes in the relationship between stimulus and desired outcome. Magescas and Prablanc (2006) trained human subjects on a target-shift paradigm similar to that commonly used in saccade adaptation. A visual target was extinguished as subjects began the reach and reappeared in a new position slightly shifted from the where it had been intially. The final location of the target (i.e. the desired outcome) depends only on the initial stimulus and not on the motor command. Subjects were able to adapt to the task and exhibited robust aftereffects in subsequent reaches. Adaptation is, however, substantially slower compared to adaptation to force fields or rotations of visual feedback (Diedrichsen et al., 2005). This kind of disturbance corresponds to a task disturbance. The required motor command in each of these cases is very similar, however the nature of learning under the proposed cerebellar learning models is quite different and, as in the case of the VOR, depends on the cerebellar architecture assumed.

3.4.1 Reaching model

Reaching movements appear to be planned as a visually estimated difference vector **dx** between current hand location and target location (Krakauer et al., 2000; Shadmehr and Wise, 2005). A simplified model is illustrated in Figure 3.9. Based on this difference vector, a suitable change in joint angles **du** is selected by the fixed controller *B*. We maintain our label *B* for this controller from the previous model of the VOR where it denotes 'brainstem', although here it denotes primary motor cortex. In general, the 'motor command' **du** will depend also on the current set of joint angles **u**; for simplicity, in our experiments, we consider a single initial joint position **u**. The final observed hand position is then given by the forward kinematics *P* which represents a

mapping from the change in joint angles **du** to a change in observed hand position **dy**,

$$\mathbf{dy} = P(\mathbf{du}). \tag{3.47}$$

Note that this P includes both the forward kinematics of the arm, which map joint angles into hand position, and any distortions of visual feedback such as a rotation of visual feedback about the initial hand position.

Meanwhile, the target may be shifted mid-reach with the shift S determining the difference vector $\mathbf{dy}^*$ of the shifted target and, therefore the desired observed change in hand position,

$$\mathbf{dy}^* = S(\mathbf{dx}). \tag{3.48}$$

The error $\widetilde{\mathbf{y}}$ in the observed hand position is used to guide adaptation of the controller and is given by the difference between the the actual and desired change in observed hand position,

$$\widetilde{\mathbf{y}} = \mathbf{dy}^* - \mathbf{dy}. \tag{3.49}$$

Adaptation in our model is mediated by the cerebellar pathway which may be connected with the motor cortex B through either a feedforward or a recurrent pathway. We model the cerebellar output as being constructed from a weighted sum of radial basis functions defined over the input space. The combination weights are learnt using the same gradient-descent learning rule as in previous sections. The error in the cerebellar output was estimated by transforming the error in hand position appropriately according to the architecture used, as described in Section 3.2. For the feedforward architecture, this corresponded to transforming the output error through a linearization of the original inverse kinematics mapping (without any rotation of visual feedback taken into account). For the recurrent architecture, this simply corresponded to using the raw observed output error, since the initial stimulus-desired outcome mapping S is simply the identity. More technical details are given in Appendix B.

We set up a 10×10 square grid of targets around the initial position of the hand (given by the initial joint-angles θ_0 (see Figure 3.10(a)). The goal was to find a suitable change of joint angles **du** such that the resulting change in hand position brought the hand in line with the target.

Two separate disturbances were applied requiring adaptation, the first corresponding to a task disturbance, the second a plant disturbance. In the first condition, we implemented a target-shifting paradigm along the lines of the experiment presented in (Lurito et al., 1991; Magescas and Prablanc, 2006). During the reach, the position of

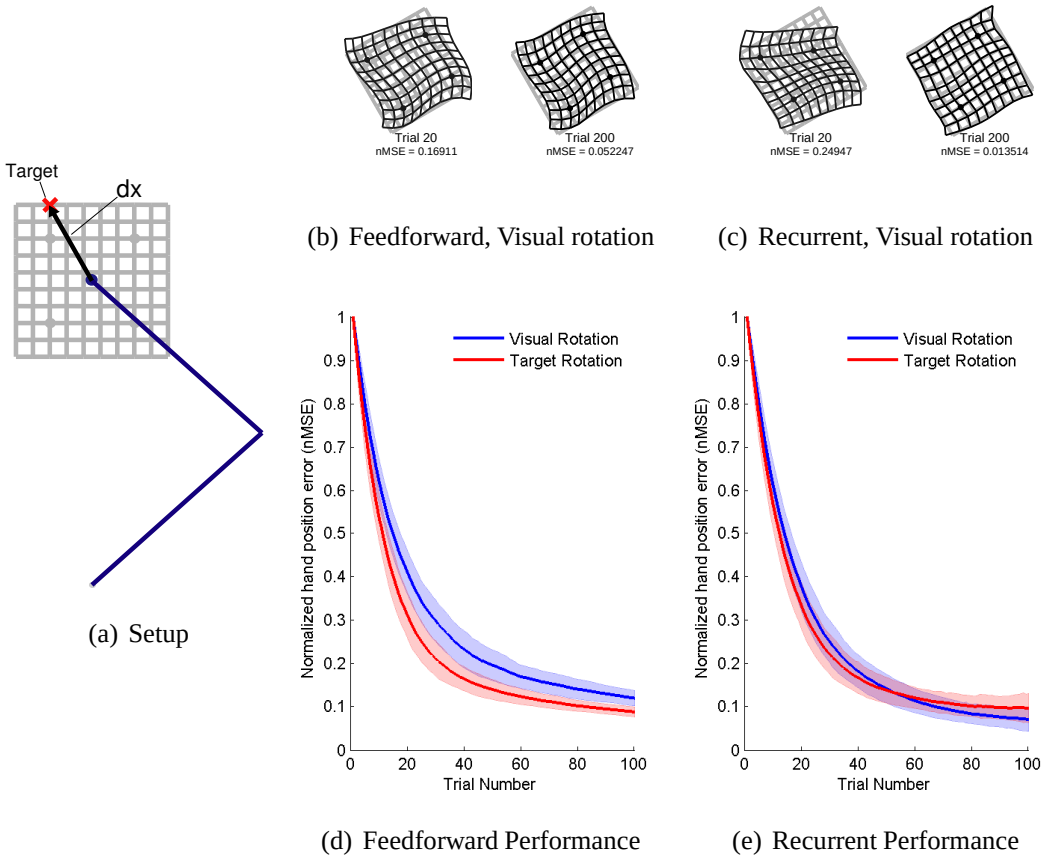

(a) Setup

(b) Feedforward, Visual rotation

(c) Recurrent, Visual rotation

(d) Feedforward Performance

(e) Recurrent Performance

Figure 3.10: Learning kinematic control of a two-link planar arm. (a) Experimental setup of arm and grid of observed targets. Difference vector **dx** is estimated from seen target positions (which may be rotated from the actual positions) and this constitutes the stimulus. (b)-(c) Grid of learnt hand positions following 30^o visual rotation for feedforward and recurrent architectures after 20 and 200 trials. Light grey grid shows the actual (rather than seen) final location of targets. Dark grid shows the grid of hand positions attained while testing reaching to all targets following the indicated number of training trials. (d) - (e) Normalized global mean squared hand position error as a function of the number of trials. Shaded regions indicate standard deviation of error across multiple training runs with training targets presented in different (random) sequences. Visual rotation and target rotation are compared for each architecture.

each target was shifted by rotating it about the initial hand location by an angle $-\psi$. In the second condition, we implemented a rotation of the visual field by angle ϕ about the initial hand location. This led to a rotation of both the stimulus **dx** and the estimated error $\widetilde{\mathbf{y}}$. To ensure that the set of stimuli used (i.e. visually estimated difference vectors **dx**) was the same in both conditions, the grid of targets was rotated by angle $-\phi$ for the visual rotation condition. The mapping to be learnt by the cerebellum C and the set of stimuli used were identical across conditions when $\phi = \psi$. The only difference between conditions was the nature of the error signal and how it related to the error in the cerebellar output.

A sequence of 200 reaching movements was simulated to a random sequence of the 100 targets and this was repeated 100 times with different randomly selected target sequences. The same target sequences were used for each architecture and for each condition. Figure 3.10 illustrates the results of learning under the different architectures and across the two different conditions. In particular, (d) and (e) show the normalized mean squared global test error (nMSE), averaged over all targets and all sessions, as a function of the number of reach trials performed for visual and target rotations of 45 $^\circ$. For the feedforward architecture, it is particularly clear that performance is impaired under the visual rotation condition relative to the target rotation condition, in accordance with the theory. For the recurrent architecture, there was less difference in performance between conditions with marginally better asymptotic average performance under the visual rotation condition.

To demonstrate more clearly the effect that different kinds of transformation had on the quality of learning for different architectures, we examined the trend in reach errors during learning for a small subset of targets (marked with dots in the grid in Figure 3.10(a)). We sampled the final hand position obtained during test trials to these targets after every 10 training trials. Because of the strong effect of the order of training targets on learning, we averaged these positions over 100 different training runs with different randomly selected target sequences to obtain an impression of the general trends of learning in each condition. The paths of these average positions as training proceeds are plotted in Figure 3.11, along with the true target locations. For the feedforward architecture, under the target-shift condition (Figure 3.11(b)), the error estimate used for training is almost equal to the true error and, consequently, the improvement from trial-to-trial comes close to following a straight line in task space. Under the visual rotation condition (Figure 3.11(a)), however, the effect of using a poorer estimate of the error is clearly seen in the fact that the trial-to-trial trend in reach errors does not

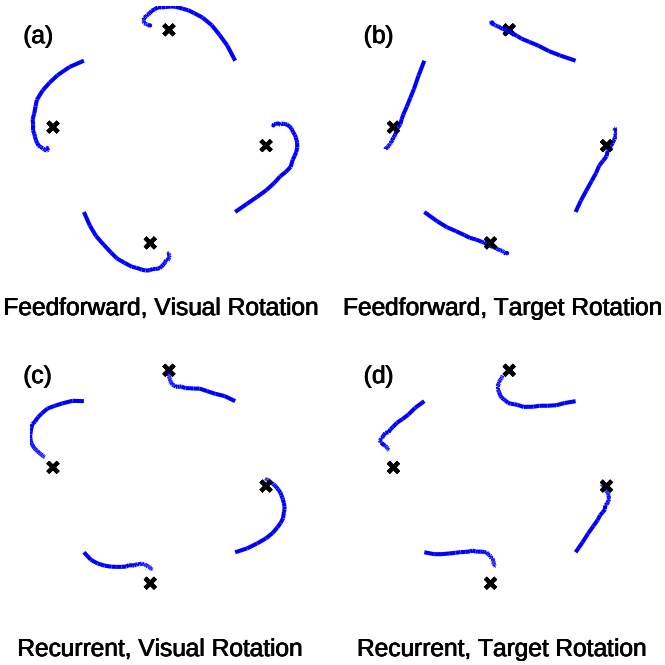

Figure 3.11: Time-course of learning for selected targets in response to either visual feedback rotations or target rotations, using either the feedforward or recurrent cerebellar architecture. The true target locations are marked by a '×'.

follow a straight line but an indirect, curved one.

Under the recurrent architecture, there is still a clear difference between the two conditions. However in the visual rotation condition (Figure 3.11(c)), where we expect the cerebellar output error estimate to be correct, the trial-to-trial trend in final hand position is not straight, as in the feedforward / target shift combination, but has slight curvature. This is due to the fact that there is a nonlinear relationship between the improvement in the cerebellar weights and improvements in task-space performance. So although the improvement takes the shortest path in cerebellar weight-space, this does not necessarily correspond to the shortest path of improvement in task space. The trend for the target-shift condition (Figure 3.11(d)), is not much further from a straight line than that for visual rotation condition. There is however, a clear distinction between patterns of adaptation between the trends for the feedforward and recurrent architecture models.

To highlight the fact that learning in the recurrent architecture really was better for the visual rotation condition than for the target rotation conditions, we quantified the

quality of the estimate of the cerebellar output error in each condition by computing the average overlap between the estimated and true error, given by $\widehat{\tilde{\mathbf{c}}}^T\tilde{\mathbf{c}}/\tilde{\mathbf{c}}^T\tilde{\mathbf{c}}$. An overlap of 1 or close to 1 indicates a good approximation while an overlap of 0 indicates that the estimated error and the true error are perpendicular. Table 3.2 shows how this overlap varies with increasing ψ and ϕ. As expected, the estimated error was close to perfect in the case of the feedforward architecture / target shift combination and the recurrent architecture / visual rotation combination, independent of the magnitude of the transformation. For the other two conditions (feedforward with visual rotation and recurrent with target rotation), the quality of the estimate clearly diminished with increasing extent of visual field or target rotation.

As was the case for the VOR, the recurrent architecture was unstable in some circumstances with divergence of the motor command during iteration of the recurrent loop. For transformations with $\psi > 60^\circ$ or $\phi > 60^\circ$, this led to a total breakdown of learning for all targets (indicated by '—' in the table). For transformations of magnitude $\psi = 45^\circ$ or $\phi = 45^\circ$ the divergence of the motor command was only apparent for some targets and not for others. This caused a large discrepancy between the estimated cerebellar output and the error in hand position for these particular targets, leading to the large variation in overlap recorded in Table 3.2.

3.5 Overcoming the distal error problem

The primary motivation for introducing the recurrent architecture model was to overcome the distal learning problem faced by the more conventional forward architecture when adapting to plant disturbances (Porrill et al., 2004). We have shown, however, that the recurrent architecture suffers from a similar distal learning problem under task disturbances. The feedforward architecture does not suffer from this task-based distal learning problem in the same way that the recurrent architecture does not suffer from the plant-based distal learning problem. Whichever architecture is chosen, the problem of distal errors cannot be avoided altogether, although certain behaviours may be more susceptible to different categories of disturbance.

Several other solutions to overcoming the distal learning problem have been proposed. Jordan and Rumelhart (1992) proposed that a forward model, $\dot{\mathbf{x}} = f(\mathbf{x},\mathbf{u})$ be initially learnt using the sensory error, in which case there is no distal learning problem, and that future sensory errors could be converted into motor errors using knowledge gained from this forward model. The learnt forward model enables estimation of the

		Average $\widehat{\widetilde{\mathbf{c}}}^T\widetilde{\mathbf{c}}/\widetilde{\mathbf{c}}^T\widetilde{\mathbf{c}} \pm$ (s.d.)					
Architecture	Condition	15 °	30°	45 °	60°	75 °	90°
Feedforward	Vis. Rotation	$.96 \pm .17$	$.87 \pm .33$	$.72 \pm .48$	$.49 \pm .61$	$-.03 \pm .15$	$-.04 \pm .17$
	Target Shift	$1.00 \pm .01$	$1.00 \pm .01$	$1.00 \pm .02$	$1.00 \pm .02$	$1.00 \pm .03$	$1.00 \pm .03$
Recurrent	Vis. Rotation	$1.00 \pm .00$	$.99 \pm .11$	1.05 ± 1.83	—	—	—
	Target Shift	$.97 \pm .00$	$.85 \pm .11$	$.82 \pm 2.24$	—	—	—

Table 3.2: Quality of cerebellar output error estimates under different conditions.

forward Jacobian $J_{\hat{f}}$ which can then be inverted to find the inverse Jacobian $(J_{\hat{f}})^{-1}$, which is what we require to transform sensory errors into motor errors. [1] Although this method is theoretically sound, it is not very plausible biologically since it relies on calculations involving parameters which are assumed to be stored in synaptic weights and are therefore not accessible.

A more biologically plausible solution was offered by Gomi and Kawato (1990), who proposed that, rather than an explicit error signal, the output of an existing feedback controller, $\mathbf{u}_{FB}$ could be used as a proxy for motor error to train a feedforward controller. This method effectively assumes that the combined feedforward and feedback commands are a good approximation to the desired feedforward command,

$$\mathbf{u}^* \approx \mathbf{u}_{FF} + \mathbf{u}_{FB} \quad \Longrightarrow \quad \tilde{\mathbf{u}} = \mathbf{u}^* - \mathbf{u}_{FF} = \mathbf{u}_{FB}. \tag{3.50}$$

Feedback-error learning is however, not really a solution to the distal error problem. It is simply an alternative mechanism of obtaining an approximation to the motor error. It is consequently no more robust against the risks of drastic changes in the dynamics model than the feedforward architecture model we have been discussing, since the feedback controller must effectively approximate the dynamics just as before. Successful feedback-error learning relies on the fact that the feedback control is stable. If the dynamics change such that this is no longer the case, e.g. moving the hand while wearing inverting prism goggles, then the feedback error approximation will worsen the learnt internal model, rather than improve it. The primary appeal of feedback error learning appears to be its simplicity and biological plausibility. However a number of recent studies have showed evidence that corrective movements are unnecessary for motor learning to occur (Wallman and Fuchs, 1998; Tseng et al., 2007), casting doubt on the feedback-error learning framework as a model of motor learning.

Abdelghani et al. (2008) proposed that the Jacobian could be learnt directly from experience by tracking changes in performance error over time and linking this to changes that have been made to the controller. While this idea appears promising, it relies on differentiation of potentially noisy error signals, which would exacerbate the impact of noise in the signals.

Shibata and Schaal (2001) implemented a feedback-error learning based biomimetic model (Gomi and Kawato, 1990) of the VOR. Here, the output of an existing feedback controller is used as an approximation to the motor error e_u for training a function approximator (i.e. cerebellum). The optokinetic response (OKR) is a reflex which

[1] Note that the inverse function theorem tells us that $(J_{\hat{f}})^{-1} = J_{\hat{f}^{-1}}$.

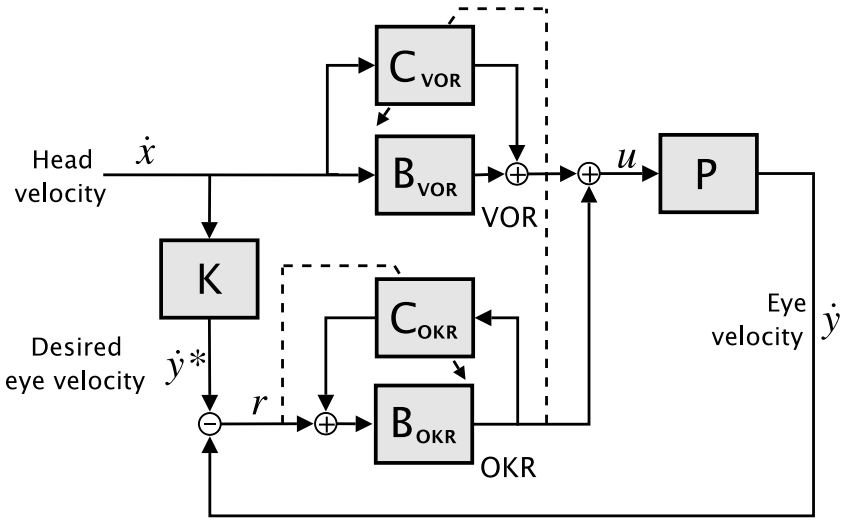

Figure 3.12: Composite model of VOR/OKR adaptation. The VOR is implemented in a feedforward architecture. The optokinetic response (OKR) is implemented through a recurrent architecture. Retinal slip serves as the training signal for the OKR. Output of the OKR serves as the training signal for the VOR.

generates compensatory eye movements in response to retinal slip. Shibata and Schaal likened this to a conventional feedback controller and used the output to train the function approximator according to the standard feedback-error-learning framework. However, this framework inherits all the problems of the forward architecture. The feedback controller implicitly contains a model of the plant dynamics and if these dynamics change, the feedback controller may no longer generate suitable suitable motor commands or training signals. One solution to this problem is to independently adapt the OKR in addition to the VOR.

In Section 3.1.1 we described how, in the VOR, learning the kinematic relationship between head velocity and desired eye velocity is a central component of adaptation. For the OKR, the analog of head velocity is retinal slip. Unlike head velocity, however, the relationship between retinal slip and desired eye velocity is veridical. Kinematics therefore doesn't play a role in the OKR and adaptation of the OKR *can* be described purely in terms of learning the inverse dynamics. Consequently, the recurrent architecture is ideally suited for adaptation of the OKR, since, as outlined above, it is robust against dynamics transformations.

We therefore propose a biomimetic VOR/OKR model, based on feedback-error-learning, in which the OKR adapts to dynamics disturbance employing a recurrent cerebellar architecture framework. The output of the OKR then also acts as a training

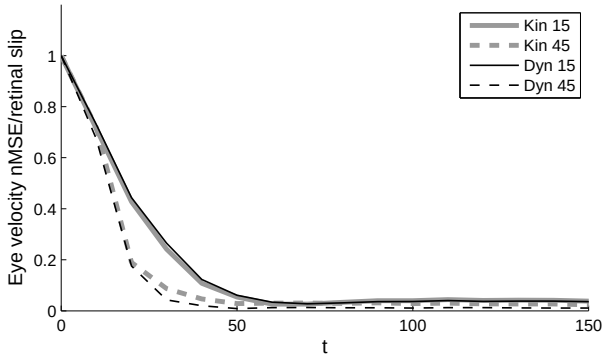

Figure 3.13: VOR composite architecture performance under task (Kin) and plant (Dyn) disturbances.

signal for the VOR, which employs the feedforward architecture as in the model of Shibata and Schaal (2001). This full joint adaptive FEL model of the VOR and OKR is illustrated in Figure 3.12.

3.5.1 Simulations

We evaluated the performance of the composite architecture under the same task and plant disturbances described in Section 3.2.3. The results are plotted in Figure 3.13. As expected, the recurrent loop in the OKR feedback controller became unstable during adaptation to large plant disturbances ($\theta > 60^\circ$). Otherwise, however, learning was stable. The contribution to the overall motor command eventually came entirely from the VOR, indicating that the VOR adaptation was complete and there was no retinal slip.

Figure 3.14 compares the performance of all three architectures under both dynamics and kinematics transformations. The composite architecture outperforms both the feedforward and recurrent architectures under both kinematic and dynamic transformations of the plant.

3.6 Conclusion

We have compared and contrasted two previously proposed architectures for cerebellar-based motor adaptation - one feedforward and one recurrent - initially in quite general theoretical terms and then in the context of two specific behaviours - vestibulo-ocular reflex adaptation and reach adaptation.

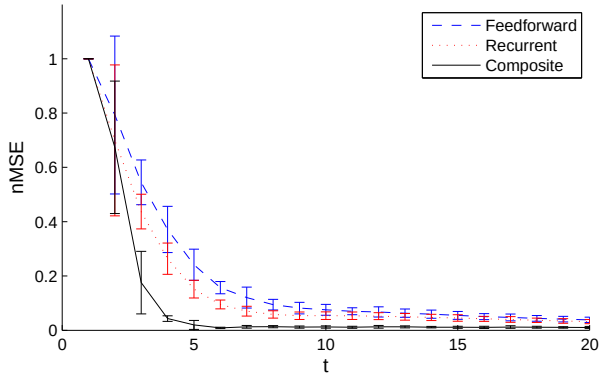

(a) Dynamics transformation: Viscous curl field ($\theta = 45°$).

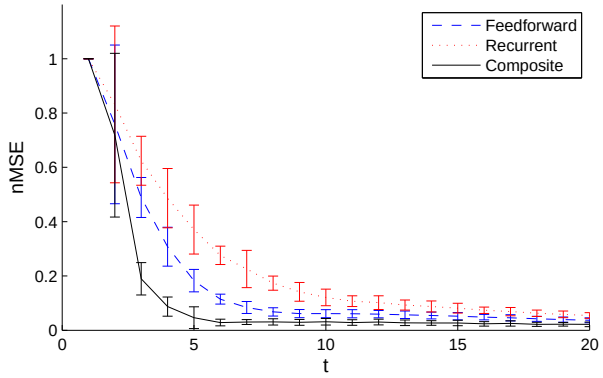

(b) Kinematics transformation: Visual field rotation ($\psi = 45°$).

Figure 3.14: Performance of all architectures controlling a linear, viscous plant (see text for details) under typical task and plant disturbances. Here, the task disturbance is a rotation of the visual field by 45°while the plant disturbance is a rotation of the viscosity field by 45 °.

The central computational difference between the two cerebellar architectures lies in their relative capabilities in adapting to two broad classes of sensorimotor disturbance: i) changes in the mapping between stimulus and desired outcome and ii) changes in the mapping between motor command and movement outcome. The distinction between these two classes of disturbance is not always obvious and has often been overlooked in the past. Because of differences across architectures in how the distal error signal is related to cerebellar output error, the patterns of adaptation under these two disturbances classes are qualitatively different. Learning in the recurrent architecture is impaired in response to task disturbances but not plant disturbances, while learning in the feedforward architecture is impaired under plant disturbances, but not task disturbances.

In order to illustrate and validate the theoretical argument, we have simulated learning under both architectures in three biological motor adaptation settings - the VOR, saccades and reaching. In each case we have highlighted examples where either the stimulus-desired outcome relationship or the motor command-outcome relationship may be subject to change either naturally or through experimental manipulation. The simulations confirm our theoretical predictions. However the results also largely indicate that error-driven learning is quite robust with successful, if slowed, learning even when the approximating error signal is not that accurate. Only in extreme cases, when the approximated cerebellar output error is either not correlated or negatively correlated with the true error, is learning not possible at all.

A major problem identified with the recurrent architecture, however, is the threat of instability in the recurrent loop. As a result of this instability, learning was more likely to fail under the recurrent architecture than the feedforward architecture, even under plant disturbances, where it is expected to perform well. It is possible, however, that these instability problems may be rectifiable in a biologically-plausible manner through transfer of learning from the cerebellum to the brainstem (Porrill and Dean, 2007a).

We have shown that task and plant disturbances can have different effects on adaptation, even though they may initially produce similar patterns of errors. While the distinction between these disturbance classes has been noted previously (Jordan and Rumelhart, 1992; Shadmehr and Wise, 2005), here we have highlighted specific examples in the context of the VOR, saccades and reaching and considered the implications for models of motor learning in these settings.

It is difficult, however, to draw any firm conclusions on what architecture the brain actually uses based purely on behavioural data. Actual learning rules in the cerebellum are considerably more complex than the simplified versions we have assumed here and the details of these learning rules are likely to have as much impact on learning as the architecture-dependent effects we have highlighted here. Moreover, it appears that, in reaching tasks, subjects respond fundamentally differently to the two kinds of disturbances, as can be seen through different generalization patterns (Magescas and Prablanc, 2006) and different brain activity (Diedrichsen et al., 2005).

Chapter 4

A Bayesian model for concurrent sensory and motor adaptation

In Chapter 2, we argued that human motor adaptation comprises multiple components - kinematic and dynamic, for example. Most computational models of motor adaptation, however, tend to consider just a single component of adaptation. Where are there are multiple components of adaptation, the nervous system is faced with a credit assignment problem: which component was responsible for the error? The Bayesian framework provides a principled solution to this problem. Recent work has shown that models of human motor adaptation based on this principle agree well with observed human behaviour (Körding et al., 2007b; Krakauer et al., 2006; Berniker and Körding, 2008).

All of these models, however, have proposed that the problem of credit assignment among multiple components of adaptation is solved based primarily on prior knowledge about the disturbance statistics. As we noted in Section 1.3, however, utilizing information from multiple sensory modalities - primarily proprioception in addition to vision - is likely to also be of critical importance. In this Chapter, we propose a Bayesian model of adaptation in which both visual and proprioceptive observations are used, as well as prior knowledge about the disturbance variability, to guide adaptation. We begin, however, by reviewing how vision and proprioception are modelled in the cue integration literature.

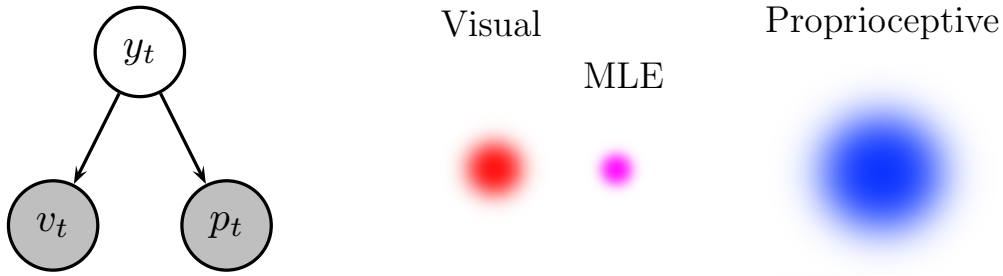

Figure 4.1: Left: A simple generative model of visual and proprioceptive observations given hand position. Subjects receives noisy visual (v_t) and proprioceptive (p_t) observations of his otherwise unknown hand position. Right: The maximum-likelihood estimate (MLE) optimally combines visual and proprioceptive observations according to their uncertainties.

4.1 Integration of visual and proprioceptive cues for state estimation

Sensory information is inherently noisy (Faisal et al., 2008), but we depend on it in order to make decisions about how to move and how to adapt. We are interested in the question of how to combine visual and proprioceptive observations of performance in order to guide motor adaptation. Though this question has not previously been adequately addressed at a computational level, one issue which has been modelled extensively is the question of how to integrate multiple sensory cues for state estimation.

Even when we cannot see our hands, we still have a vivid perception of it's location in space from proprioception. The term 'proprioception' typically refers to the collective output of multiple kinds of sensory systems in the musculoskeletal periphery, including muscle afferents, Golgi tendon organs and even skin mechanoreceptors. For the purposes of this thesis, we will assume that proprioception amounts to a noisy observation of the location of the hand in extrinsic space.

Although visual acuity on the retina may be very good, visual estimation of hand position can also be noisy. This is largely attributable to the fact that mapping a location on the retina into an extrinsic reference frame to guide movement requires knowledge of the neck and head and eye posture. Knowledge of this posture is typically available via noisy proprioception. Therefore, when referring to a 'visual' estimate of hand position, we are implicitly talking about proprioception in the neck, head and eyes.

Two distinct, noisy estimates of hand position can be combined into a single es-

timate which is more reliable (Ernst and Banks, 2002). Suppose, then, that we wish to estimate hand position based on visual and proprioceptive observations. Figure 4.1 illustrates a simple generative model of this scenario. The true hand position y is not observable directly, but only through noisy visual and proprioceptive observations:

$$v = y + N(0, \sigma_v^2) \tag{4.1}$$

$$p = y + N(0, \sigma_p^2). \tag{4.2}$$

We assume that the visual and proprioceptive observation noises are independent with variances σ_v^2 and σ_p^2 respectively.

The true position of y can be estimated via maximum likelihood estimation, Our estimate of y is therefore given by

$$\hat{y} = \arg\max_y p(v, p|y). \tag{4.3}$$

The likelihood $p(v, p|y)$ is given by

$$p(v, p|y) = \exp\left\{ -\frac{(v-y)^2}{2\sigma_v^2} - \frac{(p-y)^2}{2\sigma_p^2} \right\}. \tag{4.4}$$

The value of y maximizing the likelihood also maximizes the log-likelihood. Since this is quadratic in y, it is straightforward to maximize analytically. The solution is a weighted sum of the individual estimates:

$$\hat{y} = w_v v + w_p p, \tag{4.5}$$

where

$$w_v = \frac{\sigma_p^2}{\sigma_v^2 + \sigma_p^2} \tag{4.6}$$

$$w_p = \frac{\sigma_v^2}{\sigma_v^2 + \sigma_p^2}. \tag{4.7}$$

This estimate has variance $(\frac{1}{\sigma_v^2} + \frac{1}{\sigma_p^2})^{-1}$, which is strictly less than the individual unimodal variances, confirming the intuition that combining information from multiple sources in this way improves our estimate of the position of the hand.

Experimentally, it is typically found that the estimated hand position is slightly closer to the visual cue than the proprioceptive cue (van Beers et al., 1996), as in the illustration in Figure 4.1. Within the model, this would be consistent with a greater uncertainty in proprioception than in vision, i.e. $\sigma_p^2 > \sigma_v^2$.

This estimation principle can easily be extended to multiple-dimensional estimates of hand position. In a 2-dimensional workspace, the uncertainties associated with visual and proprioceptive cues become covariance matrices Σ_v and Σ_p. These matrices may represent anisotropic uncertainties. For instance, vision is likely to be more reliable along the visual plane than in depth (van Beers et al., 1999). These anisotropic variances give rise to the unexpected prediction that the MLE may not necessarily lie along the straight line between the two individual estimates. Remarkably, this is exactly what is observed in humans when presented with discrepant visual and proprioceptive cues (van Beers et al., 1999).

In some cases, when the discrepancy between sensory modalities is very large, it becomes rather unlikely that the two modalities truly represent the same stimulus. This intuition can be formalized in terms of Bayesian model selection (Körding et al., 2007a) between scenarios in which the two sensory observations available either derive from the same source, and scenarios where they do not. Such models typically predict that sensory fusion will occur provided the discrepancy between senses lies below some threshold. Beyond this threshold, the conflicting sensory cues are interpreted as two distinct percepts. These models tend to agree well with subjects reported perception of whether a single or multiple stimuli were present (Körding et al., 2007a; Hospedales et al., 2007; Hospedales and Vijayakumar, 2008, 2009). We do not focus on the case of large discrepancies in this thesis, however it is important to consider these kinds of models in interpreting other experimental results.

Provided the individual sensory estimates are not too discrepant, however, the generative model in Figure 4.1, along with the maximum likelihood estimation framework appears to provide a very promising model of how humans integrate visual and proprioceptive information to estimate hand position.

4.2 Adaptation of vision and proprioception

In the previous Section, we saw how to integrate information from two noisy sensory modalities. If, however, two cues are persistently discrepant by about the same amount, it is likely that there is a systematic miscalibration of one modality or the other. Such discrepancies can be eliminated by adapting the senses over time so that they become re-aligned.

When vision is shifted experimentally, either through prism goggles, or by shifting the location of a cursor on a screen, people tend to adjust both their visual and pro-

proprioceptive judgements of location. One way to measure this sensory adaptation is to ask subjects either to point straight ahead with eyes closed (tracking any changes in proprioception) or to identify a visual cue which they judge to be straight ahead (Hay and Pick, 1966; Redding and Wallace, 1996; Hatada et al., 2006). A difficulty with these kinds of methods is that the concept of 'straight-ahead' is rather subjective. An alternative method for measuring sensory adaptation is to use sensory alignment tasks in which subjects align an unseen hand with either a visual cue, or their other hand, without any contact possible between the hands (van Beers et al., 2002; Simani et al., 2007).

Although the alignment tests offer a more precise and unambiguous measure of sensory adaptation, they are limited by the fact that only the relative calibration between any two modalities can be measured. The 'straight-ahead' tasks, by contrast, yield absolute estimates. Typically, only the right hand is exposed during adaptation, and the left hand is assumed to be unaffected and is used as a neutral probe to test the extent of any visual or right hand proprioceptive shift. In any case, both methods typically yield qualitatively similar results. We would like to be able to predict exactly how much adaptation we will observe in vision vs proprioception.

Sensory adaptation can be modelled by extending the generative model in Figure 4.1 to include additional parameters r^v and r^p corresponding to unknown biases in visual and (right hand) proprioceptive observations,

$$v_t = y_t + r^v + N(0, \sigma_v^2) \tag{4.8}$$

$$p_t = y_t + r^p + N(0, \sigma_p^2). \tag{4.9}$$

These biases may either be due to internal miscalibration, or due to some deliberate experimental manipulation. We assume that the subject maintains estimates of these disturbances over time, which we denote by $\hat{r}_t^v$ and $\hat{r}_t^p$. Changes in these disturbance estimates correspond to sensory adaptation. For now, we assume that $\hat{r}^v$ corresponds exactly to the error in the vision-left hand alignment test, and that $\hat{r}^p$ corresponds to the error in the left-hand to right-hand alignment test. These assumptions about the nature of sensory adaptation are well-supported by experimental data (Simani et al., 2007).

The subjects recalibrated visual and proprioceptive estimates of hand position, $\hat{y}^v$ and $\hat{y}^p$, are then given by subtracting their disturbance estimates from their raw observations, i.e.

$$\hat{y}_t^v = v_t - \hat{r}_t^v \tag{4.10}$$

$$\hat{y}_t^p = p_t - \hat{r}_t^p. \tag{4.11}$$

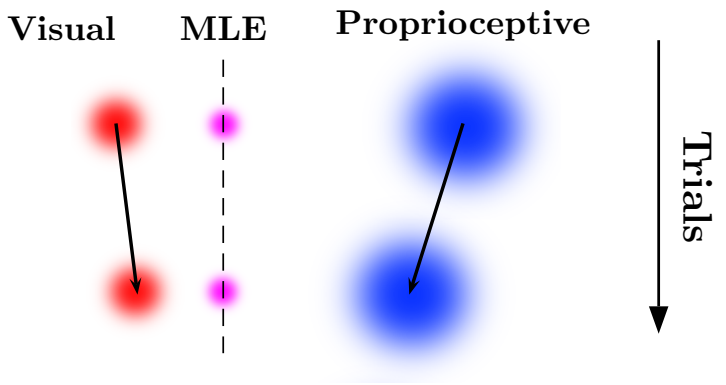

Figure 4.2: Illustration of the MLE-based sensory adaptation model. Visual and proprioceptive estimates are gradually adapted towards the MLE.

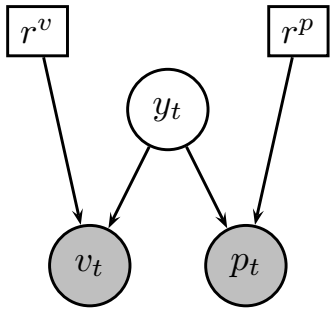

Figure 4.3: Maximum-likelihood adaptation (MLA) model. As figure 4.1, only now unknown disturbances r^v, r^p bias each observations of his hand position. In the MLA model, these are treated as *parameters* of the model. Estimates $\hat{r}_t^v$ and $\hat{r}_t^p$ of these parameters are maintained via an online EM-like procedure.

These adjusted hand position estimates can then be combined according to Equation 4.5 to yield an integrated estimate of hand position which has compensated for the miscalibrations.

4.2.1 Maximum-likelihood based sensory adaptation model

How should subjects adapt their estimates of r^v and r^p? Clearly, the goal is to eliminate any discrepancy between the calibrated hand position estimates $\hat{y}^v$ and $\hat{y}^p$. However, there is a whole family of adaptation rules that would lead to this result, each having different relative adaptation rates for vision and proprioception and therefore leading to different patterns of adaptation. Ghahramani et al. (1997) proposed that the hand position estimates should be adjusted in such a way that the hand position MLE remains unchanged. This principle is illustrated in Figure 4.2. Computationally, this is

achieved by the following update rules for $\hat{r}_t^v$ and $\hat{r}_t^p$:

$$\hat{r}_{t+1}^v = \hat{r}_t^v + \eta w_p \left[\hat{y}_t^p - \hat{y}_t^v\right], \tag{4.12}$$

$$\hat{r}_{t+1}^p = \hat{r}_t^p + \eta w_v \left[\hat{y}_t^v - \hat{y}_t^p\right], \tag{4.13}$$

where η is some fixed adaptation rate and w_v and w_p are the MLE combination weights defined in Equations 4.6 and 4.7. Importantly, the adaptation is driven purely by the discrepancy between the two unimodal estimates of hand position. We will refer to this adaptation model as *maximum likelihood adaptation* (MLA).

As an external observer, we can average out the observation noise the subject experiences to get a clearer idea of the general trends we expect to see in a subject adapting according to these update rules. Noting that $\mathbb{E}[\hat{y}^v] = y + r_t^v - \hat{r}_t^v$ and adopting a more compact notation we can rewrite Equations 4.12 and 4.13 as

$$\mathbb{E}[\Delta\hat{\mathbf{r}}_t] = \eta \begin{pmatrix} -w_p & w_p \\ w_v & -w_v \end{pmatrix} (\mathbf{r}_t - \hat{\mathbf{r}}_t), \tag{4.14}$$

where $\mathbf{r}_t = \begin{pmatrix} r_t^v \\ r_t^p \end{pmatrix}$. Note that while Equations 4.12 and 4.13 are expressed in terms of quantities the subject observes, Equation 4.14 is expressed in terms of the estimation error $\mathbf{r}_t - \hat{\mathbf{r}}_t$. Rewriting the update in this way, however, provides clearer insight into the nature of the adaptation.

An alternative interpretation of this learning rule is as an online expectation-maximization (EM) procedure in the graphical model shown in Figure 4.3. In this model, r^v and r^p are treated as *parameters* of the generative model. The E-step of the EM procedure corresponds to finding the MLE of y_t and the M-step corresponds to gradient ascent on the likelihood of r^v and r^p.

It should be noted that Ghahramani et al. (1997) originally proposed this model in the context of visual/auditory cue integration, offering strong supporting experimental evidence. There is an obvious appeal in generalizing this model to visual/proprioceptive adaptation. There has, however, been no direct attempt to test this model in that context. It has nevertheless proved a popular general theory of sensory adaptation. van Beers et al. (2002) applied this principle to estimate the relative observation uncertainties between vision and proprioception along different directions in space, based on differences in the relative extent of sensory adaptation - directly assuming that sensory adaptation is governed by Equation 4.14.

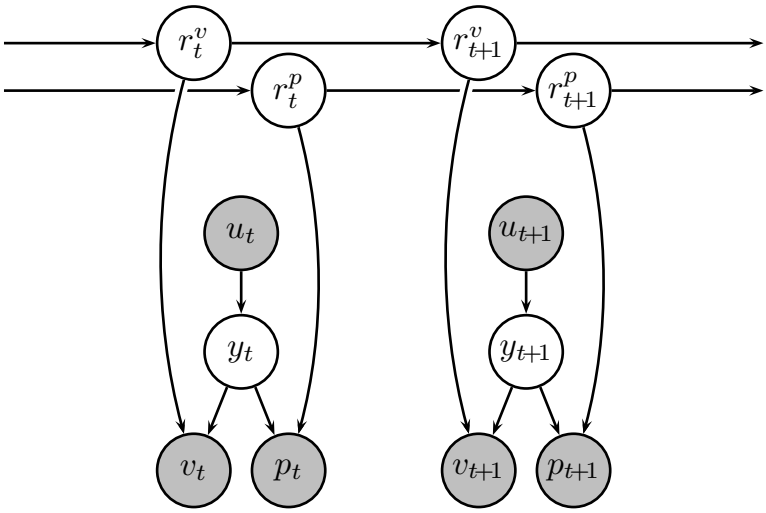

Figure 4.4: Bayesian sensory adaptation model. On each trial, known motor command u_t leads to unknown new hand position y_t. Visual and proprioceptive observations, v_t and p_t are noisy and biased by unknown sensory disturbances r_t^v and r_t^p. These disturbances are also assumed to vary randomly but smoothly between trials.

4.2.2 A Bayesian model of sensory adaptation

The MLE approach treats the miscalibrations r^v and r^p as fixed parameters which are iteratively estimated. In reality, however, it is likely that they are not fixed, but constantly varying. Knowledge of the statistical properties of this variation could potentially be exploited to improve sensory adaptation. While it is reasonable to assume that visual and proprioceptive miscalibrations evolve independently, the rate of variability may be quite different across modalities, and may not necessarily bear any relation to the observation noise. While a greater tendency for, say, proprioception to drift out of calibration could be captured in the model of Ghahramani et al. by inflating the proprioceptive observation uncertainty, a more principled approach to dealing with this issue is to model the variability directly, treating r^v and r^p as dynamic (i.e. time-varying) random variables, rather than fixed parameters. This leads to the generative model illustrated in Figure 4.4.

The subject might assume that each modality drifts out of calibration according to some random walk:

$$r_{t+1}^v = a_v r_t^v + N(0, q^v) \tag{4.15}$$

$$r_{t+1}^p = a_p r_t^p + N(0, q^p). \tag{4.16}$$

Or, more compactly,

$$\mathbf{r}_{t+1} = A\mathbf{r}_t + N(0,Q). \tag{4.17}$$

Here the diagonal matrices A and Q determine the decay rate and the variability of the disturbances respectively. These parameters capture any prior knowledge the subject might have about the nature of visual vs proprioceptive disturbances.

We assume that the subject issues a known motor command u_t which, along with motor execution noise, determines the new hand position

$$y_t = u_t + N(0,\sigma_y^2). \tag{4.18}$$

The observations are given by

$$v_t = y_t + r_t^v + N(0,\sigma_v^2) \tag{4.19}$$

$$p_t = y_t + r_t^p + N(0,\sigma_p^2). \tag{4.20}$$

We can write this in the more usual Kalman filter observation model form as

$$\mathbf{z}_t = H\mathbf{r}_t + \varepsilon_t, \tag{4.21}$$

where $\mathbf{z}_t = \begin{pmatrix} v_t - u_t \\ p_t - u_t \end{pmatrix}$ and H is equal to the 2×2 identity matrix.

$$\begin{pmatrix} v_t \\ p_t \end{pmatrix} = \begin{pmatrix} u_t \\ u_t \end{pmatrix} + \begin{pmatrix} 1 & 0 \\ 0 & 1 \end{pmatrix} \mathbf{r}_t + \varepsilon_t, \tag{4.22}$$

with $\varepsilon_t \sim N(0,R)$ and

$$R = \begin{pmatrix} \sigma_v^2 + \sigma_u^2 & \sigma_u^2 \\ \sigma_u^2 & \sigma_p^2 + \sigma_u^2 \end{pmatrix}. \tag{4.23}$$

The subject adapts by inferring the total disturbance $\mathbf{r}_t$ on each trial based on his prior, characterized by mean $\hat{\mathbf{r}}_{t|t-1}$ and uncertainty $P_{t|t-1}$, and the observations $\mathbf{z}_t$, leading to a posterior estimate with mean $\hat{\mathbf{r}}_{t|t}$ and uncertainty $P_{t|t}$.

Importantly, the covariance matrix of the observation noise is *not* diagonal. This is because the motor execution noise induces correlations between the visual and proprioceptive observations of hand position. As a result, there will typically be correlations in the estimates of r^v and r^p. In other words, if $p(\mathbf{r}_t) \sim N(\hat{\mathbf{r}}_{t|t}, P_{t|t})$ is the subject's posterior estimate after trial t, $P_{t|t}$ may not be diagonal.

Due to the linear relationships and Gaussian noise models we have assumed, inference in this model is equivalent to Kalman filtering. Details of the Kalman filter

updates are provided in Appendix A. Ultimately, the KF framework leads to the following update of the disturbance estimate:

$$\hat{\mathbf{r}}_{t|t} = A(\hat{\mathbf{r}}_{t-1|t-1} + K_t(\mathbf{z}_t - H\hat{\mathbf{r}}_{t|t-1})). \tag{4.24}$$

Assuming, for simplicity that A is the identity matrix (in practise it is usually estimated to be very close), we can average over the observation noise and find the expected update

$$\mathbb{E}\left[\Delta\hat{\mathbf{r}}_{t|t}\right] = K_t H(\mathbf{r}_t - \hat{\mathbf{r}}_t). \tag{4.25}$$

As in Equation 4.14, the update is linear in the subject's estimation error. Furthermore, since the model itself is stationary (i.e. H, Q and R don't vary over time), the Kalman gain K_t will converge to a constant.

One advantage of this model over the MLA model is that the various sources of uncertainty are represented as distinct parameters which have clear interpretations in a generative model. There is no arbitrary learning rate - the learning rate emerges as a consequence of the noise parameters.

Another important difference, however, between this and the MLA model is the presence of a prior on the hand position y_t. This is naturally provided by the motor command u together with the associated motor execution noise σ_u^2, both of which are assumed to be known to the subject. Effectively this constitutes a prediction based on a forward model of the hand. Using this additional information enables comparison with the ground truth. If both vision and proprioception shifted equally in the same direction, there would be no way of recognizing this in the MLA model. In the KF model, however, this could be recognized and adapted to accordingly.

The MLE model can easily be amended to include the extra knowledge available from the motor command u, in which case updates very similar to the Kalman filter model can be obtained. Let us assume an additional estimate $\hat{y}_t^u = u_t$ is available, with a corresponding weight w_u, so that the full MLE, integrating 3 modalities now is given by

$$\hat{y}_t = w_v(v_t - \hat{r}_t^v) + w_p(p_t - \hat{r}_t^p) + w_u u_t. \tag{4.26}$$

Note that w_v and w_p will now be correspondingly smaller, so that $w_v + w_p + w_u = 1$. We assume the updates in this case are obtained by adapting both visual and proprioceptive estimates toward the MLE. The resulting update is given by

$$\mathbb{E}[\Delta\hat{\mathbf{r}}_t] = \eta \begin{pmatrix} (1-w_v) & w_p \\ w_v & (1-w_p) \end{pmatrix} (\mathbf{r}_t - \hat{\mathbf{r}}_t). \tag{4.27}$$

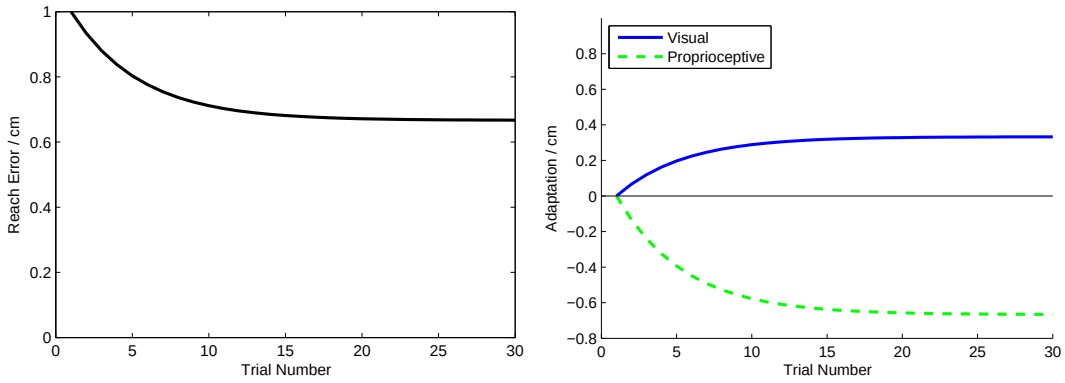

Figure 4.5: Pattern of reach errors (left) and sensory recalibration (right) over 30 trials, as predicted by the MLA sensory adaptation model (described in Section 4.3.1) following exposure to a 1cm shift in visual feedback.

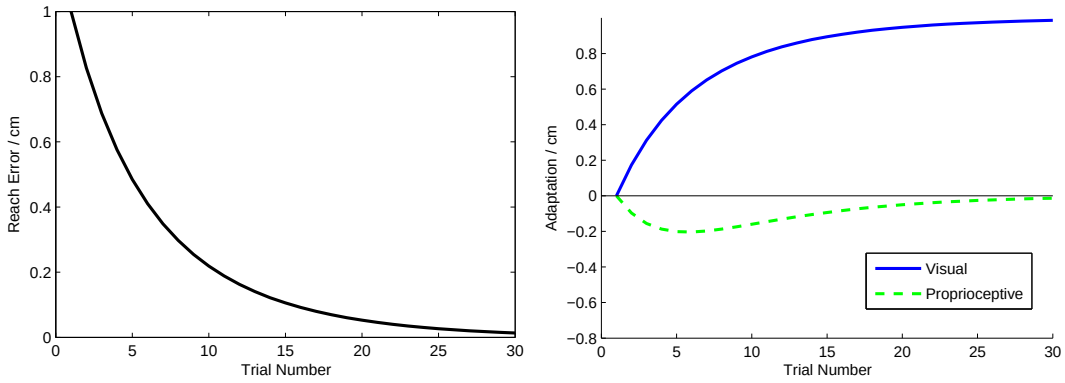

Figure 4.6: Pattern of reach errors (left) and sensory recalibration (right) over 30 trials, predicted by the Bayesian sensory adaptation model (described in Section 4.3.1) following exposure to a 1cm shift in visual feedback.

Note that the earlier MLA model is a special case of this one in which $w_v = 1 - w_p$.

If this matrix has full rank, adaptation will be asymptotically exact. The determinant is given by

$$\det M = w_p(w_v - 1)w_v(w_p - 1) - w_v^2 w_p^2 = w_v w_p(1 - w_v - w_p), \tag{4.28}$$

implying that the matrix is degenerate if $w_v + w_p = 1$, which is only the case when we assumed no prior knowledge about hand position from a forward model.

In this case, however, the MLE itself becomes biased towards the motor prediction. Both the visual and proprioceptive estimates will ultimately converge on the motor prediction, leading ultimately to identical predictions to the Kalman filter filter model.

In order to examine the differences between these models more clearly, we consider a toy scenario in which subjects perform reaching movements to a visual target under

shifted visual feedback. The subject observes the target at a location v_t^* in his visual field. The subject chooses his motor command to be $u_t = v_t^* - \hat{r}_t^v$ so that the final observed hand position matches that of the target, i.e. $\mathbb{E}[v_t] = v_t^*$. He then receives actual observations v_t and p_t. Figure 4.5 shows how sensory adaptation and improvements in reaching are predicted to proceed by the MLA sensory adaptation model. Predictions of the Bayesian sensory adaptation model are shown in Figure 4.6.

The MLA model appropropriately predicts that adaptation will be partly visual and partly proprioceptive, but fails to capture completeness of reach adaptation, since reach performance only improves by as much as vision is recalibrated. The Bayesian model predicts complete reach adaptation, but only because, ultimately, 100% of the sensory adaptation is visual, which does not agree with experimental data. Some transient proprioceptive adaptation is predicted early on, but this component disappears before reach adaptation becomes complete.

This poses a problem. Both models predict some aspects of experimental data well, but neither model seems satisfactory. In the next Section we consider possible ways to extend these purely sensory adaptation models to include a motor component of adaptation, which will enable accurate predictions about both sensory adaptation and reach performance.

4.3 Interactions between sensory and motor adaptation

We would like to have a model of reach adaptation which is able to predict the trends in both sensory recalibration and reach performance. As we saw in the simulations in the previous section, models based purely on sensory adaptation are unable to achieve this: We know that visual adaptation during reaching is incomplete, i.e. the amount of adaptation is less than the imposed disturbance. If we assume, as we have done above, that planning of feedforward reaching movements depends only on vision, then we can never have a situation where reach adaptation is complete but visual adaptation is incomplete. The fact that subjects learn to successfully reach the target despite incomplete visual recalibration suggest that they additionally learn a correction to their movements as well as recalibrating their senses.

This idea has been suggested frequently in the past (HARRIS, 1963; Welch, 1974; Redding and Wallace, 1996). A particularly clear demonstration of this additional component of adaptation was provided by Simani et al. (2007). In their study, one group of subjects performed reaching movements, while another group performed a

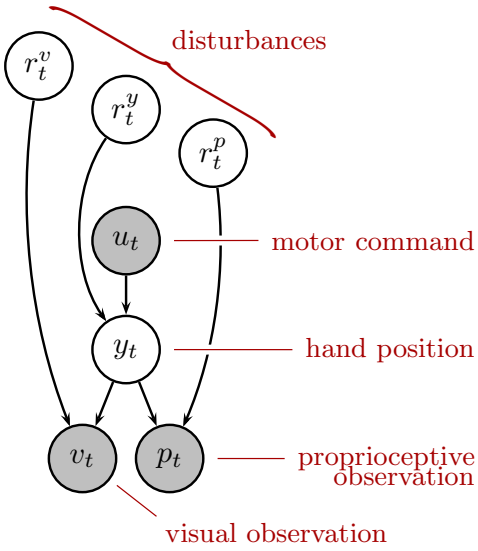

Figure 4.7: Graphical model of a single reach in a motor adaptation experiment. Motor command u_t, and visual and proprioceptive observations of hand position, v_t and p_t, are available to the subject. Three distinct disturbances affect observations: A motor disturbance r_t^y may affect the hand position y_t given the motor command u_t. Visual and proprioceptive disturbances, r_t^v and r_t^p, may affect the respective observations given hand position.

tracking task. While the extent of sensory adaptation was about the same for both groups, the group which performed reaching movements during exposure exhibited a significantly stronger reach aftereffect. This result, in particular the fact that subjects who performed a tracking task during exposure exhibited such a small reach aftereffect, strongly suggests that the subjects who performed reaching during exposure, were able to do so through an additional component of adaptation. We refer to this component as a *motor component* of adaptation, distinguishing it from the sensory components corresponding to recalibrations of vision and proprioception.

4.3.1 Independent sensory and motor adaptation model

Although no explicit computational model of concurrent sensory and motor adaptation has been previously proposed, it is straightforward to augment the MLA model of sensory adaptation model, described above, with a state-space model, as described in Section 2.3, describing the adaptation of an additional motor component of adaptation $\hat{r}^y$. The observed hand position error $\tilde{y}$ in Equation 2.13 can be replaced with the difference between the desired hand position, and the MLE of hand position $\hat{y}^{MLE}$.

This leads to the following adaptation rule for the motor component of adaptation:

$$\hat{r}^y_{t+1} = \hat{r}^y_t + \gamma(\hat{y}^*_t - \hat{y}^{MLE}_t), \tag{4.29}$$

where $\hat{y}^*_t = (v^* - \hat{r}^v_t)$ is the estimated desired hand location, and γ is some fixed adaptation rate.

We can expand Equation 4.29, using the fact that $u_t = v^*_t - \hat{r}^v_t$, along with the expression for $\hat{y}^{MLE}_t$ given in Equation 4.5, to obtain.

$$\mathbb{E}[\Delta\hat{\mathbf{r}}_t] = \gamma\left[-w_v r^v_t - w_p r^p_t - 1\right]. \tag{4.30}$$

Taking this motor adaptive component together with the sensory adaptation model of Ghahramani et al., the overall update for this model is given by

$$\Delta\hat{\mathbf{r}}_t = \eta \begin{pmatrix} w_p & -w_p & 0 \\ -w_v & w_v & 0 \\ -\gamma w_v & -\gamma w_p & -\gamma \end{pmatrix} (\mathbf{r}_t - \hat{\mathbf{r}}_t). \tag{4.31}$$

This combined model encapsulates a tacit assumption which is commonly made - that sensory and motor adaptation are distinct processes. The sensory adaptation component is driven purely by discrepancy between the senses, as in the model by Ghahramani et al. (1997), while the motor adaptation component only has access to a single, fused estimate of hand position and is driven purely by estimated performance error.

4.3.2 Unified Bayesian sensory and motor adaptation model

Rather than constructing an overall model of sensory and motor adaptation from existing models covering various sub-components of the problem, a normative, Bayesian approach considers a full generative model of the problem at hand and asks how the nervous system should adapt given this model.

We extend the generative model to include an unknown motor disturbance r^y_t. The generative model for a single trial is illustrated in Figure 4.7. This motor disturbance affects the relationship between the motor command u_t and hand position y_t,

$$y_t = u_t + r^y_t + N(0, \sigma^2_y). \tag{4.32}$$

As before, the subject does not observe the hand position directly, but receives noisy and potentially shifted visual and proprioceptive observations, according to Equations 4.19 and 4.20. The subject selects his actions so that $\mathbb{E}\left[y_t | \hat{\mathbf{r}}_{t|t-1}\right] = 0$,

$$u_t = v_t - \hat{r}^y_{t|t-1} - \hat{r}^v_{t|t-1}. \tag{4.33}$$

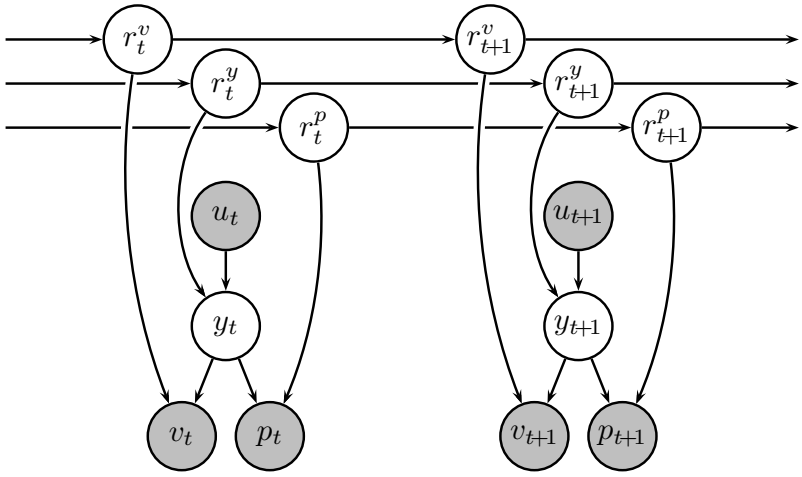

Figure 4.8: Bayesian combined sensory and motor adaptation model. As in 4.7, only now the subject assumes that disturbances vary randomly, but smoothly, from trial to trial.

As before, the latent state dynamics are characterized by a random walk

$$\mathbf{r}_{t+1} = A\mathbf{r}_t + N(0,Q), \tag{4.34}$$

now with $\mathbf{r} = \begin{pmatrix} r_t^v \\ r_t^p \\ r_t^y \end{pmatrix}$, $A = \begin{pmatrix} a^v & 0 & 0 \\ 0 & a^p & 0 \\ 0 & 0 & a^y \end{pmatrix}$, $Q = \begin{pmatrix} q^v & 0 & 0 \\ 0 & q^p & 0 \\ 0 & 0 & q^y \end{pmatrix}$. Again, these parameters summarize the statistics of the usual fluctuations in sensory calibration errors and motor plant dynamics, which the sensorimotor system must adapt to on an ongoing basis, reflecting the fact that the subject is able to utilize prior knowledge about the disturbances to improve estimation and therefore adaptation. This leads to a dynamic generative model, which is illustrated in Figure 4.8. This model gives a complete probabilistic description of how a subject's observations will depend on the disturbances, and how these disturbances may vary from trial to trial.

As in the purely sensory adaptation model in the previous section, the observations can be easily expressed as a linear combination of the latent disturbances:

$$\mathbf{z}_t = H\mathbf{r}_t + \varepsilon_t, \tag{4.35}$$

with $\mathbf{z} = \begin{pmatrix} v_t - u_t \\ p_t - u_t \end{pmatrix}$, $\varepsilon \sim N(0,R)$ and $R = \begin{pmatrix} \sigma_v^2 + \sigma_u^2 & \sigma_u^2 \\ \sigma_u^2 & \sigma_p^2 + \sigma_u^2 \end{pmatrix}$ as in the pure sensory adaptation model, but now $H = \begin{pmatrix} 1 & 0 & 1 \\ 0 & 1 & 1 \end{pmatrix}$. Full details of the Kalman filter

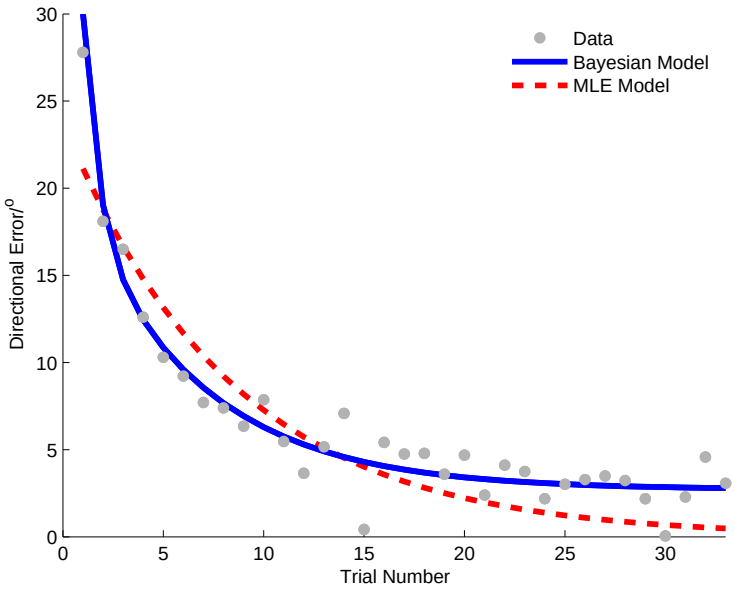

Figure 4.9: Model comparison with visuomotor adaptation data. The Bayesian model (solid blue line) and MLE-based model (dashed red line) were fitted to performance data (filled circles) from a visuomotor adaptation experiment (Krakauer et al., 2006). Both models made qualitatively similar predictions about how adaptation was distributed across components.

updates are given in Appendix A. The expected update to the mean (i.e. neglecting observation noise) is given by

$$\mathbb{E}[\Delta\hat{\mathbf{r}}_t] = K_t H(\mathbf{r}_t - \hat{\mathbf{r}}_t). \tag{4.36}$$

The Kalman gain K_t is now a 2-by-3 matrix, which converges to a constant provided A, Q, H and R remain constant.

We have described two alternative models of visuomotor adaptation which we have claimed can account for both the motor and sensory components of adaptation. We fitted both models to performance data from a visuomotor adaptation experiment (Krakauer et al., 2006) to validate this claim. In this study in which this data was taken from, subjects performed visually guided reaching movements to a number of targets. Visual feedback of hand position (given via a cursor on a screen) was rotated by 30^o relative to the starting position of each movement. The mean directional error (averaged over targets and over subjects) over trials is plotted in Figure 4.9. The Matlab function `lsqnonlin` was used to find the parameters for each model which minimized the sum of the error between the data and the predictions of each model. Since only the values of the noise coefficients relative to one another were relevant to the adapta-

tion, we assumed that the motor noise σ_u^2 was equal to 1. This left 4 free parameters for the MLE-based model $(\sigma_v^2, \sigma_p^2, \eta, \gamma)$. For the Bayesian model we assumed that all disturbances had the same timescale, i.e. all elements of **a** were the same, leaving 6 free parameters $(\sigma_v^2, \sigma_p^2, q^v, q^p, q^u, a)$. The results of the fits are shown in Figure 4.9. The spread of adaptation across components of the model was qualitatively similar between the two models, although no data on perceptual aftereffects was available from this study for quantitative comparison. The Bayesian model clearly displays a closer fit to the data and the Akaike information criterion (AIC) confirmed that this was not simply due to extra parameters ($AIC = 126.7$ for the Bayesian model vs $AIC = 159.6$ for the MLE-based model).

Although the Bayesian model appears to describe the data better, this analysis is by no means conclusive. Furthermore, the similar scope of predictions between the two models means that gathering additional data from alignment tests may not provide any further leverage to distinguish between the two models. There is, however, a more striking difference in predictions between the two models. While the MLE-based model predicts there will be sensory adaptation *only* when there is a discrepancy between the senses, the Bayesian model predicts that there will also be sensory adaptation in response to a motor disturbance such as an external force applied to the hand). Just as a purely visual disturbance can lead to a multifaceted adaptive response, so can a purely motor disturbance, with both motor and sensory components predicted, even though there is never any discrepancy between the senses.

This occurs because there are three unknown disturbances, but only two observations on each trial. There are therefore many combinations of disturbances which can account for the observations on each trial. Because of the subject's assumptions about how the disturbances vary over time (i.e. Equation 7.10), explanation which assign credit to all three disturbances are more likely than the true disturbance which was experienced.

This prediction enables us to distinguish decisively between the two models. The hypothesis that movement errors caused by motor disturbances leads to sensory adaptation is easily tested, which we do in the next chapter. Before proceeding to the details of the experiment, however, we briefly describe how the MLA model can be extended to include three components of adaptation, rather than 2. This 3-component MLA model, gives rise to the same qualitative predictions as the Bayesian model.

4.3.3 Sensory/motor MLA model

The maximum-likelihood based sensory adaptation model can be extended to include an additional motor component of adaptation. This yields a corresponding third estimate of hand position $\hat{y}_t^u$ which can be understood as a forward model prediction of hand position given previous motor commands. We now have three estimates of hand position:

$$\hat{y}_t^v = v_t - \hat{r}_t^v \tag{4.37}$$

$$\hat{y}_t^p = p_t - \hat{r}_t^p \tag{4.38}$$

$$\hat{y}^u = u_t + \hat{r}_t^y. \tag{4.39}$$

As in the two-disturbance case, the disturbance estimates are updated in such a way that these estimates gradually converge towards the MLE, which in this case is given by

$$\hat{y}_t^{MLE} = w_v \hat{y}_t^v + w_p \hat{y}_t^p + w_u \hat{y}_t^u. \tag{4.40}$$

This leads to a similar set of update rules to before.

The maximum likelihood estimate (MLE) $\hat{y}_t$ of the true hand position y_t is given by

$$\hat{y}_t = w_v \hat{y}_t^v + w_p \hat{y}_t^p + w_u \hat{y}_t^u, \tag{4.41}$$

where $w_v = \frac{\sigma_v^{-2}}{\sigma_v^{-2}+\sigma_p^{-2}+\sigma_u^{-2}}$, with the weights for the other modalities defined analagously.

According the MLE principle, each disturbance estimate is updated by adjusting that estimate towards the MLE in such a way that the MLE remains unchanged. This is achieved by adapting the estimate for each modality towards the MLE as follows:

$$\Delta \mathbf{r} = \eta \Omega \begin{pmatrix} \hat{y} - \hat{y}^v \\ \hat{y} - \hat{y}^p \\ \hat{y} - \hat{y}^u \end{pmatrix}, \tag{4.42}$$

where η is some fixed adaptation rate and

$$\Omega = \begin{pmatrix} w_v - 1 & 0 & 0 \\ 0 & w_p - 1 & 0 \\ 0 & 0 & 1 - w_u \end{pmatrix}. \tag{4.43}$$

Note that the change in r_t^u is opposite in sign to those for r^v and r^p, since this component is *added* to the motor command, rather than subtracted when calculating the corresponding hand position estimate.

This three-component MLA model (MLA3) shares many of the properties of the Bayesian model. The update equation for the Bayesian model is simply given by the Kalman filter update equation:

$$\Delta\hat{\mathbf{r}} = KH(\mathbf{r} - \hat{\mathbf{r}}). \tag{4.44}$$

Here, K is the Kalman gain, and H is the disturbance-observation matrix $\begin{pmatrix} 1 & 0 & 1 \\ 0 & 1 & 1 \end{pmatrix}$.

A similar linear update rule can also be derived for the MLE-based model. We can expand $\hat{y} - \hat{y}^v$ using Equations 4.37 and 4.41, leading to

$$\hat{y}_t - \hat{y}_t^v = (w_v - 1)(r_t^v - \hat{r}_t^v) + w_p(r_t^p - \hat{r}_t^p) + w_u(\hat{r}_t^y - r_t^u), \tag{4.45}$$

which is linear in $(\mathbf{r}_t - \hat{\mathbf{r}}_t)$. Similar expressions follow for $\hat{y}_t - \hat{y}_t^p$ and for $\hat{y}_t - \hat{y}_t^u$, resulting in

$$\Delta\mathbf{r}_t = \eta\Omega \begin{pmatrix} w_v - 1 & w_p & -w_u \\ w_v & w_p - 1 & -w_u \\ w_v & w_p & 1 - w_u \end{pmatrix} (\mathbf{r}_t - \hat{\mathbf{r}}_t). \tag{4.46}$$

This recovers an update rule of the same form as Equation 4.44.

4.4 Summary

In this chapter, we have examined models of sensory adaptation, comparing previous models in which sensory adaptaiton is driven purely by sensory discrepancy, with a Bayesian model in which disturbances are inferred from observations based on a full generative model of disturbances and observations.

In the next chapter, we test the strong prediction made by the Bayesian model that movement errors caused by a perturbing force field will lead to sensory adaptation, as well as motor adaptation to the force field. Note that this prediction is shared by the 3-component MLA model described immediately above.

Chapter 5

Experimental Methods and Results

In Chapter 4, we derived a model of concurrent sensory and motor adaptation based on the principle that adaptation proceeds according to Bayesian inference of disturbances given observed errors. Whereas previous models have supposed that sensory adaptation is driven purely by discrepancy between sensory modalities and is independent of movement errors, our Bayesian model predicts a strong coupling between sensory and motor adaptation. In particular, it predicts that adaptation to a force field, in which there are movement errors but no discrepancy between vision and proprioception, will also lead to sensory adaptation. In this chapter we describe experiments which tested and confirmed this hypothesis. Table 5.1 provides a summary of all the experiments reported in this chapter.

5.1 Experimental setup and design

11 right-handed subjects performed a series of trials consisting of reaching movements interleaved with perceptual alignment tests. Subjects grasped the handle of a robotic manipulandum with their right hand throughout the experiment. This hand was not visible directly, but a cursor was displayed via a mirror/flat screen monitor setup (Figure 5.1(a)) to be exactly co-planar and aligned with the handle of the manipulandum. In the movement phase, subjects made an out-and-back reaching movement towards a visual target with their right hand. The visual target was randomly selected from a group of 5 targets all located 15cm from the starting hand position, but distributed along an arc +/- 5°around the straight-ahead direction. In the visual localization phase, a visual target was displayed randomly in one of the same 5 positions and the subjects moved their left fingertip, which was also not visible, to the perceived location of the target. In

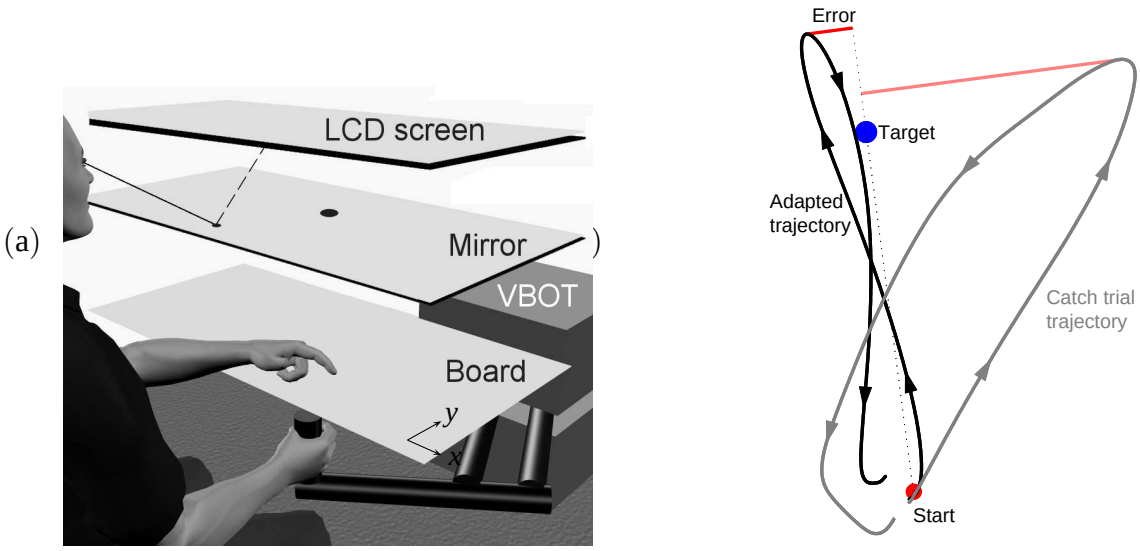

Figure 5.1: (a) Experimental Setup, (b) Sample trajectories and performance error measure

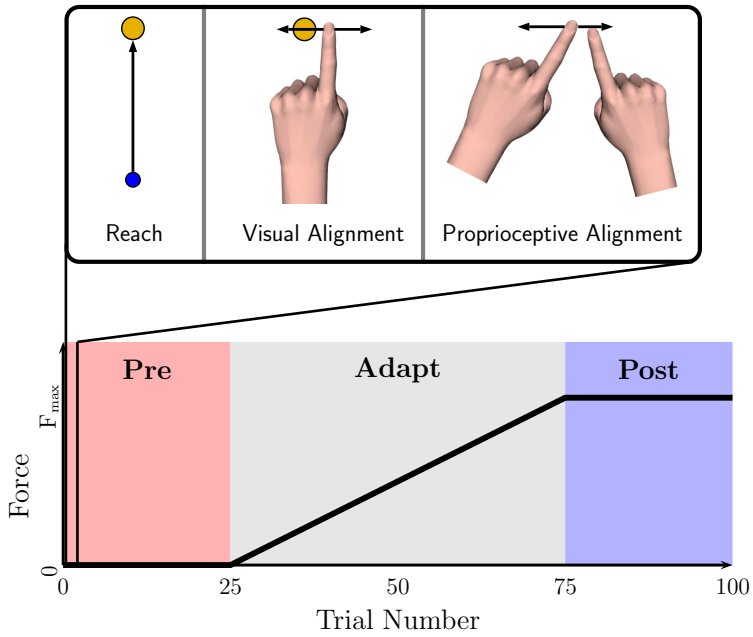

Figure 5.2: Experimental procedure. Experiment consisted of 100 trials. Each trial consistent of three phases: A reaching movement, a visual alignment test and a proprioceptive alignment test. A velocity-dependent force was applied to the hand during the reaching movements, the strength of which was increased from 0 to maximum between trials 26-75.

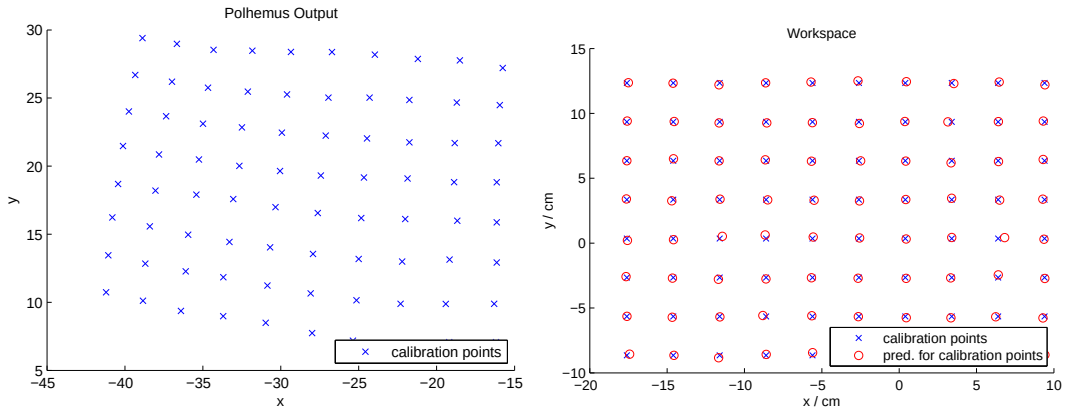

Figure 5.3: Distortion of the electromagnetic position tracking system (a) and recalibration (b).

the proprioceptive localization phase, the right hand was passively moved to a random target location (selected from the same 5 locations as before) with no visual cue of its position, and subjects moved their left fingertip to the perceived location of the right hand. Neither hand was directly visible at any time during the experiment. Subjects were given a tactile marker to mark a 'home' position for their left hand, where they held their left hand in between alignment tasks.

Left fingertip positions were recorded using an electromagnetic Polhemus motion tracker. Optical tracking was not practical due to occlusion issues. The presence of metallic objects around the workspace led to some distortion of the magnetic field and consequently distortion of the position measurements obtained. This was compensated for through a recalibration of the motion tracker: The output of the Polhemus tracker was measured at points on a uniform grid in the workspace with a spacing of 2cm. The mapping from the Polhemus output to the true location on the calibration grid was estimated using Gaussian process regression (Rasmussen and Williams, 2006) (see Figure 5.3), which was found to lead to very reliable reconstruction of the calibration grid and smooth interpolation between sampled points.

Subjects were given 25 baseline trials with zero external force, after which a force field was gradually introduced. A leftward lateral force was applied to the right hand during the reaching phase, the magnitude of which was proportional to the forward velocity $\dot{y}$ of the hand, i.e.

$$F_x = -a\dot{y}. \tag{5.1}$$

The force was applied only on the outward part of the movement (i.e. only when $\dot{y} > 0$). After steadily incrementing a during 50 adaptation trials, the force field was then kept

Table 5.1: Summary of experiments. See text for details of different conditions.

	Force dir.	Reach type	Drift test?	Tactile marker?
Exp. 1	L only	Out and back	No	Yes
Exp. 2	L and R	Out only	No	Yes
Exp. 3	L and R	Out and back	Yes	Yes
Exp. 4	L and R	Out only	No	No

constant at $a = 0.3\,N/(cms^{-1})$ for a further 25 post-adaptation test trials. All subjects received a catch trial after the final test trial, in which the force field was turned off.

The particular force field used was chosen so that the cursor trajectories (and motor commands required to counter the perturbation) would be as close as possible to those used to generate the linear trajectories required when exposed to a visuomotor shear (such as was used by van Beers et al. (2002)). Figure 5.1(b) shows two trajectories from a typical subject, one from the post-adaptation test phase and one from the catch trial after adaptation. During the initial outward part of the catch trial trajectory, the initial movement is very straight, implying that similar motor commands were used to those required by a visuomotor rotation or shear.

5.2 Experiment 1 results

5.2.1 Force field adaptation leads to sensory adaptation

We compared the average performance in the visual and proprioceptive alignment tests before and after adaptation in the velocity-dependent force field. The results are summarized in Figure 5.4(a). Most subjects exhibited small but statistically significant shifts in performance in both the visual and proprioceptive alignment tests. Two subjects exhibited shifts which were more than two standard deviations away from the average shift and were excluded from the analysis. We found significant lateral shifts in both visual and proprioceptive localization error in the direction of the perturbation (both $p < .05$, one-tailed paired t-test). Figure 5.4(b) shows the same data for the direction perpendicular to the perturbation. The initial alignment bias in this direction was, surprisingly, quite high (around 10cm). There was no shift in alignment bias in either modality, which is consistent with the fact that there was no perturbation in that direction.

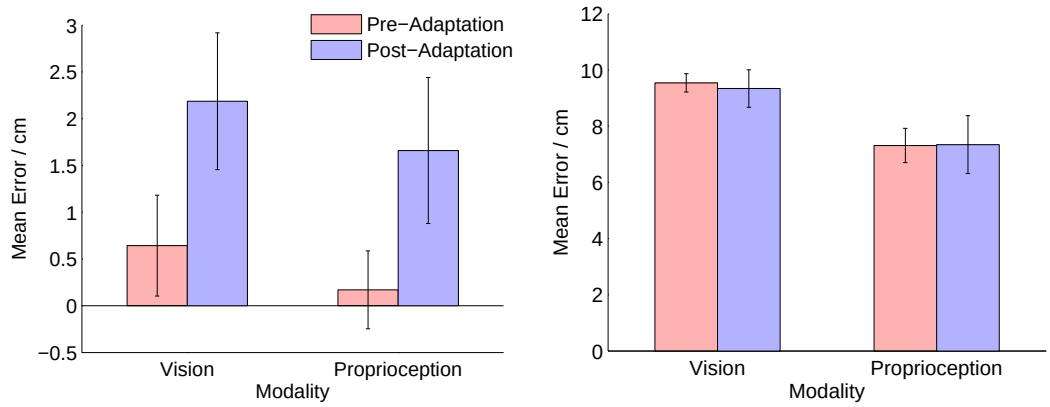

(a) x-direction (b) y-direction

Figure 5.4: (a) Average lateral (in direction of the perturbation) localization error across subjects before vs after adaptation, for vision and proprioception. Error bars indicate standard errors. (b) Same plots for y-direction

The amount of sensory adaptation varied substantially between subjects. After applying a Bonferroni correction, we found that 3 of the 12 subjects exhibited a significant shift in visual alignment bias, and 4 of the 12 subjects exhibited significant shifts in proprioceptive alignment bias ($p < .05$, two-tailed t-test with Bonferroni correction applied). Figure 5.5 illustrates the data for all subjects. Visual and proprioceptive shifts were positively correlated ($r = .5923$).

5.2.2 Model fits to data

We quantified subjects' performance in the reaching task as the perpendicular distance between the furthest point in the trajectory and the straight line passing through both the start position and the target (Figure 5.1(b)). We fitted the Bayesian model and the distinct sensory/motor MLA/SS model to the average data measured across subjects by finding parameters which minimized the squared error between the mean predictions of the model (i.e. when simulated without any noise) and the mean subject performance. Performance in the reaching, visual alignment and proprioceptive alignment tasks were weighted equally. The model predictions for the alignment test were additionally offset by the mean subject alignment error over the first 25 trials, in order to compensate for the initial bias exhibited by subjects. The Matlab function `lsqnonlin` was used to perform the optimization.

Figure 5.6 illustrates the averaged data along with the optimized fits for both mod-

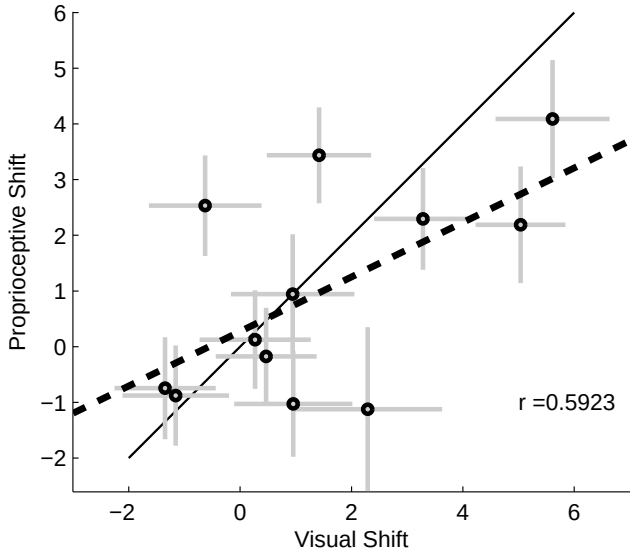

Figure 5.5: Correlation between visual alignment shift and proprioceptive alignment shift following force field adaptation. Each data point represents a single subject. Grey bars indicate standard error in the shift estimates for each subject in each modality. Solid black line represents line of equality between visual and proprioceptive shifts. Dashed black line represents line of best fit to the data.

els. Both models were able to account reasonably well for the trends in reaching performance across trials (Figure 5.6(a)). Note that since the force field was introduced incrementally, the errors remained small, therefore the motor execution noise tends to dominate. Figures 5.6(b) and 5.6(c) show the model fits for the perceptual localization task. The Bayesian model is able to account for both the extent of the shift and the timecourse of this shift during adaptation. Since there was never any discrepancy introduced between vision and proprioception, the MLA/SS model predicted no change in performance in these tasks.

5.3 Experiment 2: Controlling for left hand proprioceptive drift

The results of the previous section strongly support the Bayesian model. As predicted by the model, we observed rightward shifts in alignment bias following adaptation to a leftward force field. In the previous section, we assumed that these changes were caused by recalibrations of the visual and right-hand proprioceptive estimates of hand

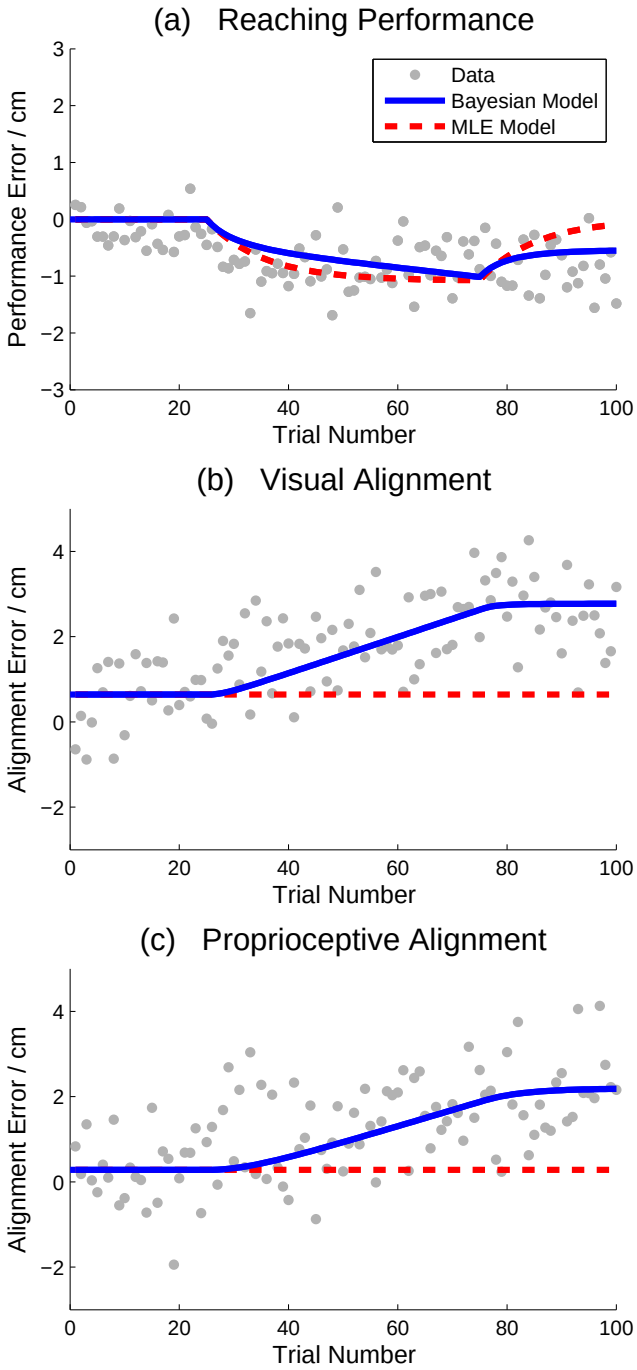

Figure 5.6: Trial-by-trial data and model fits. (a) Reaching error, (b) Visual alignment test error, (c) Proprioceptive alignment test error. The Bayesian (solid blue lines) and MLE-based (dashed red lines) were fitted to averaged data across subjects (circles).

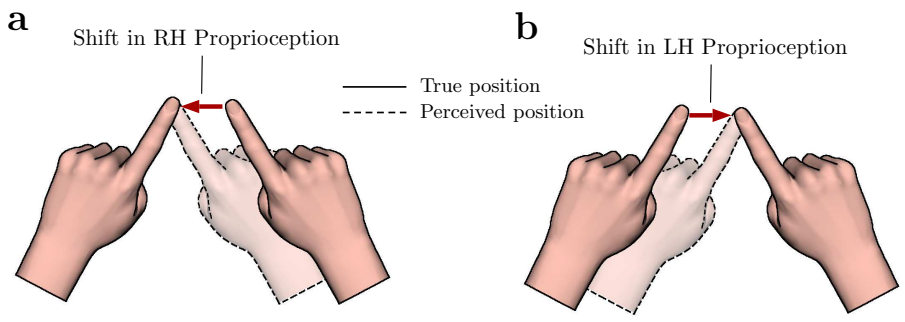

Figure 5.7: Two alternative causes of a shift in proprioceptive alignment bias. A measured *leftward* shift could be due to either: (a) a leftward shift in right hand proprioception, *or* (b) a rightward shift in left hand proprioception. interpretations of the results of Experiment 1.

position. However, the LH to RH alignment tests only enable us to measure the *relative* calibration between LH and RH proprioception.A rightward shift in proprioceptive alignment bias might equally have been caused by a leftward shift in left hand proprioception. These alternative causes of an observed shift in alignment in alignment test peformance are illustrated in Figure 5.7. The shift in alignment bias could also clearly be caused by a combination of shifts in left hand and right hand proprioception. The same is true for shifts in visual alignment bias.

Since the shifts in the LH-VIS and LH-RH alignment tests were comparable, a plausible alternative interpretation of our result is that the shifts in visual and proprioceptive alignment biases were caused by a single shift in LH proprioception, rather than separate, correlated shifts in RH and VIS. If the results were due to a shift in LH proprioception, this would likely be unrelated to the force field which was applied to the right hand, and could simply reflect a natural bias for LH to drift toward the left.

To control for this possibility, we tested a further two groups of subjects. This time, half of the subjects received a rightward force, while the other half received a leftward force. As in Experiment 1, the magnitude of the force was proportional to the forward velocity of the hand. In this second experiment, we had subjects perform outward-only reaches, rather than the out-and-back reversal movements used in Experiment 1. Since proprioceptive drift is known to be exacerbated by movement (Desmurget et al., 2000; Brown et al., 2003), we kept movement of the left hand to a minimum in Experiment 2 by only having subjects perform the alignment tests in the baseline and testing blocks, and not during the middle block of 50 adaptation trials.

If the results in Experiment 1 were caused by a tendency for left hand proprioceptive

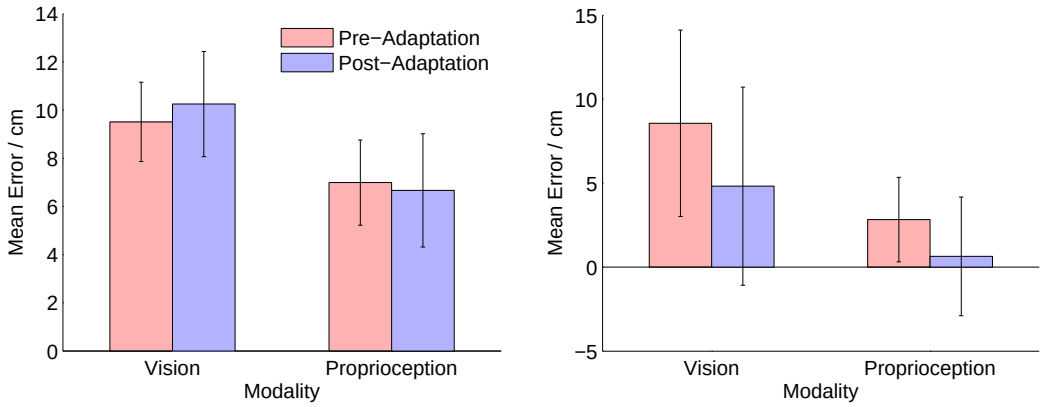

(a) Leftward force (b) Rightward force

Figure 5.8: Comparison of alignment test performance before vs after adaptation, in 5.8(a) leftward force and 5.8(b) rightward force groups.

tion to drift to the left, independently of the presence of the force field, then we would expect there to be no difference between the two groups. However if the alignment test shifts really were directly caused by adaptation to the force field, then we would expect to see opposite shifts in the two groups.

5.3.1 Experiment 2 results

6 subjects received a leftward force and 6 subjects received a rightward force. Figure 5.8 compares the alignment biases before and after adaptation for both groups. There is a clear difference in patterns of adaptation between subjects who received a leftward force and subjects who received a rightward force. The *shift* in visual alignment bias exhibited by the leftward force group was significantly different from that exhibited by the rightward group ($p < .05$, 1-tailed t-test). The shifts in proprioceptive alignment bias were not found to be significant ($p = .495$, 1-tailed t-test).

Figure 5.9 shows visual and proprioceptive shifts for all subjects. There is a clear distinction between leftward and right force groups. Visual and proprioceptive shifts across the two groups were correlated ($r = .653$).

The mean visual shift across all subjects (leftward and rightward) was around 1cm to the left, and this was comparable with the mean shift in proprioception. This can likely be attributed to proprioceptive drift in the left hand having a slight rightward bias, i.e. subjects tended to believe their left hand was further to the right than it actually was.

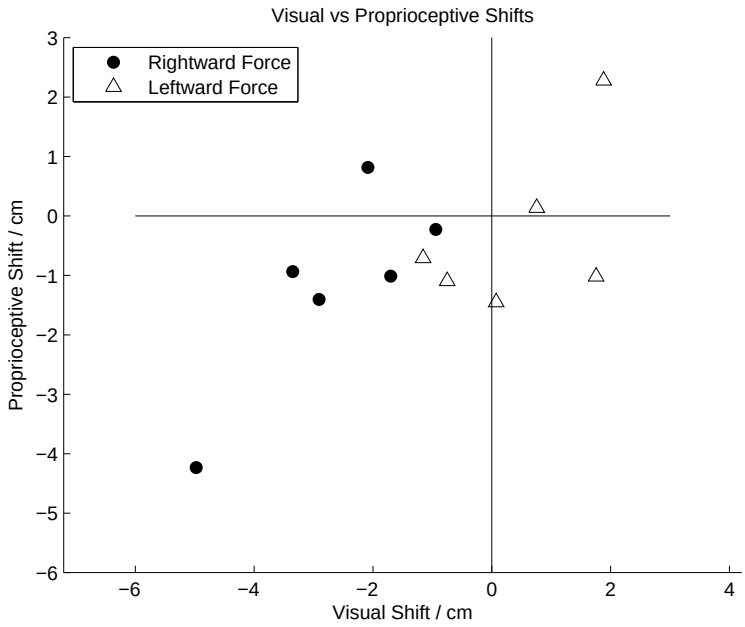

Figure 5.9: Summary of individual subjects. Each point represents a single subject. Filled circles indicate rightward force subjects. Open triangles represent leftward force subjects.

The lack of a significant shift in proprioception is at odds with the results of Experiment 1. There were two principle differences in experimental methods that may have accounted for this: i) Movements were out-and-back in Experiment 1, but outward-only in Experiment 2. ii) The experimental setup was slightly different in Experiment 2, possibly leading to slightly greater visibility of the upper arms. It is not clear, however, how these differences might lead to a stronger effect on vision than proprioception.

5.4 Additional Experiments

In addition to Experiments 1 and 2, we also performed two experiments which were less succesful in finding significant differences between leftward and rightward force conditions. The experimental setup in these further two experiments were slightly different to the other two experiments, as explained below. We include the results of these experiments here since they may of interest and we speculate below as to the reason why no significant effect was observed in these experiments. For convenience, Table 5.1 summarized the differences between experiments 1-4.

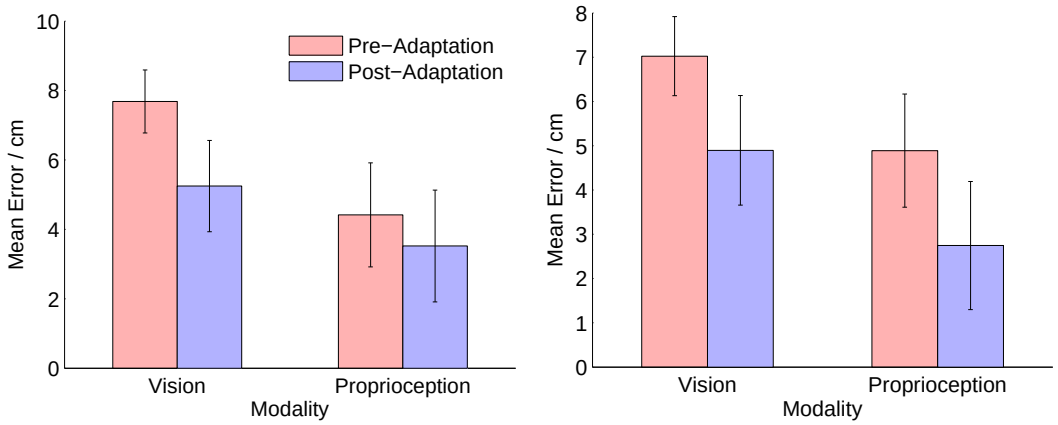

(a) Leftward Force (b) Rightward Force

Figure 5.10: Results from the drift test experiment. Bars show mean visual and proprioceptive shifts (a) Leftward force group, (b) Rightward force group.

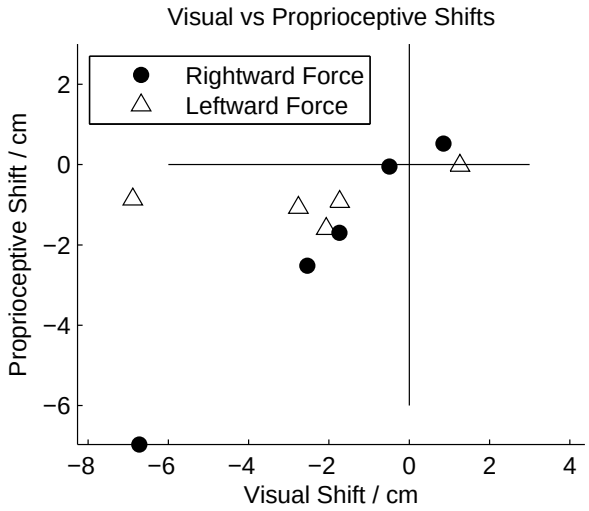

Figure 5.11: Detailed results from the drift test experiment. Each point shows visual and proprioceptive shifts for a single subject. Subjects who received a rightward force are indicated by a black circle. Subjects who received a leftward force are indicated by a white triangle.)

5.4.1 Experiment 3

In a further experiment (Experiment 3), we attempted to quantify the drift in each subjects' left hand by performing an additional 'drift test' on each trial. The experimental setup design was similar to Experiment 1. Subjects performed out-and-back reaching movements in the presence of a either a leftward or a rightward force, with alignment tests in between each reach trial. However, an additional component was

included: Following the proprioceptive alignment test, subjects were asked to move their left hand forward to a remembered point a few centimetres straight ahead of a tactile marker. We hypothesized that if the proprioceptively felt location of the left hand drifted, then this would affect the planned change in joint angles for moving to the remembered location and therefore affect the final measured endpoint, cf. (Sober and Sabes, 2003; Scheidt et al., 2005).

While some drift did occur in the location of subjects' left hand during the drift test, we found that this was uncorrelated with changes in alignment test performance. More interestingly, in this experiment we found no significant difference in shifts in alignment bias between subjects who received a leftward force, and subjects who received a rightward force. The mean shifts in vision and proprioception across subjects are summarized in Figure 5.10. In both conditions, both visual and proprioceptive alignment biases shifted leftward by around 2cm. It is clear that there is no difference in average shift between leftward and rightward groups, contrary to the results from Experiments 1 and 2. Data from all subjects is shown in Figure 5.11. These data further supports the view that there is little difference between these two groups, particularly if the two outlying data points (i.e. the one subject from each group which exhibited a large leftward visual shift) are ignored.

5.4.2 Experiment 4

The lack of any force-related shifts in alignment bias in these subject groups may have been due to increased uncertainty in the location of the left hand. We tested this hypothesis in a further experiment (Experiment 4) in which subjects did not receive a tactile marker for their left hand. The mean visual and proprioceptive shifts across subjects are shown in Figure 5.12. A scatter plot of all subjects is plotted in Figure 5.13. These results follow the same trend as the previous experiment in which the additional drift test was included: There is clearly no difference between subjects who received a leftward force and subjects who received a rightward force.

We conclude from these two experiments that an increase in uncertainty in the left hand caused subjects to change their strategy while performing the alignment tests - possibly switching to a more habitual strategy which was independent of any changes in right hand and left hand sensory calibration.

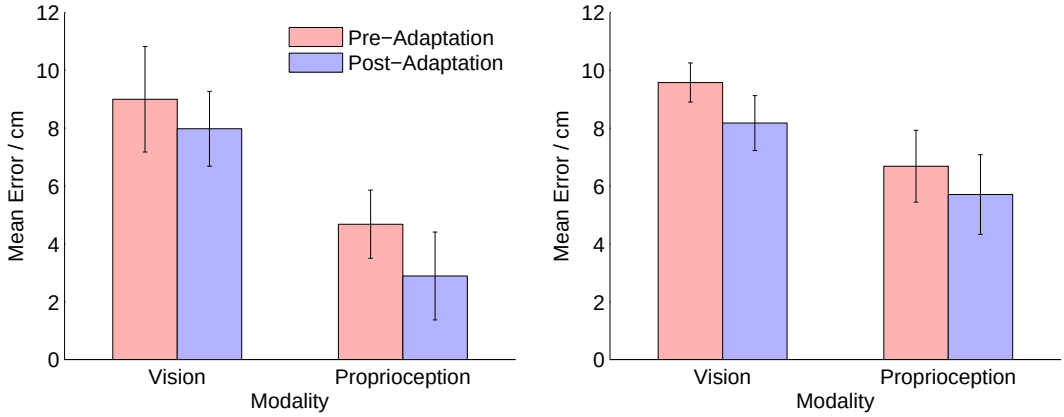

(a) Leftward Force (b) Rightward Force

Figure 5.12: Results from sessions in which subjects received no tactile marker for the left hand. Bars show mean visual and proprioceptive shifts (a) Leftward force group, (b) Rightward force group.

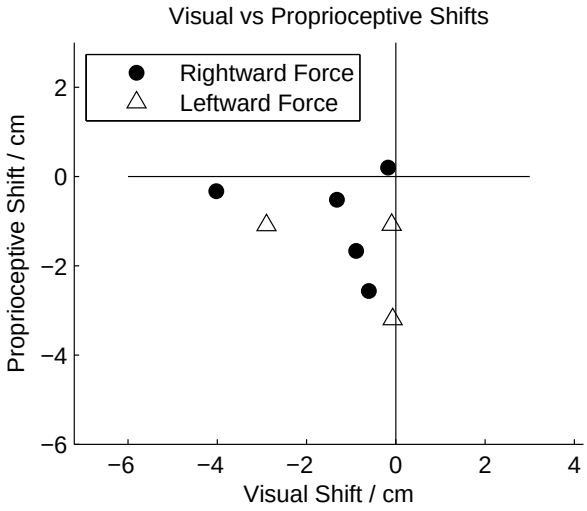

Figure 5.13: Detailed results from sessions in which subjects received no tactile marker for the left hand. Each point shows visual and proprioceptive shifts for a single subject. Subjects who received a rightward force are indicated by a black circle. Subjects who received a leftward force are indicated by a white triangle.)

5.5 Analysis of the components of adaptation

All of the three-component (i.e. 2 sensory, 1 motor) adaptation models we have considered here lead to a learning rule of the form

$$\Delta \mathbf{r}_t = D(\mathbf{r}_t - \hat{\mathbf{r}}_t). \tag{5.2}$$

We can analyse the behaviour of such a learning rule by considering the eigenvectors of the adaptation matrix D. In each model, this matrix turns out to have one zero eigenvalue with eigenvector $(-1,-1,1)^T$. This eigenvector corresponds to unobservable changes in the disturbance vector in which equal visual and proprioceptive shifts are accompanied by an equal and opposite shift in hand position, so that the overall perception of hand position does not change. The two remaining eigenvectors correspond to two distinct components of learning which adapt at different timescales. The timescales of each component is determined by its associated eigenvalue.

This view of the models reveals that there are essentially two components to any such model (since there is one direction in **r**-space which cannot be observed and is therefore not adapted along). The models differ primarily among the kind of components that they are able to predict given the parameters of the model. Given estimates of the parameters of each model, we can now consider these components quantitatively.

Figure 5.14(a) illustrates the components of adaptation of the Bayesian model, given the parameters that were learnt from data. Figure 5.14(b) provides a similar illustration for the MLA model. Note that in both cases, there is one eigenvector with eigenvalue zero, with eigenvector $[1,1,-1]$. This null component reflects the fact that no adaptation occurs when a motor disturbance shifts the true position of the hand, but both vision and proprioception are shifted in the opposite direction, giving the subject the illusion that nothing has changed.

The adaptation matrix for the distinct sensory/motor adaptation rule in Section 4.3.1 is

$$M = \begin{pmatrix} w_p & -w_p & 0 \\ -w_v & w_v & 0 \\ -\gamma w_v & -\gamma w_p & -\gamma \end{pmatrix}. \tag{5.3}$$

Optimizing the open parameters leads to the eigenvectors which are illustrated in Figure 5.14(c).

As can be seen, there is one component which is predominantly visual, and one component comprising a combination of proprioception and dynamics. The existence of these components suggest that vision can be adapted largely independently of proprioception and dynamics, but that proprioception and dynamics tend to adapt in tandem. This also suggests the possibility of distinct neural substrates for these two components.

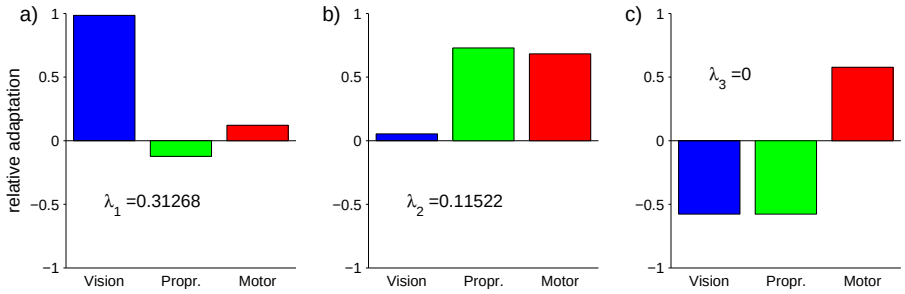

(a) Bayesian model

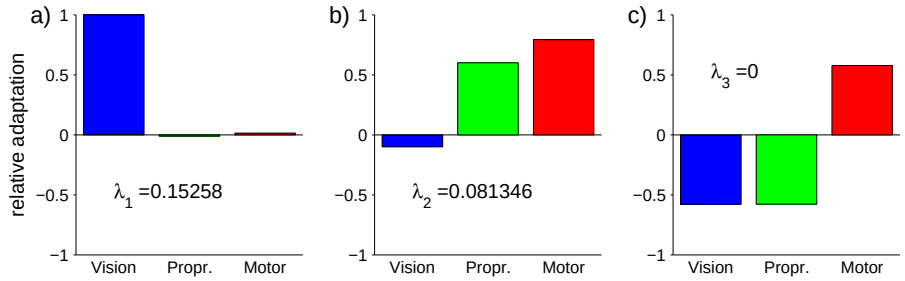

(b) 3-component MLA model

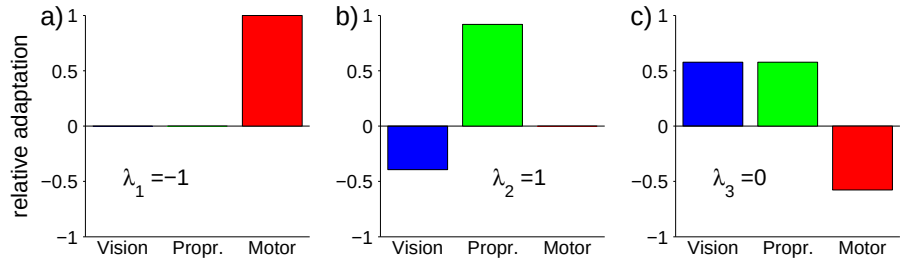

(c) Distinct sensory/motor adaptation model

Figure 5.14: Components of adaptation for the different sensory/motor adaptation models. These components are eigenvectors of the adaptation update matrix. The associated eigenvalues determine the rate of adaptation of each component.

5.6 Conclusions

Our experimental results show that adaptation of reaching movements in a force field results in shifts in visual and proprioceptive spatial perception. Furthermore, we have discounted the possibility that these shifts were simply caused by a bias in the extend of LH proprioceptive drift by comparing the results of adaptation to force fields in opposing directions.

This novel finding strongly supports the Bayesian model, which predicted such adaptation, and refutes alternative models in which sensory adaptation is assumed to occur independently of motor adaptation.

The Bayesian model was able to account for the trends in both reaching performance and alignment test errors on a trial-to-trial basis.

Overall, our results suggest that the nervous system solves the problems of sensory and motor adaptation in a principled and unified manner, supporting the view that sensorimotor adaptation proceeds according to optimal estimation of encountered disturbances.

Chapter 6

Conclusions and Discussion

6.1 Distal learning and control architectures

In this thesis we have considered the problem of sensorimotor adaptation where there may be multiple kinds of disturbance present. In Chapter 3 we examined the issue of distal learning. Cerebellar-based control architectures which rely on adaptation of an inverse internal model face a distal learning problem in which the relationship between sensory errors and errors in the internal model output (motor errors) is not precisely known, or may be computed using outdated information, if the dynamic or kinematic properties of the plant change (Jordan and Rumelhart, 1992). One solution to this problem which has been proposed (Porrill et al., 2004; Porrill and Dean, 2007b) is to employ an alternative control architecture which instead employs a forward internal model. A major contribution of this thesis has been to show that such control architectures still suffer from a distal learning problem when the properties of the *task* change, i.e. when the relationship between stimuli and requirements for succesful task completion change. We have given examples where these *task disturbances* may arise naturally in a variety of behaviours, including the VOR, saccades and reaching and catching.

Chen-Harris et al. (2008) proposed a model of saccade adaptation in which the cerebellum learns a forward model of the oculomotor plant. This model shares some similarities with the VOR adaptation model of Porrill et al. (2004) - the cerebellum acts in a recurrent loop with a feedforward controller, computing a forward model of the plant from motor commands issued by the controller. These models differ, however, in which brainstem input the cerebellar output modulates. In the Chen-Harris et al. model, the output of the cerebellum forms an estimate of the state of the plant to give

to the brainstem controller. In the Porrill et al. model, the output of the cerebellum augments the *stimulus*. However, only the Porrill et al. model successfully circumvents the distal learning problem. The Chen-Harris model suffers from distal learning issues under both plant *and* task disturbances.

In simulations, we found that the problems posed by distal learning only impair adaptation significantly in cases where disturbances are severe, such as rotations of visual feedback of more than 90 degrees. Avoidance of distal learning issues may not be such a primary consideration for the motor system. Though the two models we considered give rise to different predictions about the timecourse of learning at the behavioural level, these predictions depend strongly on the assumed plasticity laws in the cerebellum. It is therefore difficult to draw any firm conclusions about what kind of architecture may be being employed based on behavioural data.

Another reason why it may be difficult to draw conclusions based on behavioural level patterns of adaptation is that adaptation at the behavioural level may in fact be dictated by behavioural-level phenomena. The normative modelling approach proposes precisely this: that patterns of adaptation are dictated by inferences about the environment, rather than by low-level neural plasticity laws.

6.2 Multiple components of adaptation

In Chapter 1 we proposed the normative idea that the motor system should maintain multiple components of adaptation, each represented as an internal model, corresponding to the multiple potential types of disturbance to which the motor system may be exposed. This was primarily motivated by considering the differences between adapting to kinematics and dynamics disturbances. We argued that, from a normative perspective, these two kinds of disturbances should be adapted to differently since they are likely to require different patterns of generalization. Behavioural seems to support this idea (Shadmehr and Mussa-Ivaldi, 1994; Krakauer et al., 1999).

Returning to theory, however, it may not be so easy to distinguish between these two kinds of disturbance. Discrepancies between visual and proprioceptive feedback should enable the nervous system to distinguish between visual and dynamics disturbances. However, issues of noisy sensory feedback mean that this task is not entirely trivial. Furthermore, sensory feedback itself is liable to drift out of calibration.

In Chapter 4 we considered the closely related problem of concurrent sensory recalibration and motor adaptation. We examined previous models in which sensory

adaptation is driven purely by discrepancy between visual and proprioceptive feedback, and extended these to include an additional motor component based on the linear state-space modelling approach.

We derived an alternative Bayesian model in which sensory miscalibrations and motor disturbances are jointly inferred from sensory feedback based on a full generative probabilistic model of the observations given the disturbances. This model correctly predicts the distributed nature of adaptation among sensory and motor components when visual feedback is shifted. However it also predicts that, in a force field adaptation task where there is no discrepancy between sensory modalities but there are movement error, there will also be sensory adaptation. In Chapter 5 we tested and confirmed this prediction.

6.3 Unresolved questions and future work

Although there is strong evidence in favour of the notion of sensory recalibration, there are still skeptics. Smeets et al. (2006) argued against the idea of sensory adaptation, arguing instead that apparrent shifts in multimodal estimates of hand position can be explained by a simple reweighting of two fixed unimodal estimated. They tested subjects ability to align their hand to a moving target with and without visual feedback of hand position. Much like the subjects we tested, most subjects exhibited some bias in the alignment during an initial block of trials without visual feedback. When visual feedback was introduced, this bias was immediately eliminated. According to our model, the existence of the bias should have prompted subjects to recalibrate their senses to eliminate the bias. When visual feedback was again removed, however, subjects movement errors gradually drifted back towards the same bias that had been observed in the very first block. Smeets et al. show that these results are consistent with a model in which senses are not adapted, only *reweighted*. They assume that a visual estimate of hand position is maintained, even when vision is removed, but that the uncertainty in this visual estimate increases as more movements are made. Thus the relative weight of proprioception steadily increases with trial number once vision is removed.

It is not immediately clear how to reconcile this result with our model. One possibile explanation, however, is that subjects do not necessarily believe that the cursor they observe on the screen truly corresponds to their hand position. In the study by Smeets et al., the cursor was simply a cube in 3-dimensional space. When visual feedback is available, subjects are able to perform visually-guided feedback control.

This need not, however, lead to adaptation of proprioception in the sense that we have demonstrated here if they do not believe that the cursor represents their true hand position. The gradual drift back towards the initial level of performance might represent a gradual forgetting of (what the subject perceives to be) the display offset. Should the display offset be changed by the experimentor, however, the subject may be inclined to believe that this is more likely to be due to a miscalibration of his own vision system than a change in the display - which he has no reason to believe will change with time. Hence there may be a difference between how the subject initially learns the kinematics of the 'tool' under control, and how the subject later utilizes this information to recalibrate his own senses.

Sober and Sabes (2005) showed that varying the quality of visual feedback led to varying strategies for integration with proprioception. When a visual estimate of joint angles was available, for instance, this led to greater reliance on visual feedback than when end-effector location alone was provided.

It seems that such flexibility is also present during adaptation - the relative extent of visual and proprioceptive adaptation under shifted visual feedback is different when subjects view a cursor compared with when view their whole hand. Adaptation when wearing prism goggles is also substantially more rapid than adapation using virtual displays. This difference might also reflect partial attribution of errors to the display, rather than the subject's own somatosensory system. Scheidt et al. (2005) addressed the question of how vision and proprioception contribute to motor adaptation by 'clamping' visual feedback during reaching movements to a straight line between the starting and target positions, while perturbing the true hand position with a velocity-dependent force field. They found that the visual clamp led to very little adaptation of reaching movements. In fact, hand trajectories on catch trials were even in the *same direction* as the perturbed trajectories, the opposite direction from what one would expect during adaptation.

Scheidt et al. propose that their results can be explained by a misestimation of the initial posture of the arm, i.e. a shift in right-hand proprioception. In our model, we assumed that proprioception played no role in the planning of reaching movements and was only utilized in judging movement errors. Other studies have also highlighted the importance of proprioceptive estimates of initial hand location for reaching (Sober and Sabes, 2003, 2005).

One difficulty in comparing Scheidt et al.'s experiment with our own is that they employed multiple targets, whereas we used just a single target. Extending the model

to account for multiple targets is not straightforward.

Incorporating initial position into our model would be difficult but not impossible. One difficulty is that not much is known about how shifts in proprioception generalize between different locations in space. Simani et al. (2007) found some generalization to other locations of the workspace, however more extensive future research is required to characterize the full nature and extent of this generalization.

6.3.1 Extension to multiple reach directions

We have only considered reaching movements to a very small group of targets contained within a 25°range. This was a deliberate choice to avoid modelling difficulties associated with generalization to targets in different directions. Extending our model to include multiple target directions is far from straightforward. One requirement of such a model would likely be that the generalization characteristics of the different components would be different. One might expect the visual disturbance to generalize extrinsically, and the proprioceptive disturbance to generalize intrinsically. The motor component could be either. Indeed there may be multiple motor components relating to e.g. the arm and the environment (Kluzik et al., 2008). These different motor components may exhibit different generalization properties (Berniker and Körding, 2008).

In principle, such a model can be represented in terms of a Kalman filter in which the output is constructed from a linear combination of nonlinear basis functions, as in 2.5, with the weights corresponding to the unknown disturbance. This gives rise to a model in which the nonlinearity manifests itself as changes in the observation matrix from one trial to the next. However, there is a slightly more subtle difficulty we encounter when trying to formulate this model. All of the Bayesian models we have considered here, as well as the other Kalman filter-based models we have described which have been proposed elsewhere, are formulated as *forward models*. Learning is achieved by adapting this forward model. Action selection is achieved by inverting it to find u. In the linear models considered here and elsewhere, inverting the forward model is trivial. In a nonlinear model, however, it is not.

Considering a deterministic, nonlinear model with a single observation but several nonlinear disturbance components:

$$y = \sum \mathbf{r}_i^y \phi(u). \tag{6.1}$$

It is far from trivial to attempt to solve this equation for u given some desired hand

position y^*. Including multiple observations, noise, etc. complicates matters even further.

The generalization patterns we observe in subjects are consistent with an inverse model representation, rather than a forward model representation. An extrinsic generalization pattern would emerge from some representation with basis functions of the form $y = \sum \mathbf{w}_i \phi_i(v^*)$, rather than $v = \sum \mathbf{w}_i \phi_i(y)$. Learning inverse models, however, we encounter the problem of distal learning, as discussed in Chapter 3. The Bayesian framework is not exempt from the distal learning problem. Representing an inverse model using a Kalman filter amounts to assuming a probabilistic model in which the motor command u is *generated by* the sensory stimuli, v say, i.e.

$$p(r_t, u_t, v_t) = p(r_t)p(v_t)p(u_t|r_t, v_t), \tag{6.2}$$

rather than

$$p(r, u, v) = p(r)p(u)p(v|r, u), \tag{6.3}$$

as assumed in a forward model formulation. Ultimately this will lead to updates of the form

$$r_{t+1} = r_t + K_t(u_t^* - u_t), \tag{6.4}$$

where the term in brackets is the difference between the 'true' motor command u_t^* and our actual (estimated) motor command u_t. This amounts exactly to the distal learning problem described in Chapter 3, since we cannot observe this error directly, we can only observe its sensory consequences.

6.3.2 Predictions about uncertainty

Although the Bayesian and state-space modelling approaches can lead to very similar predictions, there are two key advantages to the Bayesian modelling approach. Firstly, the learning rate, which is chosen fairly arbitrarily in the state-space model formulation, is determined in the Bayesian framework by the structure of the generative model. In simple models with a single disturbance and a single observation of performance, it has been shown that learning rate is sensitive to changes in feedback uncertainty and uncertainty in the disturbance (Burge et al., 2008). In our model of multimodal sensorimotor adaptation, in which there are three unknown disturbances and two observations, the learning rate becomes a 2×3 adaptation matrix. The structure of the generative model determines the properties of this matrix and this is essentially where the prediction of interaction between sensory and motor adaptation arises from.

Another important feature of Bayesian models, however, is that they predict that changes in the observation structure from trial to trial (i.e. the matrix H in the Kalman filter formulation described in Section 2.4.1) will affect the uncertainty in disturbances and consequently the rate of adaptation. In the settings in which we have applied our model, the observation structure has remained fixed, therefore these aspects of the Bayesian modelling approach have not been tested. Our generative model makes very clear predictions about how adaptation will proceed if, say, visual feedback is removed. The effect of changing observation structure has been examined elsewhere (Krakauer et al., 2006; Körding et al., 2007b; Wei and Körding, 2008), with some evidence found in support of Bayesian models of the kind we have proposed. However, not all predictions of this framework turn out to be supported experimentally. Huang and Shadmehr (2007) found that increasing inter-trial intervals led to greater adaptation to errors experienced on the previous trial, rather than increased sensitivity to errors on subsequent trials, as the Bayesian framework would suggest.

Any negative experimental results indicate the limit of these kind of models. There will inevitably be discrepancies between the physiological and computational abilities of the brain, and normative principles which we expect to be reflected in their behaviour. Observations of behaviour deviating from optimality is, in a sense, just as enlightening, if not more so, than observations of optimal behaviour, since the latter may point to physiological constraints which can potentially be correlated with brain structure and function, paving the way for a deeper understanding of how the brain controls movement of the body. Nevertheless, a thorough understanding of normative principles is essential in order to draw this distinction and recognize whether an observed behaviour reflects a physiological constraint, or a behavioural strategy.

Appendix A

Kalman filter update equations

This basic probabilistic framework can be extended to arbitrary linear dynamical systems, with general form

$$\mathbf{r}_{t+1} = A_t \mathbf{r}_t + \eta_t \tag{A.1}$$

$$\eta_t \sim N(0, Q_t), \tag{A.2}$$

$$\mathbf{z}_t = H_t \mathbf{r}_T + \varepsilon_t \tag{A.3}$$

$$\varepsilon_t \sim N(0, R_t). \tag{A.4}$$

Here, A_t is a (potentially time-varying) matrix which describes any underlying dynamics of the disturbance. In a motor control context this is typically assumed to be either the identity I, or αI, where α is some number slightly less than 1, e.g. $\alpha = .999$. This describes disturbances which tend to gradually decay over time, with α the decay rate. Interestingly, this decay factor is the only way in which these linear adaptation models can capture incomplete learning. If we think of the α as a 'forgetting factor', learning becomes incomplete when the amount learned from errors on one trial becomes equal to the amount of forgetting on that trial.

The volatility of the disturbances, Q_t, is usually assumed to be diagonal, since multiple disturbances should decay independently. H_t is the observation matrix, and describes how the latent disturbances are manifested in the observations. R_t is the covariance matrix of the observations on trial t.

The prior over the disturbance is now given by a multivariate Gaussian with mean $\hat{\mathbf{r}}_{t|t-1}$ and covariance matrix $P_{t|t-1}$. We similarly represent the posterior mean and covariance by $\hat{\mathbf{r}}_{t|t}$ and $P_{t|t}$.

The derivation of the update equations (finding the posterior mean and covariance matrix) follows the same basic logic as the 1-dimensional case presented in the previous section, however it is slightly more involved due to the (potentially) multi-dimensional nature of the disturbances and observations. The general algorithm is given by the following equations. First, a prediction step, in which the prior for trial t is computed from the posterior of the previous trial:

$$\hat{\mathbf{r}}_{t|t-1} = A\hat{\mathbf{r}}_{t-1|t-1}, \tag{A.5}$$

$$P_{t|t-1} = AP_{t|t}A^T + Q_{t-1}. \tag{A.6}$$

Then an update step based on the incoming observations:

$$\tilde{\mathbf{z}}_t = \mathbf{z}_t - H_t\hat{\mathbf{r}}_{t|t-1} \tag{A.7}$$

$$S_t = H_tP_{t|t-1}H_t^T + R_t \tag{A.8}$$

$$K_t = P_{t|t-1}H^TS^{-1} \tag{A.9}$$

$$\hat{\mathbf{r}}_{t|t} = \hat{\mathbf{r}}_{t|t-1} + K_t\tilde{\mathbf{z}} \tag{A.10}$$

$$P_{t|t} = (I - K_tH_t)P_{t|t-1} \tag{A.11}$$

Note that, in general, this model permits learning of nonlinear disturbances also, provided they are represented as a linear combination of nonlinear basis elements, as in Eqn 2.5. Here $\mathbf{r}_t$ corresponds to the weights $\mathbf{w}$, and H_t takes the role of the nonlinear basis elements.

Appendix B

Computational methods for cerebellar modelling

The same pattern of training was used and very similar control and learning algorithms were employed for simulating each of the behaviours discussed here. Table B.1 outlines the basic algorithm underlying all of the simulations.

In each case, an initial motor command-outcome mapping P_0 and an initial stimulus-desired outcome mapping S_0 were specified. The algorithm then simulated cerebellar-based adaptation to a new pair of mappings P_1 and S_1 (in practice only one was varied at a time) using either a feedforward (FF) or recurrent (REC) architecture.

A sequence of stimuli $\mathbf{x}_{1:T}$ was selected. For the VOR, this $\mathbf{x}_t$ represented a discrete-time series of head velocity measurements with a discretization timestep of $.01s$. For reaching, each $\mathbf{x}_t$ represented a difference vector movement plan for a single trial.

The fixed controller B generates motor commands which are optimal under the initial conditions P_0 and S_0, i.e.

$$B(\mathbf{x}_t) = P_0^{-1}(S_0(\mathbf{x}_t)). \tag{B.1}$$

The input to the cerebellum, which we denote by $\mathbf{z}_t$, varied depending on the architecture employed and the task. For linear P and S (i.e. in the case of VOR), under the forward architecture this was equal to the stimulus $\mathbf{x}_t$, while under the recurrent architecture this was equal to the motor command $\mathbf{u}_t$.

For nonlinear P and S (i.e. reaching), $\mathbf{z}_t$ was given by a set of non-linear basis functions Φ defined over the same input space, i.e. $\mathbf{z}_t = \Phi(\mathbf{x}_t)$ for the feedforward architecture and $\mathbf{z} = \Phi(\mathbf{u}_t)$ for the recurrent architecture. The basis functions Φ were

Table B.1: Pseudocode summary of algorithm used for all simulating all behaviours simulated and for both architectures. (Exceptions for particular behaviours are given in parentheses).

Initialize:

Define stimulus sequence $\mathbf{x}_{1:T}$

$W_1 = 0$

($\mathbf{u}_0 = 0$ for VOR)

Run:

For t = 1:T

1. **Generate motor command $\mathbf{u}_t$**

   if (FF)

   $\mathbf{z}_t = \mathbf{x}_t$ (or $\mathbf{z}_t = \Phi(\mathbf{x}_t)$ for reaching)

   $\mathbf{c}_t = W_t \mathbf{z}_t$

   if (REC)

   $\mathbf{u}_t = 0$

   iterate

   $\mathbf{z}_t = \mathbf{u}_t$ (or $\mathbf{z}_t = \Phi(\mathbf{u}_t)$ for reaching)

   $\mathbf{c}_t = W_t \mathbf{z}_t$

   $\mathbf{u}_t = B(\mathbf{x}_t + \mathbf{c}_t)$

   until convergence of $\mathbf{u}_t$:

   (or $\mathbf{u}_t = B(\mathbf{x}_t + \mathbf{c}_{t-1})$ for VOR)

2. **Calculate outcome $\mathbf{y}_t$ and observed error $\widetilde{\mathbf{y}}_t$**

   $\mathbf{y}_t = P_1(\mathbf{u}_t)$

   $\mathbf{y}_t^* = S_1(\mathbf{u}_t)$

   $\widetilde{\mathbf{y}}_t = \mathbf{y}_t^* - \mathbf{y}_t$

3. **Estimate cerebellar error $\widetilde{\mathbf{c}}_t$**

   if (FF)

   $\widehat{\widetilde{\mathbf{c}}}_t = P_0^{-1}(\widetilde{\mathbf{y}}_t)$ (or $\widehat{\widetilde{\mathbf{c}}}_t = J_{P_0^{-1}} \widetilde{\mathbf{y}}_t$ for reaching)

   if (REC)

   $\widehat{\widetilde{\mathbf{c}}}_t = S_0^{-1}(\widetilde{\mathbf{y}}_t)$

4. **Update cerebellar weights**

   $W_{t+1} = W_t + \beta \widehat{\widetilde{\mathbf{c}}}_t \mathbf{z}_t^T$

End

Table B.2: Summary of model details for different behaviours.

Model Component	Notation	Description		
		VOR	Saccades	Reaching
Stimulus	$\mathbf{x}_t$	Head velocity	Target difference vector	Target difference vector
Outcome	$\mathbf{y}_t$	Eye velocity	Eye displacement	Hand displacement
Motor command	$\mathbf{u}_t$	Oculomotor torque	Motor amplitude	Change in joint angle
Motor command-outcome mapping	P	Oculomotor Dynamics	Oculomotor dynamics	Visual rotation
Stimulus-desired outcome mapping	S	Visual rotation	Target shift	Target shift

Gaussians given by

$$\Phi_i(\mathbf{o}) = e^{(\mathbf{o}-\mathbf{r}_i)^T \Sigma (\mathbf{o}-\mathbf{r}_i)}, \tag{B.2}$$

where $\mathbf{o}$ represents the appropriate input ($\mathbf{x}_t$ or $\mathbf{u}_t$) depending on the architecture. The function centres $\mathbf{r}_i$ were distributed on a uniform square grid in the input space and the metric Σ was chosen so that the width of each tuning function along each dimension was equal to twice the separation $\Delta\mathbf{r}$ between functions:

$$\Sigma = 2 \begin{pmatrix} \frac{1}{\Delta \mathbf{r}_1} & 0 & 0 \\ 0 & \ddots & 0 \\ 0 & 0 & \frac{1}{\Delta \mathbf{r}_n} \end{pmatrix}. \tag{B.3}$$

Note that $\mathbf{r}$ and Σ were different between the two architectures due to different distributions of inputs. A total of 16 basis functions in a 4×4 grid was used in each case.

The cerebellar output $\mathbf{c}_t$ was then given by multiplying the input $\mathbf{z}_t$ by the learnt cerebellar weight matrix W_t,

$$\mathbf{c}_t = W_t \mathbf{z}_t. \tag{B.4}$$

The motor command $\mathbf{u}$ was constructed differently for different architectures. For the feedforward architecture, it was given directly by the sum of the cerebellar and brainstem outputs

$$\mathbf{u}_t = B(\mathbf{x}_t) + C(\mathbf{x}_t). \tag{B.5}$$

For the recurrent architecture, when approximating continuous time dynamics, as in the VOR, the motor command was calculated as

$$\mathbf{u}_t = B(\mathbf{x}_t + C(\mathbf{u}_{t-1})). \tag{B.6}$$

For simulating single trials of reaching, the motor command was determined by iterating the equation

$$\mathbf{u}_t = B(\mathbf{x}_t + C(\mathbf{u}_t)) \tag{B.7}$$

until the difference in $\mathbf{u}$ between successive iterations was less than 0.1 %.

In some cases the recurrency led to divergence of $\mathbf{u}_t$ either while iterating within a single trial (reaching) or over time (VOR), in which case the recurrent architecture was unstable and unable to learn the task. However, this was typically only an issue for transformations of moderate to large magnitude and for less severe transformations $\mathbf{u}_t$ converged within 10-20 iterations.

The motor command $\mathbf{u}_t$ was then transformed into an observed output $\mathbf{y}$ via the (transformed) plant dynamics P_1,

$$\mathbf{y}_t = P_1(\mathbf{u}_t). \tag{B.8}$$

For reaching, the converged value of $\mathbf{u}_t$ was used for this.

$$\mathbf{y}_t = P_1(\mathbf{u}_t(1+\varepsilon_t));\ \varepsilon_t \sim N(0, 0.5^2) \tag{B.9}$$

The desired outcome at each timestep or trial, $\mathbf{y}_t*$, was calculated separately according to the (transformed) stimulus-desired outcome relationship,

$$\mathbf{y}_t^* = S_1(\mathbf{x}_t). \tag{B.10}$$

The observation error was then calculated as

$$\widetilde{\mathbf{y}}_t = \mathbf{y}_t^* - \mathbf{y}_t. \tag{B.11}$$

To estimate the error in the cerebellar output, the initial mappings between motor command and observed outcome P_0 and between stimulus and desired outcome S_0 were used, according to the theory presented in section 3.2, i.e. for the recurrent architecture,

$$\widehat{\widetilde{\mathbf{c}}}_t = \widetilde{\mathbf{y}}_t, \tag{B.12}$$

and for the feedforward architecture,

$$\widehat{\widetilde{\mathbf{c}}}_t = P_0^{-1}\widetilde{\mathbf{y}}_t. \tag{B.13}$$

Where this mapping was nonlinear (i.e. for reaching) the error was approximated to first order using a Taylor expansion,

$$\widehat{\widetilde{\mathbf{c}}}_t = J_{P_0^{-1}}(\mathbf{y}_t)\widetilde{\mathbf{y}}_t \tag{B.14}$$

where $J_{P_0^{-1}}(\mathbf{y}_t)$ is the Jacobian of P_0^{-1} at $\mathbf{y}_t$. This was estimated numerically by finite differences. Note that in all simulations S was linear, although the same principle could be used for approximating $\widehat{\widetilde{\mathbf{c}}}$ in the recurrent architecture if it were nonlinear.

Finally, the cerebellar weights were updated at each time step using a discrete-time analog of the gradient learning rule stated in section 2.2.1

$$W_t = W_{t-1} + \beta\widetilde{\mathbf{c}}_t\mathbf{p}_t^T, \tag{B.15}$$

where $\widetilde{\mathbf{c}}_t$ is the *estimated* cerebellar output error.

The learning rate β was different in each case and chosen to give approximately realistic timescales of adaptation in comparison to experimental data. The same value of β was always used for both architectures.

Appendix C

Estimating hand position in the Bayesian model

Estimating hand position via MLE as in Equation 4.5 is straightforward, but assumes that the observations v_t and p_t are conditionally independent given y_t. However in the Kalman filter model, this is no longer true, since the observations also depend on the disturbances r_t^v and r_t^p, which may not in fact be independent of one another. Estimating hand position nevertheless still turns out to be fairly straightforward in the KF model. Since we are now operating in a Bayesian framework, we refer to maximum a-posteriori (MAP) estimation, rather than MLE, since we consider the posterior distribution over $\mathbf{r}_t$.

We want to find the value of y_t which maximizes the marginal posterior $p(y_t|u_t, v_t, p_t)$. We first consider the joint posterior

$$p(y, r|u, v, p) = p(v, p|r, y)p(y|u)p(r). \tag{C.1}$$

To simplify the notation, we define $\mathbf{z} = \begin{pmatrix} v \\ p \\ u \end{pmatrix}$, $\Sigma = \begin{pmatrix} \sigma_v^2 & 0 & 0 \\ 0 & \sigma_p^2 & 0 \\ 0 & 0 & \sigma_u^2 \end{pmatrix}$, and write $\mathbf{1} = \begin{pmatrix} 1 \\ 1 \\ 1 \end{pmatrix}$. We also drop the subscripted trial index and use $\hat{\mathbf{r}}$ and P to denote the *prior* mean and covariance of $\mathbf{r}_t$.The log-probability is

$$\log p = -\frac{1}{2}(y\mathbf{1} + \mathbf{r} - \mathbf{z})^T \Sigma^{-1}(y\mathbf{1} + \mathbf{r} - \mathbf{z}) - \frac{1}{2}(\mathbf{r} - \hat{\mathbf{r}})P^{-1}(\mathbf{r} - \hat{\mathbf{r}}). \tag{C.2}$$

We wish to marginalize out $\mathbf{r}$. We achieve this by forcing the terms into a quadratic in $\mathbf{r}$, which can then be easily separated from the other terms and will be lost once the

integration is done.

$$\begin{aligned}\log p(y,r|u,v,p) &= -\tfrac{1}{2}\mathbf{r}^T(\Sigma^{-1}+P^{-1})\mathbf{r}^T - \mathbf{r}^T(\Sigma^{-1}(y\mathbf{1}-\mathbf{z})-P^{-1}\hat{\mathbf{r}}) \\ &\quad -\tfrac{1}{2}(y\mathbf{1}-\mathbf{z})^T\Sigma^{-1}(y\mathbf{1}-\mathbf{z}) - \tfrac{1}{2}\hat{\mathbf{r}}^T P^{-1}\hat{\mathbf{r}}.\end{aligned} \tag{C.3}$$

Completing the square leads to

$$\begin{aligned}\log p &= -\tfrac{1}{2}\left[r-\left(\Sigma^{-1}+P^{-1}\right)^{-1}(\Sigma^{-1}(y\mathbf{1}-\mathbf{z})+P^{-1}\hat{\mathbf{r}})\right]^T \\ &\qquad \left(\Sigma^{-1}+P^{-1}\right)^{-1}\left[r-\left(\Sigma^{-1}+P^{-1}\right)^{-1}(\Sigma^{-1}(y\mathbf{1}-\mathbf{z})+P^{-1}\hat{\mathbf{r}})\right] \\ &\quad -\tfrac{1}{2}(\Sigma^{-1}(y\mathbf{1}-\mathbf{z})-P^{-1}\hat{\mathbf{r}})^T\left(\Sigma^{-1}+P^{-1}\right)^{-1}(\Sigma^{-1}(y\mathbf{1}-\mathbf{z})-P^{-1}\hat{\mathbf{r}}) \\ &\quad -\tfrac{1}{2}(y\mathbf{1}-\mathbf{z})^T\Sigma^{-1}(y\mathbf{1}-\mathbf{z}) - \tfrac{1}{2}\hat{\mathbf{r}}^T P^{-1}\hat{\mathbf{r}}.\end{aligned} \tag{C.4}$$

After integrating out $\hat{\mathbf{r}}$, we lose the first term in Equation C.4. We can then differentiate the remaining expression (for the log marginal probability of y), and set it equal to zero to find our estimate $\hat{y}$:

$$\mathbf{1}^T\Sigma^{-1}\left(\Sigma^{-1}+P^{-1}\right)^{-1}(\Sigma^{-1}(\hat{y}\mathbf{1}-P^{-1}\hat{\mathbf{r}})-\mathbf{1}^T\Sigma^{-1}(\hat{y}\mathbf{1}-\mathbf{z})=0. \tag{C.5}$$

Solving for $\hat{y}$, we get

$$\hat{y}=\frac{\mathbf{1}^T\left[\Sigma^{-1}\left(\Sigma^{-1}+P^{-1}\right)^{-1}(P^{-1}\hat{\mathbf{r}}+\Sigma^{-1}\mathbf{z})-\Sigma^{-1}\mathbf{z}\right]}{\mathbf{1}^T\left[\Sigma^{-1}\left(\Sigma^{-1}+P^{-1}\right)^{-1}\Sigma^{-1}-\Sigma^{-1}\right]\mathbf{1}}. \tag{C.6}$$

This rather fiendish-looking expression is the best estimate of hand position. Note that $\mathbf{1}^T X\mathbf{1}$ has the effect of summing all the entries in the matrix X. In this style of notation, the usual MLE rule of Equation 4.5 would be written

$$\hat{y}=\frac{\mathbf{1}^T\Sigma^{-1}\mathbf{z}}{\mathbf{1}^T\Sigma^{-1}\mathbf{1}}. \tag{C.7}$$

Applying the matrix inversion theorem: $(A+B)^1 \equiv A^{-1}-A^{-1}(B^{-1}+A^{-1})A^{-1}$, we can simplify this further to:

$$\hat{y}=\frac{\mathbf{1}^T\left[(P+\Sigma)^{-1}-I\right]\left(\mathbf{z}+\Sigma P^{-1}\hat{\mathbf{r}}\right)}{\mathbf{1}^T(P+\Sigma)^{-1}\mathbf{1}}. \tag{C.8}$$

Bibliography

Abdelghani, M. N., Lillicrap, T. P., and Tweed, D. B. (2008). Sensitivity derivatives for flexible sensorimotor learning. *Neural Comput*, 20:2085–2111.

Albano, J. E. (1996). Adaptive changes in saccade amplitude: oculocentric or orbitocentric mapping? *Vision Res*, 36(14):2087–2098.

Baizer, J., Kralj-Hans, I., and Glickstein, M. (1999). Cerebellar lesions and prism adaptation in macaque monkeys. *J Neurophysiol*, 81(4):1960–1965.

Bastian, A. (2006). Learning to predict the future: the cerebellum adapts feedforward movement control. *Current opinion in neurobiology*, 16(6):645–649.

Bastian, A., Martin, T., Keating, J., and Thach, W. T. (1996). Cerebellar ataxia: abnormal control of interaction torques across multiple joints. *J Neurophysiol*, 76:492–509.

Bernier, P. M., Chua, R., Bard, C., and Franks, I. M. (2006). Updating of an internal model without proprioception: a deafferentation study. *Neuroreport*, 17:1421–1425.

Berniker, M. and Körding, K. (2008). Estimating the sources of motor errors for adaptation and generalization. *Nat. Neurosci.*, 11:1454–1461.

Bock, O., Pipereit, K., and Mierau, A. (2007). A method to reversibly degrade proprioceptive feedback in research on human motor control. *J. Neurosci. Methods*, 160:246–250.

Boyden, E. S., Katoh, A., and Raymond, J. L. (2004). Cerebellum-dependent learning: the role of multiple plasticity mechanisms. *Annual Review Neuroscience*, 27:581–609.

Brown, L. E., Rosenbaum, D. A., and Sainburg, R. L. (2003). Limb position drift: implications for control of posture and movement. *J. Neurophysiol.*, 90:3105–3118.

Burge, J., Ernst, M. O., and Banks, M. S. (2008). The statistical determinants of adaptation rate in human reaching. *J. Vis.*, 8(4):1–19.

Chen-Harris, H., Joiner, W. M., Ethier, V., Zee, D. S., and Shadmehr, R. (2008). Adaptive control of saccades via internal feedback. *J. Neurosci.*, 28:2804–2813.

Cheng, S. and Sabes, P. (2006). Modeling sensorimotor learning with linear dynamical systems. *Neural Computation*, 18:760–793.

Cheng, S. and Sabes, P. (2007). Calibration of visually guided reaching is driven by error-corrective learning and internal dynamics. *J Neurophysiol*, 97:3057–3069.

Coenen, O. J. and Sejnowski, T. J. (1996). A dynamical model of context dependencies for the vestibulo-ocular reflex. In *Advances in Neural Information Processing Systems*, volume 8, Cambridge, MA. MIT Press.

Conditt, M. A., Gandolfo, F., and Mussa-Ivaldi, F. A. (1997). The motor system does not learn the dynamics of the arm by rote memorization of past experience. *J. Neurophysiol.*, 78:554–560.

Desmurget, M., Vindras, P., Gra, H., Viviani, P., and Grafton, S. T. (2000). Proprioception does not quickly drift during visual occlusion. *Exp Brain Res*, 134:363–377.

Diedrichsen, J., Hashambhoy, Y., Rane, T., and Shadmehr, R. (2005). Neural correlates of reach errors. *J Neurosci*, 25:9919–9931.

Donchin, O., Francis, J. T., and Shadmehr, R. (2003). Quantifying generalization from trial-by-trial behavior of adaptive systems that learn with basis functions: theory and experiments in human motor control. *J Neurosci*, 23(27):9032–9045.

Ernst, M. and Banks, M. (2002). Humans integrate visual and haptic information in a statistically optimal fashion. *Nature*, 415:429–433.

Ethier, V., Zee, D. S., and Shadmehr, R. (2008). Spontaneous recovery of motor memory during saccade adaptation. *J. Neurophysiol.*, 99:2577–2583.

Faisal, A., Selen, L., and Wolpert, D. (2008). Noise in the nervous system. *Nature Reviews Neuroscience*, 9(4):292–303.

Franklin, D., So, U., Burdet, E., and Kawato, M. (2007). Visual feedback is not necessary for the learning of novel dynamics. *PLoS ONE*, 2:e1336.

Fujita, M. (1982). Adaptive filter model of the cerebellum. *Biological Cybernetics*, 45(3):195–206.

Ghahramani, Z., Wolpert, D., and Jordan, M. (1997). Computational models for sensorimotor integration. In Morasso, P. and Sanguineti, V., editors, *Self-Organization, Computational Maps and Motor Control*, pages 117–147. North-Holland, Amsterdam.

Gomi, H. and Kawato, M. (1990). Learning control for a closed loop system using feedback-error-learning. In *Proceedings of the 29th conference on decision and control*, pages 3289–3294.

Haith, A., Jackson, C., Miall, C., and Vijayakumar, S. (2008a). Interaction between sensory and motor adaptation predicted by a bayesian model. In Shadmehr, R. and Todorov, E., editors, *Proc. Advances in Computational Motor Control*.

Haith, A., Jackson, C., Miall, C., and Vijayakumar, S. (2008b). Unifying the sensory and motor components of sensorimotor adaptation. In *Advances in Neural Information Processing Systems*.

Haith, A. and Vijayakumar, S. (2007). Robustness of vor and okr adaptation under kinematic and dynamic transformations. In *Proc. International conference on development and learning, London (ICDL '07)*.

Haith, A. and Vijayakumar, S. (2009). Implications of different classes of sensorimotor disturbance for cerebellar-based motor learning models. *Biological Cybernetics*, 100:81–95.

Harris, C. M. and Wolpert, D. M. (1998). Signal-dependent noise determines motor planning. *Nature*, 394:780–784.

HARRIS, C. S. (1963). Adaptation to displaced vision: visual, motor, or proprioceptive change? *Science*, 140:812–813.

Hatada, Y., Rossetti, Y., and Miall, R. (2006). Long-lasting aftereffect of a single prism adaptation: shifts in vision and proprioception are independent. *Exp Brain Res*, 173:415–424.

Hay, J. C. and Pick, H. L. (1966). Visual and proprioceptive adaptation to optical displacement of the visual stimulus. *J Exp Psychol*, 71:150–158.

Hirata, Y. and Highstein, S. M. (2001). Acute adaptation of the vestibuloocular reflex: signal processing by floccular and ventral paraflocular Purkinje cells. *J Neurophysiol*, 85(5):2267–2288.

Hopp, J. J. and Fuchs, A. F. (2004). The characteristics and neuronal substrate of saccadic eye movement plasticity. *Prog Neurobiol*, 72(1):27–53.

Hospedales, T. and Vijayakumar, S. (2008). Structure inference for Bayesian multisensory scene understanding. *IEEE Transactions on Pattern Analysis and Machine Intelligence*, 30(12):2140–2157.

Hospedales, T. and Vijayakumar, S. (2009). Multisensory Oddity Detection as Bayesian Inference. *PLoS ONE*, 4(1).

Hospedales, T. M., Cartwright, J. J., and Vijayakumar, S. (2007). Structure inference for bayesian multimodal perception and tracking. In *IJCAI*.

Huang, V. S. and Shadmehr, R. (2007). Evolution of motor memory during the seconds after observation of motor error. *J. Neurophysiol.*, 97:3976–3985.

Imamizu, H., Miyauchi, S., Tamada, T., Sasaki, Y., Takino, R., Putz, B., Yoshioka, T., and Kawato, M. (2000). Human cerebellar activity reflecting an acquired internal model of a new tool. *Nature*, 403(6766):192–195.

Ingram, H. A., van Donkelaar, P., Cole, J., Vercher, J. L., Gauthier, G. M., and Miall, R. C. (2000). The role of proprioception and attention in a visuomotor adaptation task. *Exp Brain Res*, 132:114–126.

Ito, M. (2000). Mechanisms of motor learning in the cerebellum. *Brain Research*, 886(1-2):237–245.

Izawa, J., Rane, T., Donchin, O., and Shadmehr, R. (2008). Motor adaptation as a process of reoptimization. *J Neurosci*, 28:2883–2891.

Jordan, M. I. and Rumelhart, D. E. (1992). Forward models: Supervised learning with a distal teacher. *Cognitive Science*, 16:307–354.

Kawato, M. (1999). Internal models for motor control and trajectory planning. *Curr Opin Neurobiol*, 9(6):718–727.

Kawato, M. and Gomi, H. (1992). The cerebellum and VOR/OKR learning models. *Trends in Neuroscience*, 15(11):445–453.

Kitazawa, S., Kimura, T., and Yin, P. (1998). Cerebellar complex spikes encode both destinations and errors in arm movements. *Nature*, 392(6675):494–497.

Kluzik, J., Diedrichsen, J., Shadmehr, R., and Bastian, A. (2008). Reach adaptation: What determines whether we learn an internal model of the tool or adapt the model of our arm? *J Neurophysiol*.

Kojima, Y., Iwamoto, Y., and Yoshida, K. (2004). Memory of learning facilitates saccadic adaptation in the monkey. *Journal of Neuroscience*, 24(34):7531–7539.

Körding, K. P., Beierholm, U., Ma, W. J., Quartz, S., Tenenbaum, J. B., and Shams, L. (2007a). Causal inference in multisensory perception. *PLoS ONE*, 2:e943.

Körding, K. P., Tenenbaum, J. B., and Shadmehr, R. (2007b). The dynamics of memory as a consequence of optimal adaptation to a changing body. *Nat Neurosci*, 10(6):779–786.

Korenberg, A. and Ghahramani, Z. (2002). A bayesian view of motor adaptation. *Curr Psychol Cogn*, 21(4–5):537–564.

Krakauer, J. W., Ghilardi, M. F., and Ghez, C. (1999). Independent learning of internal models for kinematic and dynamic control of reaching. *Nat Neurosci*, 2(11):1026–1031.

Krakauer, J. W., Mazzoni, P., Ghazizadeh, A., Ravindran, R., and Shadmehr, R. (2006). Generalization of motor learning depends on the history of prior action. *PLoS Biol*, 4(10):e316.

Krakauer, J. W., Pine, Z. M., Ghilardi, M. F., and Ghez, C. (2000). Learning of visuomotor transformations for vectorial planning of reaching trajectories. *J Neurosci*, 20(23):8916–8924. Clinical Trial.

Lurito, J. T., Georgakopoulos, T., and Georgopoulos, A. P. (1991). Cognitive spatial-motor processes. 7. The making of movements at an angle from a stimulus direction: studies of motor cortical activity at the single cell and population levels. *Exp Brain Res*, 87(3):562–580.

Magescas, F. and Prablanc, C. (2006). Automatic drive of limb motor plasticity. *J Cogn Neurosci*, 18:75–83.

Marr, D. (1969). A theory of cerebellar cortex. *The journal of physiology*, 202(2):437–470.

McLaughlin, S. (1967). Parametric adjustment in saccadic eye movements. *Perception & Psychophysics*, 2:359–362.

Mitrovic, D., Klanke, S., and Vijayakumar, S. (2008). Adaptive Optimal Control for Redundantly Actuated Arms. In *Proceedings of the 10th international conference on Simulation of Adaptive Behavior: From Animals to Animats*, pages 93–102. Springer.

Optican, L. M. and Robinson, D. A. (1980). Cerebellar-dependent adaptive control of primate saccadic system. *J Neurophysiol*, 44(6):1058–1076.

Pipereit, K., Bock, O., and Vercher, J. (2006). The contribution of proprioceptive feedback to sensorimotor adaptation. *Exp Brain Res*, 174:45–52.

Porrill, J. and Dean, P. (2007a). Cerebellar motor learning: when is cortical plasticity not enough? *PLoS Comput. Biol.*, 3:1935–1950.

Porrill, J. and Dean, P. (2007b). Recurrent cerebellar loops simplify adaptive control of redundant and nonlinear motor systems. *Neural Computation*, 19(1):170–193.

Porrill, J., Dean, P., and Stone, J. V. (2004). Recurrent cerebellar architecture solves the motor-error problem. *Proceedings in Biological Sciences*, 271(1541):789–796.

Rabe, K., Livne, O., Gizewski, E. R., Aurich, V., Beck, A., Timmann, D., and Donchin, O. (2009). Adaptation to visuomotor rotation and force field perturbation is correlated to different brain areas in patients with cerebellar degeneration. *J. Neurophysiol.*, 101:1961–1971.

Rasmussen, C. E. and Williams, C. K. I. (2006). *Gaussian processes for machine learning*. MIT Press.

Redding, G. M. and Wallace, B. (1996). Adaptive spatial alignment and strategic perceptual-motor control. *J Exp Psychol Hum Percept Perform*, 22:379–394.

Robinson, D. (1964). The mechanics of human saccadic eye movement. *J Physiol*, 174:245–264.

Robinson, F. R., Noto, C. T., and Bevans, S. E. (2003). Effect of visual error size on saccade adaptation in monkey. *J Neurophysiol*, 90(2):1235–1244.

Scheidt, R. A., Conditt, M. A., Secco, E. L., and Mussa-Ivaldi, F. A. (2005). Interaction of visual and proprioceptive feedback during adaptation of human reaching movements. *J. Neurophysiol.*, 93:3200–3213.

Schweighofer, N., Arbib, M. A., and Kawato, M. (1998). Role of the cerebellum in reaching movements in humans. I. Distributed inverse dynamics control. *Eur. J. Neurosci.*, 10:86–94.

Scott, S. (2004). Optimal feedback control and the neural basis of volitional motor control. *Nat. Rev. Neurosci.*, 5:532–546.

Scudder, C. A., Batourina, E. Y., and Tunder, G. S. (1998). Comparison of two methods of producing adaptation of saccade size and implications for the site of plasticity. *J Neurophysiol*, 79(2):704–715. Comparative Study.

Shadmehr, R. and Mussa-Ivaldi, F. A. (1994). Adaptive representation of dynamics during learning of a motor task. *J Neurosci*, 14(5 Pt 2):3208–3224.

Shadmehr, R. and Wise, S. P. (2005). *The Computational Neurobiology of Reaching and Pointing: A Foundation for Motor Learning*. MIT Press.

Shibata, T. and Schaal, S. (2001). Biomimetic gaze stabilization based on feedback-error-learning with nonparametric regression networks. *Neural Networks*, 14(2):201–216.

Simani, M., McGuire, L., and Sabes, P. (2007). Visual-shift adaptation is composed of separable sensory and task-dependent effects. *J Neurophysiol*, 98:2827–2841.

Simpson, J., Wylie, D., and De Zeeuw, C. (1996). On climbing fiber signals and their consequence(s). *Behav Brain Sci*.

Smeets, J., van den Dobbelsteen, J., de Grave, D., van Beers, R., and Brenner, E. (2006). Sensory integration does not lead to sensory calibration. *Proc. Natl. Acad. Sci. U.S.A.*, 103:18781–18786.

Smith, M., Ghazizadeh, A., and Shadmehr, R. (2006). Interacting adaptive processes with different timescales underlie short-term motor learning. *PLoS Biol.*, 4:e179.

Smith, M. and Shadmehr, R. (2005). Intact ability to learn internal models of arm dynamics in huntington's but not cerebellar degeneration. *J Neurophysiol*, 93:2809–2821.

Sober, S. and Sabes, P. (2005). Flexible strategies for sensory integration during motor planning. *Nat Neurosci*, 8:490–497.

Sober, S. J. and Sabes, P. N. (2003). Multisensory integration during motor planning. *J Neurosci*, 23(18):6982–6992. Clinical Trial.

Straube, A., Fuchs, A. F., Usher, S., and Robinson, F. R. (1997). Characteristics of saccadic gain adaptation in rhesus macaques. *J Neurophysiol*, 77(2):874–895.

Thoroughman, K. A. and Shadmehr, R. (2000). Learning of action through adaptive combination of motor primitives. *Nature*, 407(6805):742–747.

Todorov, E. (2000). Direct cortical control of muscle activation in voluntary arm movements: a model. *Nat Neurosci*, 3(4):391–398.

Todorov, E. and Jordan, M. I. (2002). Optimal feedback control as a theory of motor coordination. *Nat Neurosci*, 5(11):1226–1235.

Todorov, E. and Li, W. (2005). A generalized iterative lqg method for locally-optimal feedback control of constrained nonlinear stochastic systems. In *Proceedings of the 2005 American Control Conference.*, pages 300–306.

Tong, C., Wolpert, D. M., and Flanagan, J. R. (2002). Kinematics and dynamics are not represented independently in motor working memory: evidence from an interference study. *J Neurosci*, 22(3):1108–1113. Clinical Trial.

Tseng, Y.-W., Diedrichsen, J., Krakauer, J. W., Shadmehr, R., and Bastian, A. J. (2007). Sensory prediction errors drive cerebellum-dependent adaptation of reaching. *J Neurophysiol*, 98(1):54–62.

van Beers, R., Sittig, A., and Denier van der Gon, J. (1996). How humans combine simultaneous proprioceptive and visual position information. *Exp Brain Res*, 111:253–261.

van Beers, R., Sittig, A., and Gon, J. (1999). Integration of proprioceptive and visual position-information: An experimentally supported model. *J Neurophysiol*, 81:1355–1364.

van Beers, R. J., Wolpert, D. M., and Haggard, P. (2002). When feeling is more important than seeing in sensorimotor adaptation. *Curr Biol*, 12(10):834–837.

Vijayakumar, S., D'Souza, A., and Schaal, S. (2005). Incremental online learning in high dimensions. *Neural Computation*, 17(12):2602–2634.

Wallman, J. and Fuchs, A. F. (1998). Saccadic gain modification: visual error drives motor adaptation. *J. Neurophysiol.*, 80:2405–2416.

Wei, K. and Körding, K. P. (2008). Uncertainty in state estimate and feedback determines the rate of motor adaptation. In Todorov, E. and Shadmehr, R., editors, *Proc. Advances in Computational Motor Control*.

Welch, R. (1974). Speculations on a model of prism adaptation. *Perception*, 3:451–460.

Wolpert, D. M., Ghahramani, Z., and Jordan, M. I. (1995). An internal model for sensorimotor integration. *Science*, 269:1880–1882.

Wolpert, D. M., R, M. C., and Kawato, M. (1998). Internal models in the cerebellum. *Trends in Cognitive Sciences*, 2:338–347.

Yutaka Hirata, P. M. B. and Highstein, S. M. (2004). Evaluation of the inverse dynamic model in cerebellum during visual-vestibular interactions at different vor gains in squirrel monkeys. *Neurocomputing*.